Bartosz Kossowski

Magnetic resonance spectroscopy - method and measurement for dyslexia and age related effects

PhD thesis
Completed in the Laboratory of Brain Imaging
of the Nencki Institute of Experimental Biology
Polish Academy of Sciences

SUPERVISORS:

dr hab. Katarzyna Jednoróg, associate professor
Nencki Institute of Experimental Biology, PAS

dr hab. Piotr Bogorodzki, associate professor
Faculty of Electronics and Information Technology
Warsaw University of Technology

Warsaw, 2020

Abstract

Biochemical environment of the brain can be studied in-vivo with magnetic resonance spectroscopy (MRS). Despite the fact that this technique is known since 1980s and available on many clinical scanners it is still considered difficult to perform and interpret. This thesis concerns theoretical, practical and experimental considerations of MRS in the context of dyslexia and age-related changes.

The standard MRS measurement enables identification of up to 20 metabolites in the brain, but not GABA, which is a major inhibitory neurotransmitter. We additionally targeted GABA with the state of the art spectral editing technique - MEGA-PRESS. The method was installed on 3 different scanners from 3 to 7 T, tested with a newly designed phantom and validated for an application study. In order to correctly address the new method in research questions, a lot effort has been made including sequence implementation, phantom tests and an in-vivo evaluation (Approach). A complete methodology of a spectroscopic measurement can be reimplemented in the future studies.

Application study concerned developmental dyslexia, which is a brain-based difficulty in acquiring fluent reading skills that affects around 10% of children. Anatomical and functional brain networks involved in typical and atypical reading are increasingly well characterized, while the underlying neurochemical bases of developmental dyslexia are almost unknown. Similarly, little is known about normal age-related metabolite changes compared to imaged based brain volumetry, diffusion and functional magnetic resonance. The first theory related to the brain chemistry suggests that dyslexia might be a consequence of neuronal hyperexcitability - heightened noise and instability in information processing due to a lack of balance in glutamate and GABA. The second suggests that the cause of reading disorder is neuronal oscillation desynchronization in the specific frequency bands driven by glutamate, acetylcholine or caused by structural organization abnormalities. Thus, we hypothesized that concentrations of glutamate, GABA, choline, and N-acetylaspartate (NAA) would differentiate the groups or correlate with the performance of behavioral tests. Additionally we aimed to explore how the age of participants influences the results in spectroscopy.

For that purpose we scanned 36 adults and 52 children (half of them with dyslexia). In contrast to the predictions based on the hyperexcitability, dyslexic individuals were not

characterized with heightened levels of glutamate or lower GABA neither in adult, nor children sample. Dyslexic individuals, irrespective of age, had significantly lower NAA than controls in the occipital cortex. NAA is considered to be a marker of neural health and viability but also plays a role in myelin synthesis. Reduced tNAA in all dyslexic subjects suggests microstructure rather than neurotransmission abnormalities.

Additionally, we found that concentration of many metabolites change with age such as NAA, choline and creatine are higher in adults than children, whereas glutamate is lower. Therefore scaling to NAA or creatine can be confounded by age, whereas water referencing used here is the most advisable method and the one with least assumptions to be made.

In sum, we developed the complete pipeline for a magnetic resonance spectroscopy measurement for the major brain metabolites with an extension to GABA. Improved tissue composition correction, acquisition protocol and data analysis greatly increased the value of such measurement in an application research. Original article and the current dissertation are a significant contribution to the neurobiology of dyslexia and its methodology.

Streszczenie

Spektroskopia rezonansu magnetycznego (MRS) umożliwia bezinwazyjne badanie środowiska biochemicznego mózgu. Pomimo tego, że technika została wprowadzona już w latach 80’ ubiegłego wieku i jest dostępna w większości skanerów rezonansu magnetycznego używanych do celów klinicznych, nadal sprawia wiele problemów przy rejestracji i nie jest łatwa w interpretacji. Ta praca ma na celu przedstawienie teoretycznych rozważań, praktycznych zastosowań oraz wyników eksperymentalnych dotyczących spektroskopii w kontekście badań nad dysleksją rozwojową i zmian metabolicznych zachodzących wraz z wiekiem.

Standardowy pomiar umożliwia obliczenie stężeń około 20 metabolitów mózgowych ale nie GABA, głównego neuroprzekaźnika hamującego. W celu wyodrębnienia sygnału GABA wykorzystaliśmy zyskującą na popularności technikę edycji widmowej przy pomocy sekwencji MEGA-PRESS. Metoda pomiarowa została uruchomiona na 3 skanerach o indukcji magnetycznej od 3 do 7 T, przetestowana i wykorzystana w aplikacyjnym badaniu na reprezentatywnej grupie. Nowa metoda badań została dogłębnie poznana dzięki samodzielnemu zaprogramowaniu sekwencji, zaprojektowaniu procesu przetwarzania danych oraz testom opartych o nowo zaprojektowany fantom chemiczny (Approach). Rekomendacje zawarte w pracy mogą zostać wykorzystane w kolejnych badaniach naukowych.

W dalszej części pracy przedstawione jest własne badanie aplikacyjne (Application), w którym opisaną metodę zastosowano celem zbadania biochemii mózgu w dysleksji rozwojowej. Osoby z dysleksją mają trudność z nauką poprawnego i szybkiego czytania, a problem ten dotyczy około 10% populacji. Anatomiczne i funkcjonalne właściwości mózgu związane z dysleksją są dosyć szczegółowo opisane w literaturze, w przeciwieństwie jednak do związanych z nią zmian biochemicznych Podobnie niewiele badań prowadzonych in-vivo z wykorzystaniem rezonansu magnetycznego opisuje zmiany metaboliczne w mózgu zachodzące wraz z wiekiem w porównaniu do badań opartych o analizę obrazów. Pierwsza z teorii etiologicznych dysleksji jest oparta o hipotezę nadmiernej pobudliwości neuronów wynikającej z nierównowagi w stężeniach glutaminianu oraz GABA. Druga teoria opiera się na badaniach elektroencefalografii mierzonej w obszarach kory słuchowej, w której zaobserwowano deficyty w specyficznych pasmach częstotliwości w synchronizacji na bodźce słuchowe. Podobnie jak w pierwszej teorii zakłócenia mogą być spowodowane przez

nieprawidłowe uwalnianie neuroprzekaźników takich jak glutaminian, acetylocholina i GABA jak również brane są pod uwagę zmiany cytoarchitektoniczne mózgu mierzone za pomocą markera takiego jak NAA. Ponadto ciekawe są zmiany metabolitów zachodzące wraz z wiekiem wśród osób z dysleksją i typowo czytających

W badaniu aplikacyjnym 36 osób dorosłych oraz 52 dzieci (~połowa ze zdiagnozowaną dysleksją) wzięło udział w sesji MRS w celu zmierzenia stężeń metabolitów w 2 obszarach mózgu. W przeciwieństwie do zakładanej hipotezy nie stwierdzono zwiększonej zawartości glutaminianu ani obniżonego poziomu GABA wśród osób z dysleksją. Co ciekawe, osoby z dysleksją niezależnie od wieku miały obniżone stężenia NAA w obszarze kory wzrokowej. NAA jest uważany za wskaźnik żywotności i funkcji neuronów jak również bierze udział w syntezie mieliny w oligodendrocytach. Obniżony poziom NAA u dyslektyków powinien kierować uwagę na zmiany raczej mikrostrukturalne niż dotyczące uwalniania neuroprzekaźników.

Dodatkowo, pokazaliśmy że stężenie wielu metabolitów zmienia się wraz z wiekiem i na przykład NAA, cholina and kreatyna mają wyższe stężenie u dorosłych niż u dzieci, natomiast zależność jest odwrotna dla glutaminianu (wyższe stężenie u dzieci). Dlatego stężenia metabolitów skalowane do NAA lub kreatyny mogą być zakłócone przez wiek badanej próby. Skalowanie metabolitów do stężenia wody jest tym samym rekomendowaną metodą, niewymagającą wielu założeń.

W niniejszej pracy został przedstawiony kompletny opis metody spektroskopii rezonansu magnetycznego do pomiaru głównych metabolitów mózgowych ze szczególnym uwzględnieniem pomiaru stężenia GABA. Warto podkreślić wprowadzone udoskonalenia dotyczące korekcji wyników ze względu na typ tkanki, opracowany protokół badania oraz analizy danych. Publikacja zamieszczona w wysoko punktowanym czasopiśmie oraz niniejsza rozprawa stanowią wkład w rozwój neurobiologii w zakresie metodologii badań oraz lepszego zrozumienia biochemicznego podłoża dysleksji rozwojowej.

Glossary of Abbreviations

13C	carbon-13
1H	hydrogen-1
31P	phosphorus-31
Ala	alanine
ARHQ	Adult Reading History Questionnaire
Asp	aspartate
Cho	choline-containing compounds
Cr/PCr	creatine/phosphocreatine
FWHM	Full width at half maximum
GABA	γ butyric acid
Gln	glutamine
Glu	glutamate
GPC	glycerophosphocholine
Lac	lactate
Lip	lipids
MRS	Magnetic resonance spectroscopy
NAA	N-acetylaspartate
NAAG	N-acetylaspartylglutamate
PA	Phonological Awareness
PCh	phosphocholine
RAN	Rapid Automatized Naming
TE	echo time
TR	repetition time

1 STATE OF THE ART

1.1 Introduction to MR spectroscopy

1.1.1 History of in-vivo spectroscopy

Magnetic resonance spectroscopy (MRS) is a nuclear magnetization measurement focused on a spectral separation of signals. Even though spectroscopy spectrum and metabolite concentrations are usually not the information of interests, all the MR experiments have to take into account spectro-spatial aspects of the signal. First experiments in that sense can be traced back to observations of Bloch (Bloch, 1946) and Purcell (Purcell et al., 1946) in 1946. However, it took a lot of time and effort to quantitatively measure metabolite concentrations in-vivo. At the beginning, separation of metabolites in nuclear magnetic resonance (NMR) spectrum was a big challenge due to magnetic field inhomogeneity in objects bigger than those used as samples in vertical NMR spectrometers. Especially compounds in 1H spectrum with a plentitude of peaks and a relatively low bandwidth of approximately 3ppm (~400 Hz at 3T) were indistinguishable. Indeed, phosphorus spectrum which extends across broader range of 15ppm (~800 Hz at 3T), was more easily accessible at that time than 1H.

In 1983 Thulborn and Ackerman (Thulborn & Ackerman, 1983) presented an in-vivo applicable framework for water-referenced phosphorus spectroscopy. It involved matching transmit coils used for phosphorus (31P) and water (1H) with a calibrated capacitor (Wray & Tofts, 1986) or by a pulse calibration procedure (Tofts, 1988). A pioneering experiment of measuring phosphorus metabolites in human brain was done at the University of California, San Francisco and published in 1989 (Roth et al., 1989). Next, as magnet design improved, 1H spectroscopy became more and more popular with its first quantitative measurement of NAA published in 1989 (Narayana et al., 1989). The measurement based on proton signal itself, without the need of switching between different nuclei, made the technique less hardware demanding and easier to apply in in-vivo applications. Further improvements in localization techniques and shortening echo time reduced j-modulation distortions and relaxation losses thus enabled identification of greater number of metabolites (Frahm et al., 1990; Michaelis et al., 1991).

Several significant improvements have been made since the establishment of measurement method: single-voxel excitation techniques - PRESS (Bottomley, 1985) and then sLASER (Lance & Michael, 1998), MEGAPRESS (Rothman et al., 1993) - j-edited spectroscopy for lactate and GABA, automated quantitatification software such as in LCModel (Provencher, 2001), just to name a few.

The performance in single voxel spectroscopy almost linearly increases with the value of magnetic induction. Firstly, magnetization (averaged angular momentum of all spins in the sample) is proportional to external magnetic field, which gives a linear increase in signal magnitude. Secondly, chemical shifts of the peaks i.e. the spectral bandwidth broaden as a whole, with theoretically no deterioration in spectral resolution, giving the opportunity for better peak separation at higher fields - see Figure 1. Steady progress in methodology has been accompanied by technological leap in magnet design and construction. Recently ultra high field - 7T magnets became available for the research as well as clinical applications. At CMRR in Minnesota there is currently the highest magnetic induction of 10.5T magnet available for humans (Ertürk et al., 2017), but there are sites trying to achieve even higher field strengths in France - 11.7T (Bihan et al., 2017), Korea (11.7T), USA (11.7T, 14T and 20T) and Germany (14T) (Ladd et al., 2018). The possibility of achieving so strong electromagnets was raised when superconductive material with higher magnetic critical field (niobium-tin) was introduced to the manufacturing process.

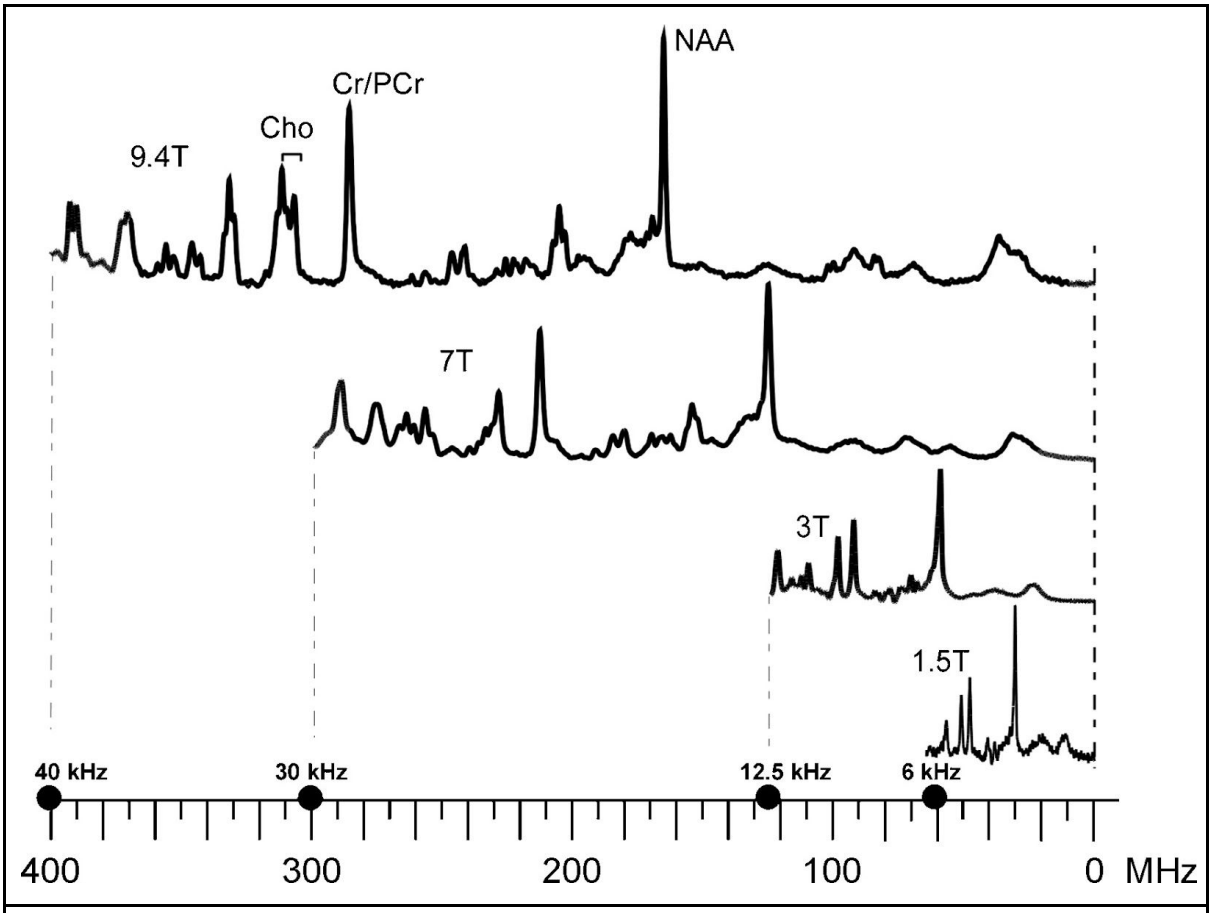

Figure 1. Spectra obtained in magnetic field from 1.5T to 9T with marked peaks of N-acetyl-aspartate (NAA), creatine/phosphocreatine (Cr/PCr) and choline (Cho). The higher magnetic field, the higher peak amplitude and the wider spectral bandwidth is (Hajek & Dezortova, 2008).

Continuous progress in MR technology have opened up new possibilities in spectroscopy applications. Recently functional magnetic resonance spectroscopy during fMRI-like stimulation has attracted attention of scientist (P. G. Mullins, 2018; Stanley & Raz, 2018). Also spatially encoded information has been incorporated with enhanced quality in a given time (Hangel et al., 2015; Strasser et al., 2017) which enables studying whole brain distribution of increased number of metabolites including neurotransmitters in the brain.

1.1.2 Principles of MR spectroscopy

Isotopes with a nonzero nuclear magnetic moment may interact with external magnetic field and undergo a phenomenon of nuclear magnetic resonance. This process consist of state of energy absorption of electromagnetic radiation (excitation) and following emission during a return to the previous, lower energy state. Both processes are characterized with specific frequency of electromagnetic radiation - Larmor frequency (1).

$$\nu_0 = \frac{\gamma}{2\pi B_0} \qquad (1)$$

The proportionality constant γ is called gyromagnetic ratio and it is specific to detectable isotopes i.e. 1H, 13C and 31P resulting in respective resonant frequency for each type of nucleus in a given external magnetic field. Other factors, which limit visibility of MRS signal, are metabolite concentration and size (mobility) of a molecule. The majority of brain metabolites can be identified by measuring one of those spectra, however the feasibility of in-vivo measurement is limited to about 20 metabolites in proton spectrum, <10 in phosphorus and ~5 metabolites in carbon spectrum (without infusion of a 13C enriched marker). Very large and heavy molecules such as lipids, are difficult to measure, because of their broad frequency spectrum (broad, low magnitude non-specific signals). Signals which give rise to a so called spectral baseline, which span across several metabolite signals causing difficulties in quantifications are classified with general term of macromolecules.

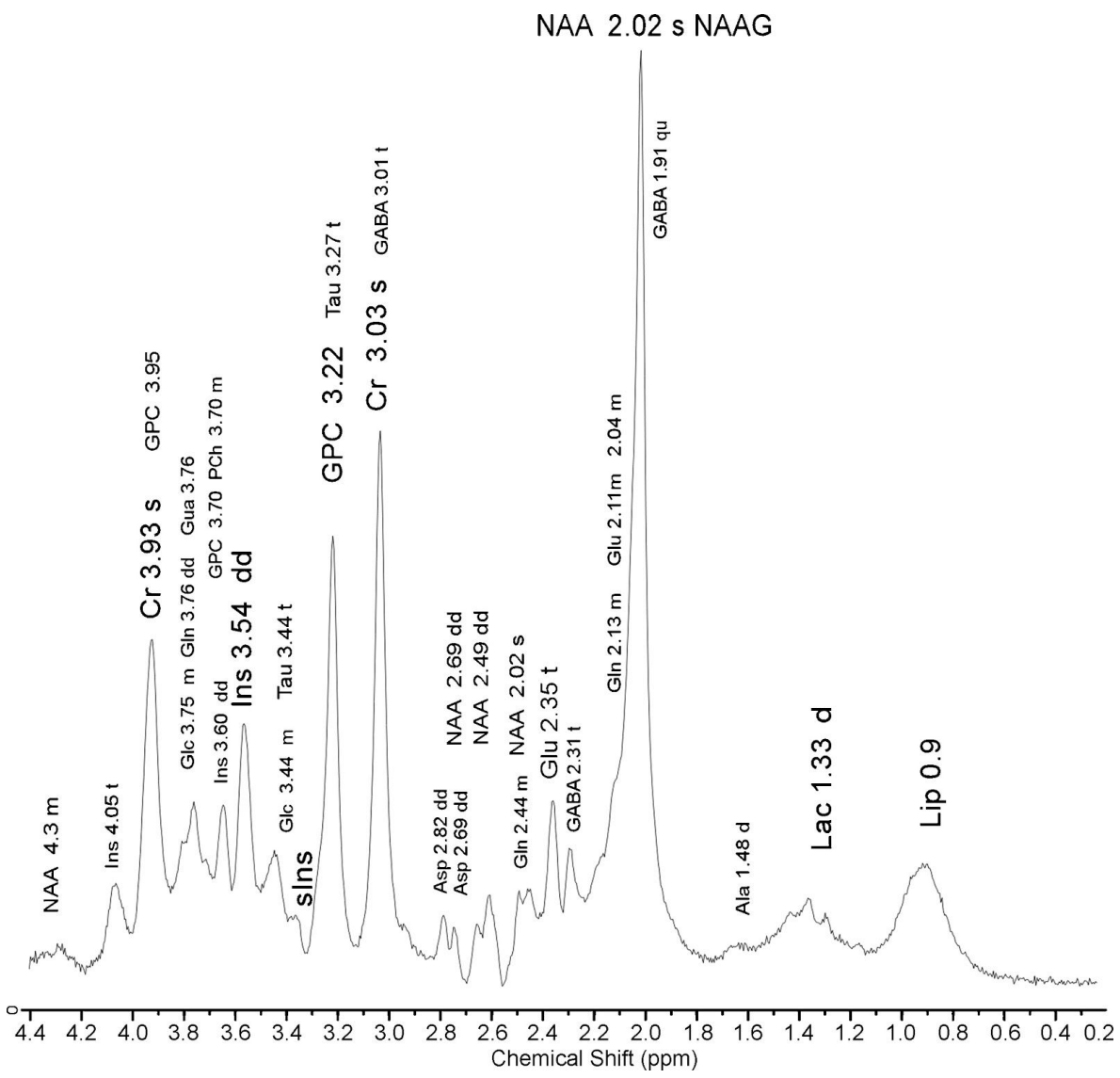

Figure 2. The interpretation of the typical 1H spectrum - NAA, N-acetylaspartate; NAAG, N-acetylaspartylglutamate; Cr/PCr, creatine/phosphocreatine; Cho, choline-containing compounds; GPC, glycerophosphocholine; Pch, phosphocholine; Ins, myo-inositol; sins, scyllo-inositol; Glc, glucose; Gln, glutamine; Glu, glutamate; Tau, taurine; Lip, lipids; Lac, lactate; Ala, alanine; GABA, γ butyric acid; Asp, aspartate (Hajek & Dezortova, 2008)

Interpretation of metabolite spectrum (Figure 2) is achievable thanks to signal properties dependant on chemical environment of molecules - electron shielding and interactions between nuclei of the same type. In chemical compounds nuclei are connected via chemical bonds and share electrons, which may group together around targeted nucleus (shield) or travel away towards attached chemical groups (unshield). Higher shielding, which creates magnetic field with opposite direction to external B_0, will lower the Larmor frequency shifting peaks in the frequency spectrum (Table 1). A spectrum can be displayed with an

absolute frequency axis in hertz [Hz] or with a use of values relative to tetramethylsilane (TMS). The latter option is commonly used as it results in a units invariant to center frequency of a magnet (magnetic field). TMS has been selected, because it is soluble and also can be easily evaporated from a sample. Its absolute frequency is higher than most of the observable compounds due to strong electron shielding, so it does not overlap with them. Eventually, it can be also utilized as a reference in carbon spectroscopy. In-vivo spectra are usually artificially calibrated based a water frequency, which is not so precise due to temperature dependence of the water peak.

Table 1. Chemical shifts in 1H spectrum for selected metabolites

Metabolite	Carbohydrate groups	Relative frequency [ppm]
NAA	-CH3, -CH2	2.01, 2.62
Cr/PCr	-CH3, -CH2	3.01, 3.90
Choline	N- (CH3)3, -CH2	3.23, 3.76

Additionally nuclei interact with each other in neighbourhood via indirect, spin-spin interaction - such as hydrogen in different carbohydrate groups. Spin of one nucleus perturbs (polarizes) the spins of the shared, bonding electrons, and the energy levels of neighboring magnetic nuclei are in turn perturbed by those polarized electrons. This leads to a lowering of the energy of the neighboring nucleus when the perturbing nucleus has one spin, and a raising of the energy when it has the other spin. Due to the fact that hydrogen is assigned with two energy states (½ & -½) in a group such as -CH2, which consist of 2 hydrogens there are 3 possible arrangements (++, +-/-+, --). In that case a local magnetic field that either adds or subtracts from neighbouring hydrogen will split its peak into 3 sub energy levels resulting in peaks multiplication in a spectrum (J-splitting) (Hahn & Maxwell, 1952). This is particularly important, that J-splitting is transferred to another proximal nucleus but does not influence the spectrum of the evoking group itself. However, J-coupling is mutual so 2 adjacent groups -CH2 and -CH3 will split each other into 3 and 4 peaks respectively (see Figure 3). More details with mathematical explanation of J-splitting will be provided in section 1.4.

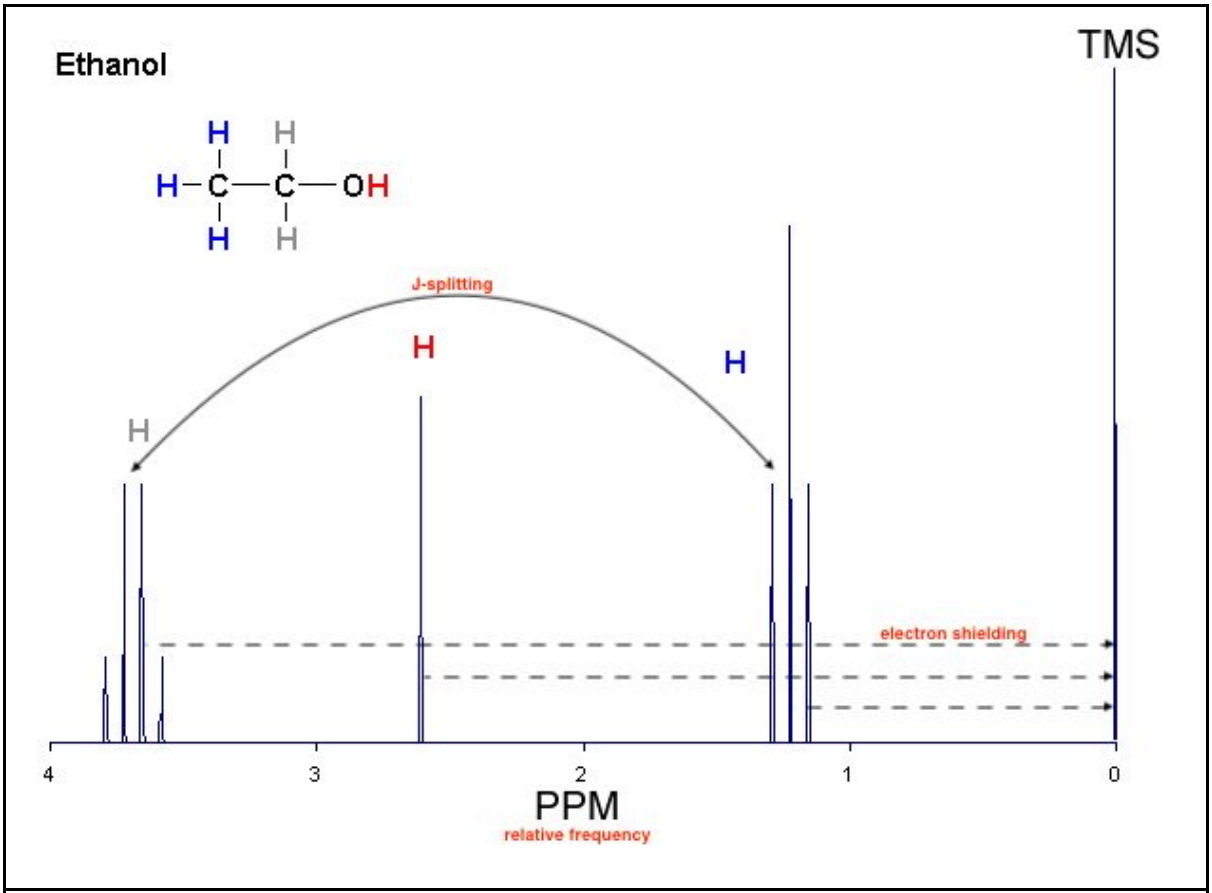

Figure 3. Ethanol 1H spectrum presents chemical shift due to electron shielding of -CH3, -CH2 and -OH groups relative to tetramethylsilane (TMS) frequency (very high shielding). Additionally, neighbouring -CH3 and -CH2 groups show reciprocal J-splitting into accordingly 3 and 4 peaks.

1.1.3 Localized single voxel spectroscopy illustrated with PRESS sequence

From previous section we learned that spins of nonzero magnetic momentum can absorb and reemit energy at a characteristic Larmor frequency. Thus, the simplest MR experiment would take radiofrequency excitation (RF pulse) and acquisition period. It is worth to mention that signal decays after excitation both due to static and dynamic field inhomogeneities. The influence of static inhomogeneities can be mitigated by the use of refocusing pulse, which inverts spin systems and produces echo signal (spin-echo (*Spin echo*, n.d.)). Thus, the simplest spin-echo experiments can be build with excitation (90) and refocusing (180) pulses. RF pulses have frequency characteristics dependent on their shape and magnitude. Combined with linearly increasing magnetic field (gradient) frequency properties (bandwidth) may be transferred to spatial domain resulting in selectivity in one of the dimensions (x,y,z) (*Slice-selective excitation*, n.d.).

Single voxel excitation technique was introduced in 1995 (Bottomley, 1985) and soon became available on all common preclinical and clinical platforms. The diagram depicted on Figure 4 shows 3 pulses sequence (PRESS sequence) which generates twice refocused echo. All three pulses combined with linear gradients are slice selective giving the opportunity to limit the volume of interest to cuboid voxel (intersection). Frequency properties of the signal are used twice here for both spatial and spectral encoding. Hence, voxel position is prone to chemical shift artifact, which is the spatial misalignment resulting from broad range of observed frequencies. Similarly to an effect of fatty tissue on water proton images, where fat appears on images shifted in reference to water signal, the voxel position in 3-dimensional space becomes shifted according to respective metabolites. Despite that due to low bandwidth pulses the classical sequence is not optimal for the use in ultra high fields (low spatial specificity) it is still considered as a gold standard for single-voxel spectroscopy (SVS).

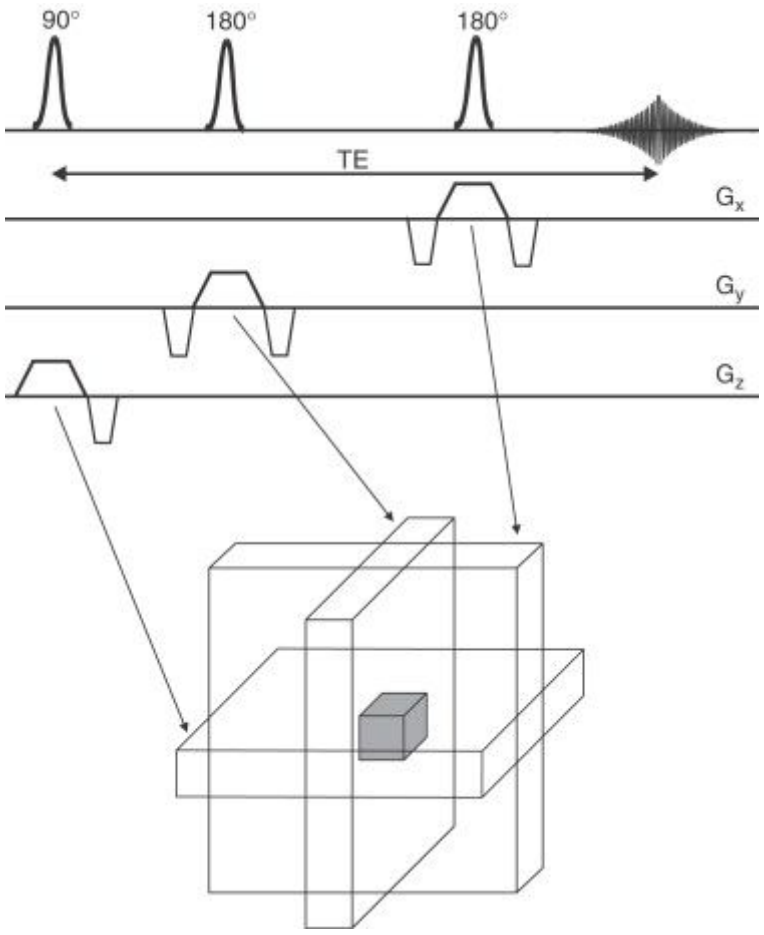

Figure 4. PRESS sequence diagram depicts: 3 pulses (90, 180, 180) followed by spin-echo signal at the top line; TE - echo time definition; 3 lines reflecting gradient pulses for spatial encoding and resulting space definition of cuboid voxel.

1.1.4 Chemical shift artifact

Chemical shift artifact is a broad term related to unexpected effects of encoding additional information in a frequency of NMR signal. On the one hand, chemical shift as a term comes from a valuable feature of frequency modulation according to local chemical environment (spectroscopy). On the other hand, artifacts related to unwanted interference between spectral and spatial information are very problematic. In MR imaging we usually focus on a specific frequency range characteristic to the most prominent water signal. However, with a frequency being used for spatial encoding we cannot neglect the effects of intercurrent resonances eg. fat, silicone and metabolites in case of spectroscopy.

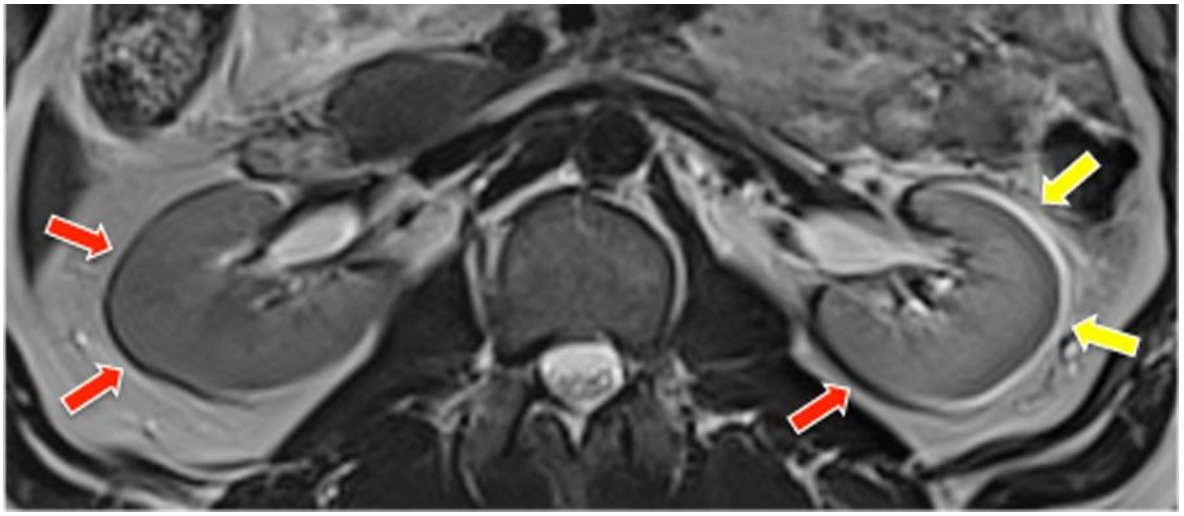

Figure 5. MR scan of a thecal sac with a gradient field decreasing from left to right during a readout phase (*Chemical shift artifact*, n.d.). Brighter fatty tissue appears shifted towards the right.

Pictorial explanation of chemical shift artifact is based on a fact that less shielded compounds (water) would shift towards higher magnetic field and more shielded ones (fat) towards lower field areas (Figure 5). In fact, static magnetic field in a scanner is not varying so much but it is the switching gradient field, which creates the shift. Thus, with a gradient field increasing from left to right brighter fatty tissue appears shifted towards the right. What is more, such an artifact does not occur horizontally in the presented image, however, that direction is also encoded by a gradient pulses. It is due to the fact that chemical shift is always present when gradient field is applied simultaneously with acquisition phase such as in case of readout direction (left-right). However, when gradient pulses precede acquisition

phase, such as in phase-encoding, they do introduce additional phase shift related to spatial (expected) and spectral (unwanted) information. In line-by-line, standard MR sequence the chemical shifts do not accumulate (are the same for each step), hence they do not cause chemical shift displacement. However, in echo planar imaging, where many lines are encoded subsequently, chemical shift accumulates in phase and is much more prominent than in readout direction.

Chemical shift displacement occurs also in an excitation/refocusing phase, when a slice-selective gradient is being played along with an RF pulse. RF pulses are designed to have a limited bandwidth corresponding to the specific range of resonance frequencies on a gradient slope. However, similarly to the readout phase less shielded compounds would shift towards higher magnetic field and vice versa. In consequence, that leads to a slice shift proportional to the difference of observed frequencies in imaging and localized spectroscopy. Eventually, in PRESS sequence there are 3 slice-selective pulses applied, which are prone to chemical shift artifact but in contrast to spectroscopic imaging the readout phase is gradient free (undistorted). Nevertheless, displacement in a voxel position due to broad range of observed metabolites leads to unexpected results (Lange et al., 2006) (Figure 6). From one perspective, voxel shift may lead to unwanted signal being introduced into the spectrum coming from outer volume (see semiLaser in section 3.1.2). However, much more complicated changes of peak shape arise from disturbance of j-coupling evolution due to refocusing of coupled spins depending on their location within a voxel (see Phantom studies in 3.1.4).

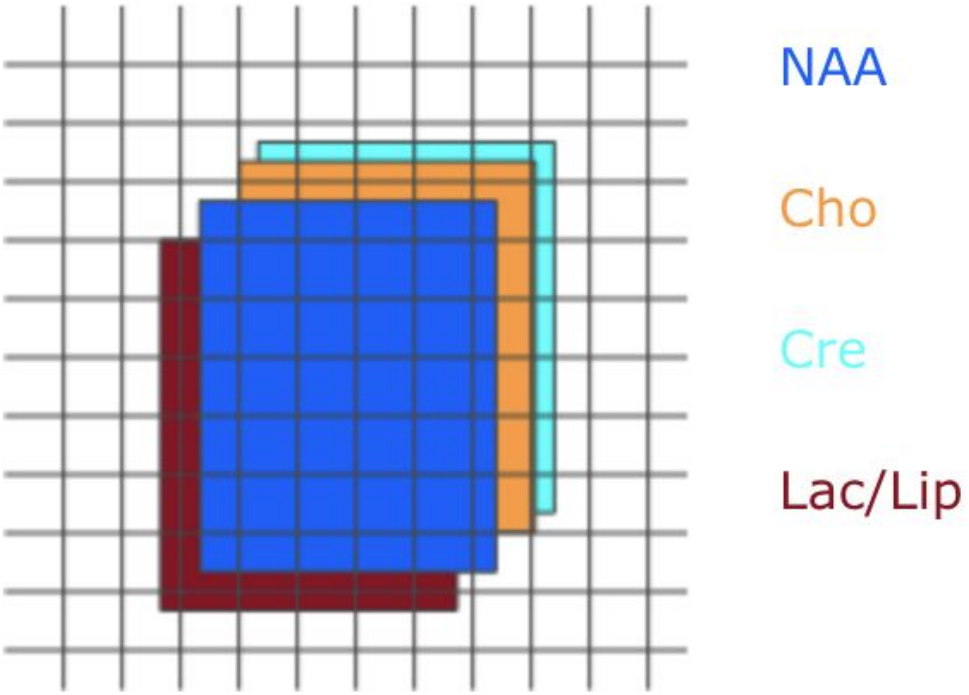

Figure 6. Two-dimensional illustration of an influence of chemical shift on a voxel position for selected metabolites.

1.1.5 Motion artifacts

The gallery of artifacts, which irreversibly deteriorate magnetics resonance spectra is very broad. A lot of them are hardware related and deep description goes beyond the scope of this thesis. However, there is a systematic review (Kreis, 2004), which is rich of common and also some more extraordinary examples. From the practical point of view motion artifact is one of the biggest issues especially in pediatric participants (Figure 7).

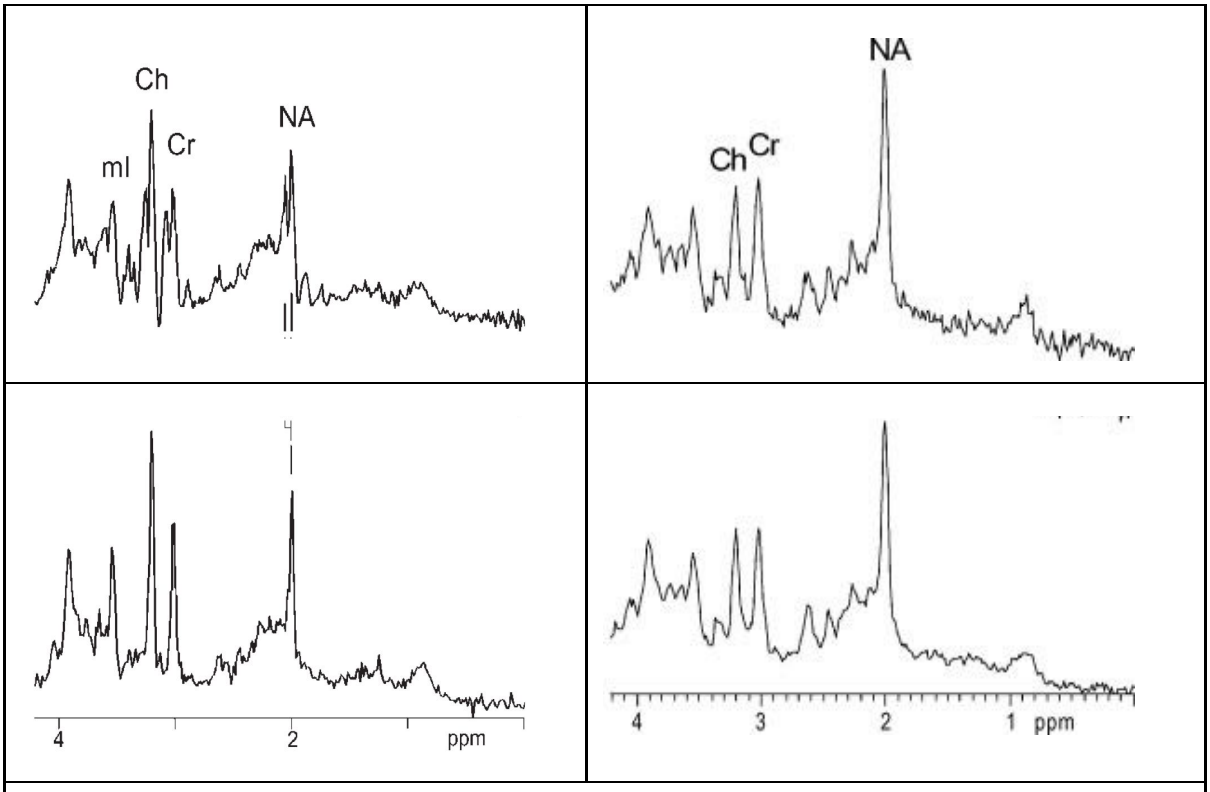

Figure 7. Motion artifacts from Kreis 2004 (Kreis, 2004). Motion artifacts observed in MRS are shown in upper row - the effect of single head movement of a neonate (upper-left) and a subject who left the scanner in midtime of acquisition (upper-right). In lower row spectra show non-deteriorated acquisition from the same participants.

Motion in a scanner can be divided into 3 groups:

- quivering or squirming of participant,
- single or repetitive head movement,
- mechanical vibrations.

All of them are very difficult to identify and even more to mitigate, however, there are a few options available to minimize the risk of artifacts. One of them is adequate head fixation, which satisfies the needs but also maintains participant's comfort inside the scanner bore. Even professional fixation cushions could not help in case of deliberate motion in children when they do not feel safe or on the opposite are too relaxed and active during the procedure. Further, we should measure motion during spectroscopy experiments, which can be based either on acquisition of additional interleaved localizers, rely on the individual spectra quality itself or employ external video recording device. What is more, spectra can be also analyzed one by one only, if they are stored in one of the raw data formats before the accumulation.

Eventually, one of the options, which is always relevant is a rapid spectroscopy acquisition, which minimizes the risk of movement by decreasing the time of an experiment. Such an acquisition could be then repeated in case of severe artifacts. Also additional localizer sequence before and after the scan are recommended to control any possible changes in the head position. Tools, which would help technicians to quickly decide, such as notification about overall shift between two scans or automated spectra quality check are extremely needed in order to make it easily applicable in a daily routine. Currently, they are not available even as additional work-in-progress packages for our platforms (GE, Siemens, Bruker).

1.2 MRS data preprocessing and quantification

Single MR measurement consists of an excitation and following acquisition of signal samples in time. Signal is being acquired in parallel from 1 or more receiving coil elements (antennas). Thus raw data matrix could have 3 dimensional size equal to coils elements by repetitions by samples. Usually, data is being accumulated across coils and repetitions into a single vector. Then, simple preprocessing operation including exponential windowing, band filtering etc. can be applied. Finally time domain signal is transformed to frequency spectrum by Fourier Transform. Such data is displayed on the screen for quality assessment and basic visual identification. That frequency plot should be saved automatically in the scan database in a DICOM format but the original data is no longer available.

1.2.1 Modelling spectra with linear combination of individual metabolite basis functions

In order to estimate concentrations of observed metabolites, quantification analyses are needed. There are several metabolite quantification programs available for research (and commercial) use. They differ in procedures, assumptions about the peak shapes, baseline modelling, macromolecule and lipid contributions, as well as in self-constraints to avoid outling results. As an input, they usually work on minimally preprocessed, already accumulated time-domain data. Currently, the most widely used is LCModel™ (Provencher, 2001), which incorporates a metabolite basis set (BS) into the fitting model. BS consists of either measured or simulated spectra from individual metabolites. The signal model consist of a set of basis functions representing individual metabolites accompanied by a few correction

factors like phase, frequency shift, individual and global peak widths. The quantities of interest, the metabolite concentrations, can be estimated from the weighting coefficients (amplitudes) of the linearly combined BS. An example composition of observed frequency peaks is shown on Figure 8. There is a number of alternatives to LCModel such as TARQUIN or AQSES (jMRUI).

TARQUIN uses a time-domain fitting combined with algorithmic approach taken from AQSES (Poullet et al., 2007). It deletes starting points from the free induction decay (FID) to eliminate quickly decaying macromolecular signal. Basis set is synthesized from simulated metabolites signal, lipids and macromolecules similarly to LCModel. To eliminate baseline, TARQUIN smooths residual signal with a convolution filter, whereas LCModel uses cubic b-splines for fitting. Programs use different sets of constraints. In addition to NAA/NAAG ratio used by both programs, LCModel uses aspartate, GABA, glucose, scyllo-Inositol. Amplitude estimates from LCModel and TARQUIN were compared using a wide range of spectra acquired on 1.5T and 3T scanners, as well as using Monte-Carlo simulations (Wilson et al., 2011) and rodent 7T data (Kossowski et al., 2017) showing high consistency.

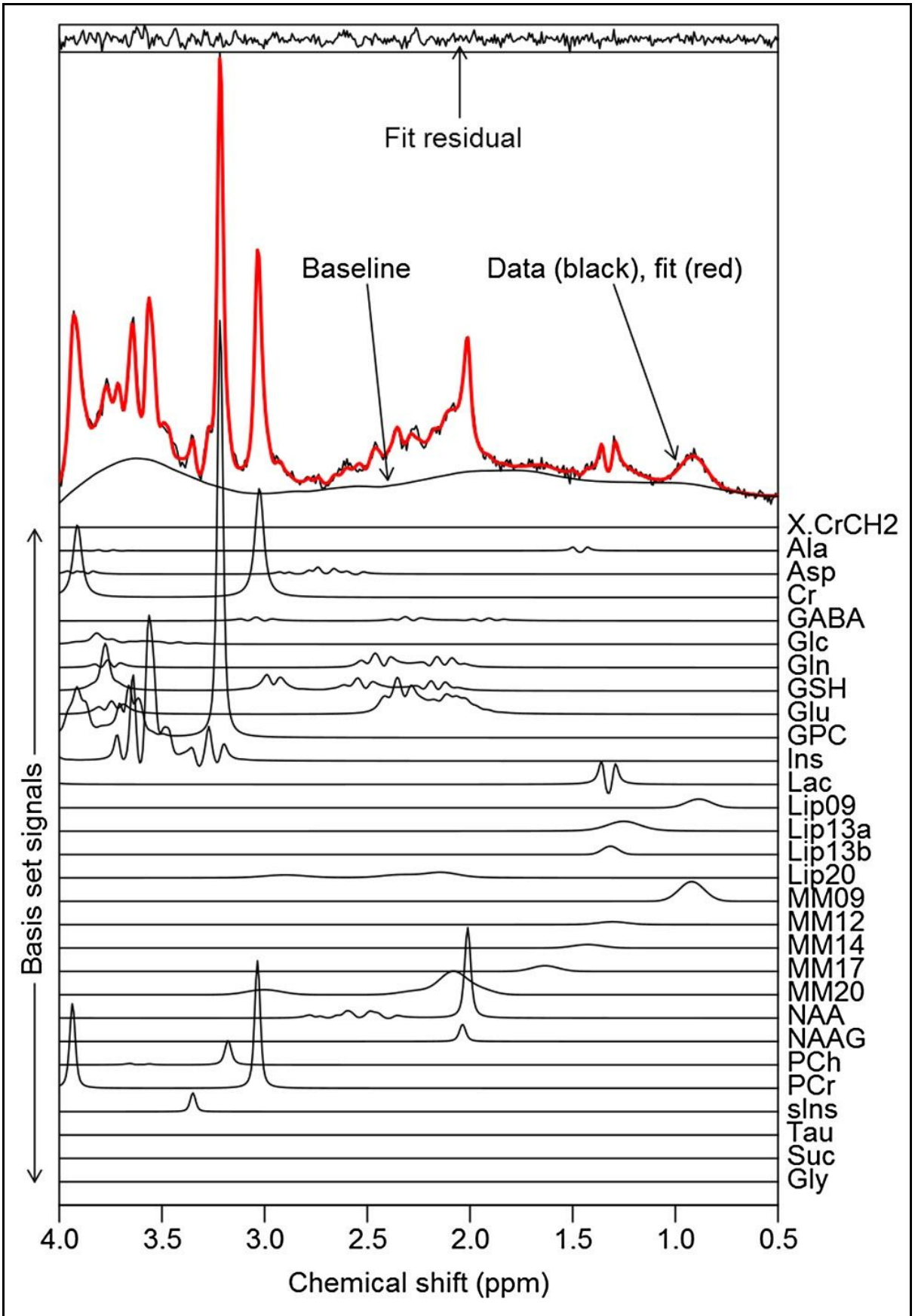

Figure 8. Pictorial representation of spectral analysis based on fitting linear combination of individual model metabolite, macromolecules and lipids spectra (Wilson et al., 2019)

1.2.2 Referencing metabolite concentration

The concentration of metabolite is proportional to the area under the spectrum. Some of the metabolites such as NAA are characterized with one dominating singlet peak (see Figure 8) which can be approximated with a gaussian shaped curve of a given magnitude and width (standard deviation). Others such as glutamate, are much more spreaded across a frequency spectrum due to a co-existence of several chemical groups and j-modulation between them. The latter are more difficult to model and fit but eventually, the area under any metabolite spectrum, will be proportional to its concentration. However, that number estimates metabolite concentration with given constants of proportionality, which may vary between measurements:

$$peak\ area \approx n_{protons} \cdot volume \cdot temperature \cdot RG \cdot Q_f$$

$n_{protons}$ - number of protons giving rise to NMR signal

Q_f - coil quality factor (coil loading)

RG - receiver gain

volume - voxel size decreased by volume of no interest (CSF, air etc.)

Apart from these variable parameters, other should be maintained stable across measurements - sequence type & parameters, magnetic field and scanner hardware, preprocessing. It becomes clear that such a raw, relative values are not useful for results generalization. Thus, a few methods are commonly used in the field to obtain comparable values across scans:

1. Peak ratio

   Under certain conditions we could assume that the concentration of some metabolites does not change. Then, we could calculate ratios of x/Cr, x/NAA and other to internally reference peaks of interest. That solution has advantage of being resistant to most of technical difficulties, hence usually gives the data with the lowest variability. That is probably why some researchers still use a creatine ratio as a standard. However, there is no such metabolite which can be considered to be stable in the human brain. Biological interpretation of any change in a ratio becomes very difficult, since it could be a change in metabolite of interest, reference or both. Especially,

creatine levels are most likely related to the amount of activity occurring in a particular region, or to the degree of vascularization of the area (C. D. Rae, 2014).

2. External referencing

   Reference signal can be also measured with a use of a standardized phantom. Reference volume can be placed together with measured object (eg. small volume attached to receiving coil) or placed after the experiment in the same location where the object had been before. Both options are prone to variation in field profiles between the two measurements. On one hand, one can apply RF transmit field nonuniformity corrections to reduce the bias between the two conditions. However, variations in a receiving field in that matter is quite difficult to account for. Therefore, external concentration referencing is not recommended in higher fields (R. A. de Graaf & de Graaf, 2019). On the other hand, there may be no alternative to such a method in case of a breast spectroscopy (varying water content) or heteronuclear experiments (13-C spectroscopy combined with 1-H reference).

3. Internal water referencing

   Internal water referencing would be the most appropriate method to calculate absolute molar concentration. However, during standard 1H MRS water signal has to be attenuated by the frequency specific water signal suppression pulses. It is due to a great difference between water and metabolite concentration (~35880 mM vs 12 mM), which would result in domination of water pool in signal power. Hence it would be challenging to acquire signals of huge and tiny magnitudes - water and metabolites altogether. Therefore we would need an additional acquisition to register undistorted water signal from the same volume and with the same sequence parameters. Luckily, water signal is so strong that usually there is no need to acquire more than 4 averages. Then metabolite estimates could be referenced to internal water signal representing water content of measured volume (Christiansen et al., 1994). Basically the method is easy to perform and overcomes all disadvantages related to technical problems of external phantoms. However, there are also a few assumptions to be made for the signal of reference:

   a. water concentration within a voxel is stable across time or participants,

b. MR properties such as T1/T2 relaxation of water within a voxel do not change.

Water content is not homogenous across the brain hence at least some additional measurement would be needed to control for voxel positition. Within the brain spectroscopy voxel, there are at least 3 tissue types such as CSF, GM, WM, which differ in both water content and water properties. According to the state-of-the-art literature (Gasparovic et al., 2006), we can estimate water concentration based on the equation concerning their relative content and relaxation times:

$$S_{H_2O_{obs}} = f_{GM} \cdot S_{H_2O} \cdot R1_{H_2O_{GM}} + f_{WM} \cdot S_{H_2O} \cdot R1_{H_2O_{WM}} + f_{CSF} \cdot S_{H_2O} \cdot R1_{H_2O_{CSF}}$$

f_X - fraction of respective tissue type within a voxel

R1 - longitudinal relaxation rate

S_{H2O} - true water signal unregarded to tissue type and respective longitudinal relaxation.

Then, corrected water concentration will be used to reference metabolite signals, which results in millimolar, averaged estimates across voxel's volume. It is worth to mention that with a single voxel spectroscopy we can only measure averaged signal within a specified volume of interest but it is not possible to distinguish signal distribution within a voxel. Indeed, metabolite distributions differ between tissue types so there is no easy way to calculate tissue specific concentrations. As an example glutamate is almost exclusively concentrated in gray matter (Figure 9), thus a voxel which contains only 50% of cortex will give us lowered estimate than it would in case of a purely cortical voxel. One of the possibilities to overcome the problem would be to measure a few (at least 2) voxels characterized with different white/gray matter ratio and calculate estimates for both types (Wang & Li, 1998). Alternatively one can utilize segmented images to obtain tissue characteristic and at least include the additional information as a covariate in a statistical model (Pugh et al., 2014).

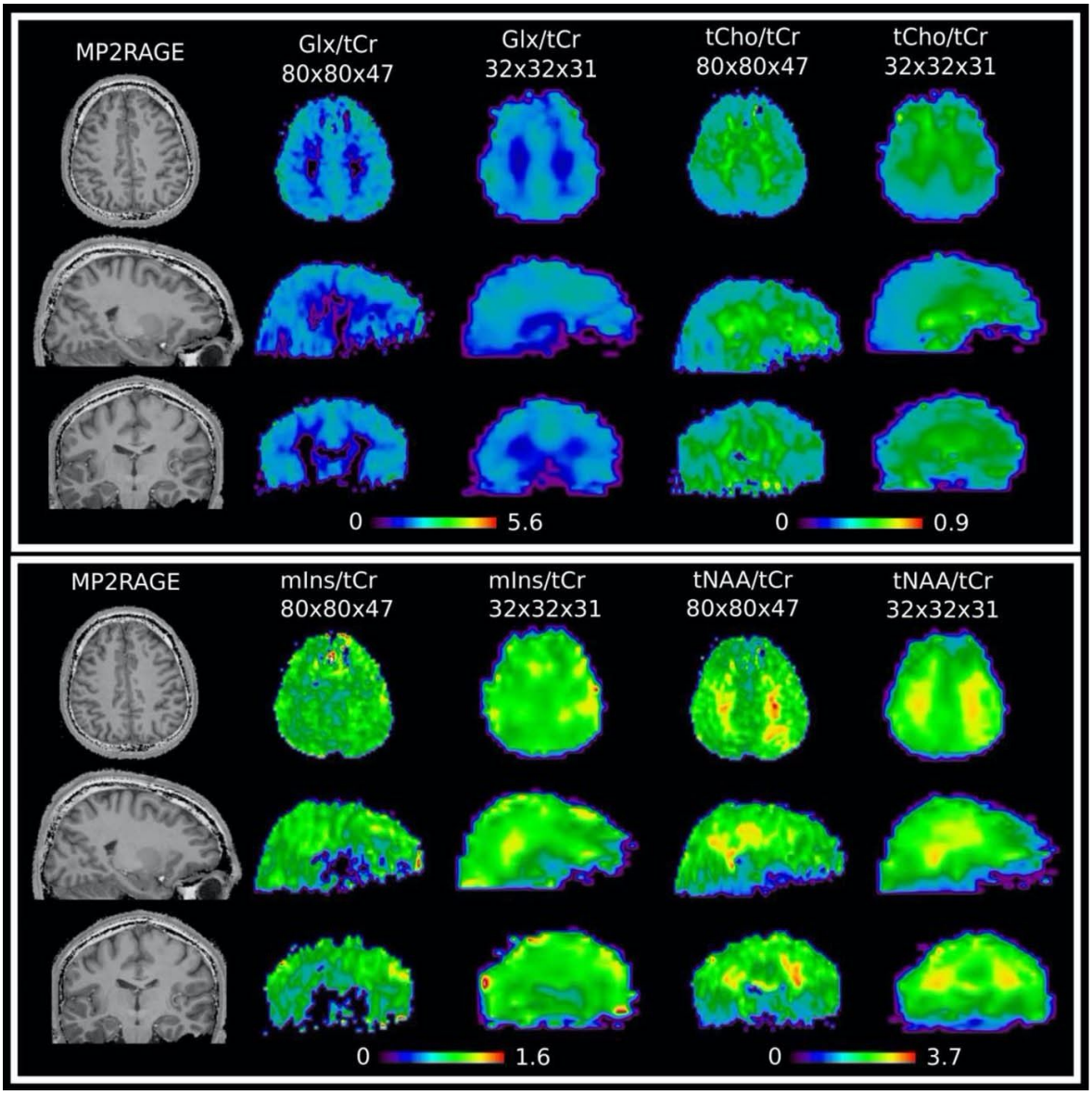

Figure 9. Distribution of metabolites within the human brain (low and high resolution) obtained with a state-of-art spectroscopic imaging technique (Hingerl et al., 2019). In a single voxel spectroscopy when a large volume of interest contains all tissue types, it depicts the partial volume effects in spectroscopy.

In summary, voxel tissue composition should be estimated based on an image segmentation (eg. in SPM12 or FSL FAST). Then, true water signal can be calculated based on tissue fractions and literature derived or measured relaxation rates. In case of pathologies the later should be used, however, it is not always feasible. Hence, ideal combined imaging and spectroscopic sessions should contain whole brain T1-relaxation map, suppressed and unsuppressed water acquisition. If there is no T1-relaxation map protocol available,

T1-weighted scan is minimally required for proper image segmentation and metabolite absolute quantification. Additional data about voxel position and composition should be published along with the concentration estimates.

1.3 Applications of 1H-MRS in neurology (selected metabolites)

Despite the fact that magnetic resonance spectroscopy is not commonly used in clinical diagnosis, its possible application in research is invaluable. On one hand the brain, viewed as complex chemical environment, can be measured quantitatively thanks to the spectra of its individual chemical components such N-acetylaspartate, choline, creatine etc. On the other hand, the brain as a neural network, can be observed with neuronal markers and neurotransmitters concentration (mainly Glu, GABA) in resting state as well as during a functional task. This short review focuses on the compounds which are the most frequently reported in the literature and are detectable with a standard 1H, 1.5-7T, single-voxel spectroscopy protocols - NAA, Cho, Cr, Glu, Gln & GABA.

N-acetylaspartate (NAA) is one of the highest concentrated molecules in the brain (after glutamate) and is easily readable from a spectrum due to prominent singlet at 2.01 ppm. NAA has long been considered a neuronal marker, due to its lowered concentration in glial tumours compared to neural tissue (Nadler & Cooper, 1972). However, more recent studies revealing higher concentration of NAA in myelin and oligodendrocytes than in neurons raise questions about its common interpretation as a neuronal marker (Nordengen et al., 2015). In fact, it is a common element of the all types of neural tissue cytoplasm. NAA is considered to serve various functions such as fluid balance (osmolarity), source of acetate for myelin synthesis (in oligodendrocytes) and is a precursor of probable neurotransmitter N-Acetylaspartylglutamate (NAAG). It has been identified as a marker in a series of disease states (Barker, 2001) such as infarcts, tumors, multiple sclerosis to name a few examples, with an interpretation of reflecting loss of neuronal fraction within a voxel. But surprisingly NAA is not always necessary for neuronal metabolism such as in case of Canavan's disease or in some individuals lacking entirely this metabolite (Martin et al., 2001). Therefore, currently NAA is considered as a marker of neuronal function and viability, but also reflecting both number of axons as well as degree of myelination and their efficiency.

Choline compounds which resonate at 3.2 ppm are mostly glycerophosphocholine (GPC) and phosphocholine (PC) as well as free choline and acetylcholine. The brain cannot

synthesise choline, thus it is transported from extracellular space and blood via the blood brain barrier. The human body can produce choline in the liver, or it may be consumed from the diet (lecithin). Plasma concentration of choline may vary from around 10μM (Löffelholz et al., 1993) to 20μM after a choline-rich meal or decrease to 5μM in dietary deficiency. Choline and its metabolites serve three purposes: structural integrity of cell membranes (phospholipid turnover), cholinergic neurotransmission (acetylcholine synthesis), and being a source for methyl groups via its metabolism. Despite the fact that phospholipids constitute around 40% of myelin, the choline signal has limited utility as a marker of myelin status due to a very short relaxation of NMR lipid signal (Laule et al., 2007). However, choline is being considered as a marker of an active myelination (turnover) when the signal is being accessible.

Creatine (Cr) facilitates recycling of adenosine triphosphate (ATP), the energy currency of the cell, primarily in muscle and brain tissue. Recycling is achieved by converting adenosine diphosphate (ADP) back to ATP via donation of phosphate groups from phosphocreatine (PCr). Both compounds (Cr and PCr) resonate at ~3.02 ppm, which makes them difficult to distinguish in quantification. Often total creatine (tCr) is reported as a sum of Cr and PCr. Creatine is derived both from diet and synthesis (also in the brain). It is exclusively available in meat, however, synthetic route is capable of meeting the requirements (i.e. in vegetarians) (C. D. Rae, 2014). Phosphocreatine can quickly regenerate ATP much faster than oxidative phosphorylation or glycolysis, thus serves as an extremely efficient buffer of energy. Indeed upon functional activation, phosphocreatine levels acutely decrease (Rango et al., 1997) but ATP levels are maintained stable (until severe decrease of oxygen when there is no supply from other pathways). Interestingly, higher creatinine levels are associated with increased neuroprotection in subsequent hypoxia. Its supplementation is beneficial in neurological and atherosclerotic diseases (Wyss & Schulze, 2002), also it was reported to reduce mental fatigue and oxygen requirements when doing a repetitive task (Watanabe et al., 2002). Total creatine concentration has been commonly used as a reference value to other metabolites. However, it is by no means a constant compound in the brain (C. D. Rae, 2014), being most likely related to the amount of activity occurring in particular region or to efficiency of vascular system (transient hypoxia).

Glutamate (Glu) is the major excitatory neurotransmitter with glutamine (Gln) as its

precursor. Both signals highly overlap in a 1.5-3T spectrum making it difficult to calculate their individual concentrations. Most often the sum of Glu and Gln is reported as Glx. However, the complexity of combined signal should be always taken into account during interpretation. Glutamate or glutamic acid is considered to be the principal excitatory neuronal signal transmitter in the brain (Platt, 2007). Release of Glu from a synaptic vesicle into a synaptic cleft causes activation of respective ionotropic receptors - AMPA, NMDA and kainate as well as slower metabotropic cascades. Opened channels allow influx of Ca^{2+} ions and consequently may trigger an action potential in the postsynaptic neuron. Glutamate may also be a potent neurotoxin, and glutamate excitotoxicity has been implicated in the pathogenesis of many devastating human neurological diseases such as stroke, amyotrophic lateral sclerosis and epilepsy (Smith, 2000). As an example, in ouabain induced stroke in rats significant rise of glutamate was found just after 2 hours from the injection (Figure 10) - research conducted during my employment in Mossakowski Medical Research Centre, Warsaw.

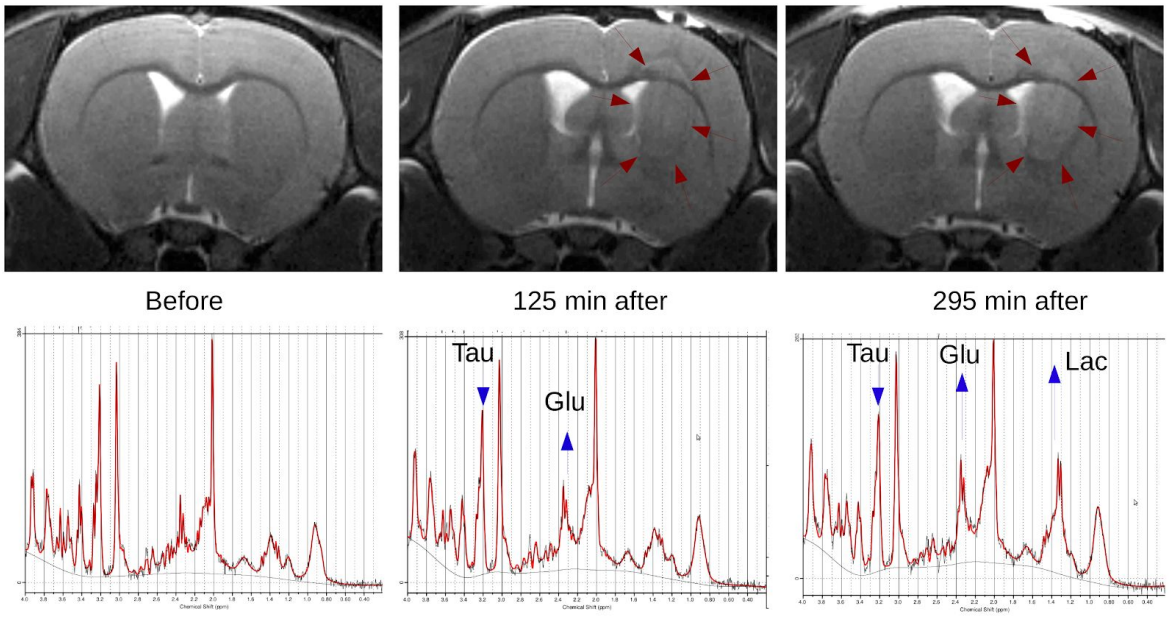

Figure 10. Ouabain induced brain stroke in rats. Bruker Biospec 7T (Mossakowski Medical Research Centre, Warsaw)

Glu is synthesized from glucose in nearly all cells of the human body other than neurons (Bak et al., 2006) due to the lack of pyruvate carboxylase. This inability has to be compensated by important resupply pathway via glutamate-glutamine cycle. Neighbouring

astrocytes collect (actively) Glu from extracellular space (i.e. synaptic cleft) maintaining its safe, low concentration at ~1μM (Anderson & Swanson, 2000). Then Glu is synthesized to Gln, which consumes ~80% of energy produced by glucose metabolism in the brain (Rothman et al., 1999). Gln in transported back to extracellular space and further into the presynaptic neurons, where Glu is resynthesized in mitochondria. The cycle is important not only to facilitate glutamate requirements of neurons but also to prevent from excessive neurotransmission after the Glu release and maintaining lower ammonia concentration (detoxification) after formation Glu from Gln.

γ-Aminobutyric acid (GABA) is a major inhibitory neurotransmitter in the brain. GABA is synthesized from glutamate and metabolised to succinic semi-aldehyde, and then to succinate. GABA has two receptor types, which are both located pre- and -post- synaptically throughout the brain (C. D. Rae, 2014). GABA also fills vesicles in the presynaptic neuron (GABAergic, inhibitory neuron) and may be released into the synaptic cleft. GABA binds to postsynaptic membrane receptors and opens up Cl^- ion channels leading to the hyperpolarization (in contrast to glutamate), which will result in decreased probability to reach the action potential threshold. GABA is synthesized from glutamate in neurons entering glutamate-glutamine cycle for resupply. Even though, it it can be efficiently reabsorbed by interneurons after its subsequent release from extracellular space, the homeostasis in the brain can be maintained only due to balanced cycle of Gln-Glu-GABA (Figure 11). The GABAergic system is involved in maintenance and modulation of many important physiological processes, including sleep, pain, motor control as well as pathological processes underlying epilepsy, anxiety, schizophrenia, developmental and neurodegenerative disorders (Möhler, 2006).

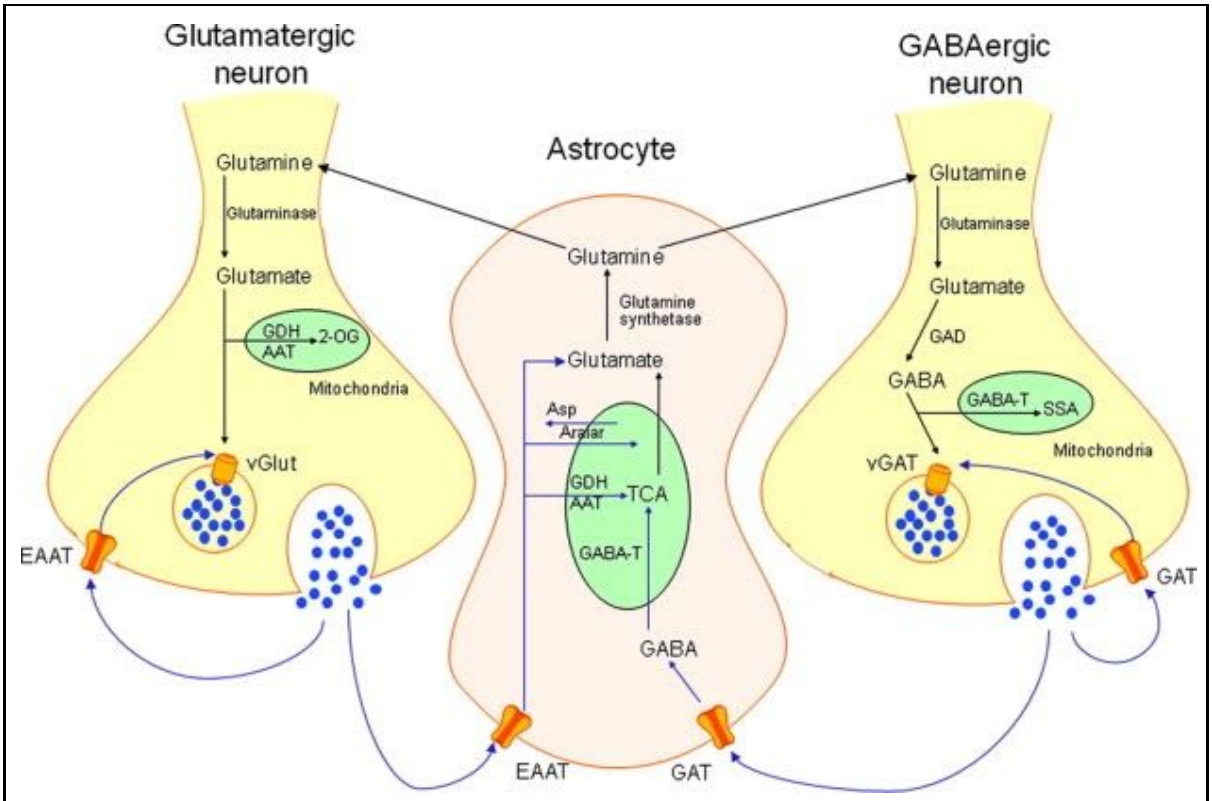

Figure 11. Glutamate, glutamine and GABA cycle. Adapted from "Glutamate and GABA synthesis, release, transport and metabolism as targets for seizure control," by Rowley, N. M., Madsen, K. K., Schousboe, A., and Steve White, H., 2012, Neurochemistry International, 61, 546-58. Copyright 2012 by Elsevier. (Rowley et al., 2012)

1.4 1-H magnetic resonance spectroscopy of GABA

GABA has 3 methylene groups (-CH2) resonating at 1.89, 2.28, 3.01 ppm. All three overlap with other more intense signals generated by glutamates, NAA and creatine (Figure 12). Because of the overlap, detection of GABA is problematic at magnetic field <3T with a standard PRESS sequence. Two common approaches were proposed to overcome the difficulties - spectral editing (Harris et al., 2017) and 2D spectroscopy with variable TE (L-COSY, J-PRESS) (Thomas et al., 2001, 2003). Despite that the two methods are comparable in performance (Prescot et al., 2018), 2D spectroscopy is considered to require longer acquisition and more complex analyses. What is more, the j-editing is considerably easier to implement on every platform, thus became a gold standard for measuring GABA.

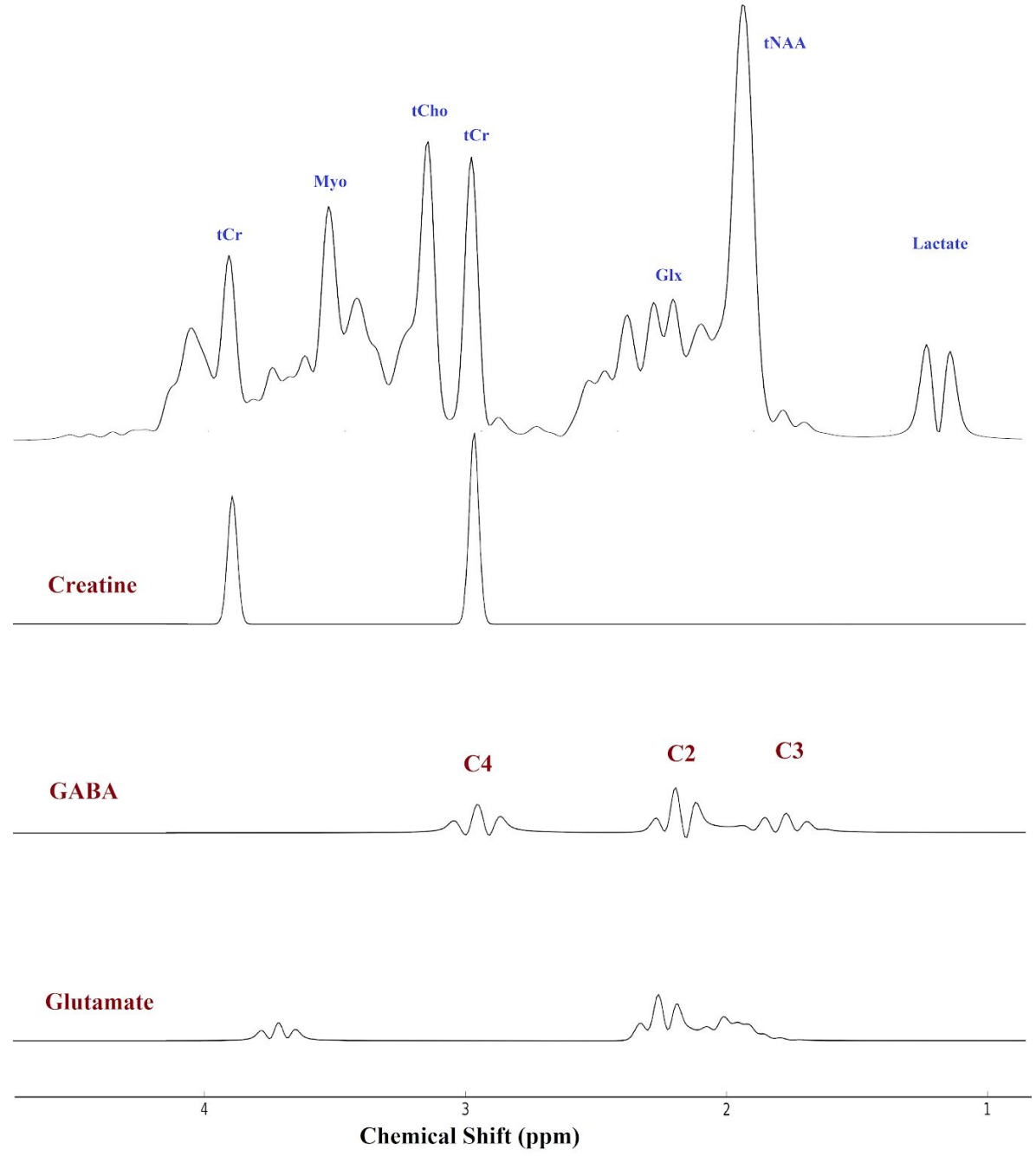

Figure 12. GABA peaks overlap with glutamates, NAA and creatine. Simulated metabolite spectrum with PRESS TE=30ms at 3T (J. M. Zhang, 2013)

J-edited spectroscopy is a technique based on a acquisition of two spectra differing only in a phase evolution of targeted peaks. Phase changes is a consequence of spin-spin interaction within single compound, neighbouring atoms. One can influence the directionality of phase evolution with a selectively applied pulses to one of the chemical groups. However,

to fully describe the physical properties of edited spectroscopy the Product Operator formalism must be used.

1.4.1 Product Operator formalism

In order to present edited spectroscopy with a meaningful mathematical apparatus we need to implement Product Operator formalism. Classical vector model of magnetization helps to build imaging sequences with standard blocks such as excitation, refocusing and acquisition phases. Whereas, MEGA-PRESS sequence additionally utilizes properties such as an evolution refocusing and J-evolution time, which are not available in the vector model. Product Operator is a formalism which weighs more on the density operator quantum theorem than a classical vector model, however, it is still easy to visualize and apply practically. Consequently, it successfully describes wider range of NMR experiments including coherence transfer (e.g. COSY) and multiple quantum coherence. For more detailed description please refer to other, academical resources (Donne & Gorenstein, 1997; Keeler, 2011).

Operators in quantum mechanics represent observable quantities such as position, momentum and energy. For a single spin, x- y- and z-components of the magnetization are represented by the spin angular momentum operators I_x, I_y, I_z. Hamiltonian (H) represents energy of the spin system. Especially, the Hamiltonian changes when a radiofrequency pulse is applied so it will help us manipulate the spin system during the experiment. For the sake of simplicity, we can focus on 3 particular Hamiltonians:

- the free precession about the z-axis $H_{free} = \Omega I_z$
- a pulse about x-axis $H_{pulse,x} = \omega_1 I_x$
- a pulse about y-axis $H_{pulse,y} = \omega_1 I_y$

Hamiltonians presented above can be pictorialy visualized as rotations of spin angular momentum about one of the axes (Figure 13).

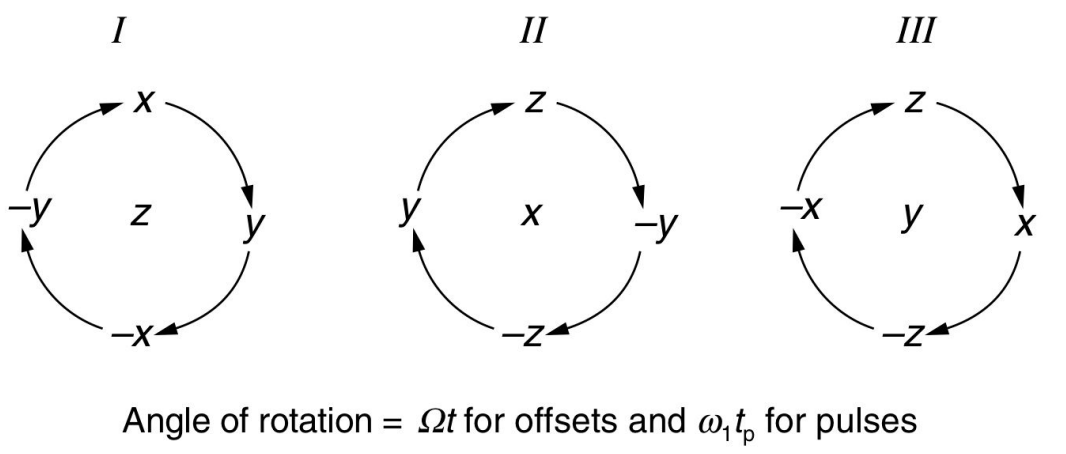

Figure 13. Pictorial representation of rotations about one of x (I), y (II) or z (III) axes representing free precession (Ωt) or pulse ($\omega_1 t$) transitions (Keeler, 2011)

As an example below is presented spin-echo experiment for 1 spin (homonuclear) system:

90° (x) → *delay* τ → 180° (x) → *delay* τ → *acquire*

1. 90° excitation

   $I_z \xrightarrow{\omega_1 t_p I_x} cos\omega_1 t_p I_z - sin\omega_1 t_p I_y$

   $I_z \xrightarrow{\frac{\pi}{2} I_x} - I_y$

2. Free precession during τ

   $-I_y \xrightarrow{\Omega\tau I_z} -cos\Omega\tau I_y + sin\Omega\tau I_x$

3. Refocusing pulse

   $-cos\Omega\tau I_y + sin\Omega\tau I_x \xrightarrow{\omega_1 t_p I_x} \sigma_{ref}$ (dealt separately below)

   (1) $-cos\Omega\tau I_y \xrightarrow{\omega_1 t_p I_x} -cos\Omega\tau cos\omega_1 t_p I_y - sin\Omega\tau cos\omega_1 t_p I_z$

   $-cos\Omega\tau I_y \xrightarrow{\pi I_x} cos\Omega\tau I_y$

   (2) $sin\Omega\tau I_x \xrightarrow{\omega_1 t_p I_x} sin\Omega\tau I_x$ (unaffected by x-axis rotation)

   $\sigma_{ref} = cos\Omega\tau I_y + sin\Omega\tau I_x$

4. Free precession during 2nd τ

   $cos\Omega\tau I_y + sin\Omega\tau I_x \xrightarrow{\Omega\tau I_z} \sigma_{echo}$ (dealt separately below)

   (1) $cos\Omega\tau I_y \xrightarrow{\Omega\tau I_z} cos\Omega\tau cos\Omega\tau I_y - sin\Omega\tau cos\Omega\tau I_x$

   (2) $sin\Omega\tau I_x \xrightarrow{\Omega\tau I_z} cos\Omega\tau sin\Omega\tau I_x + sin\Omega\tau sin\Omega\tau I_y$

$$\sigma_{echo} = (cos\Omega\tau\, cos\Omega\tau + sin\Omega\tau\, sin\Omega\tau)I_y + (cos\Omega\tau\, sin\Omega\tau + sin\Omega\tau\, cos\Omega\tau)I_x = I_y$$

In words, the offset Ω is refocused by the spin-echo sequence, even though the phase is acquired during evolution of two equal τ delays. A more complex system of 2 spins will be presented further.

1.4.2 Two-spins system J-evolution

Spin evolution under offsets and pulses in a two-spins system is based on the same operators as in a one-spin system. Nonetheless, the rotation have to be applied separately to each spin. Thus, each spin will be indexed with additional subscript: I_{1x}, I_{1y}, I_{1z}, I_{2x}, I_{2y}, I_{2z} etc. Most importantly, in a system of two magnetic particles interacting with each other, effective magnetic field will vary depending on a state of neighborhood nuclei - spin-spin or j-coupling. In a result of mutual modulation of effective magnetic field, coupling causes splitting of the adjacent spin spectrum. Two spectral lines are associated with different spin states of coupled spin and the offset is proportional to $2\pi J_{12}$, where J is an respective oscillation in the free induction signal. Hamiltonian representing the coupling is presented below:

$H_J = 2\pi J_{12} I_{1z} I_{2z}$, where J_{12} is the coupling in Hz.

J-coupling evolution as depicted on Figure 14 leads to creation to cycle between in-phase and anti-phase magnetization states. Anti-phase states are represented by operators $2I_{1x}I_{2z}$, $2I_{1y}I_{2z}$ and similarly for 2nd spin $2I_{1z}I_{2x}$, $2I_{1z}I_{2y}$, describe transverse magnetization of one spin (x or y) with respect to the coupling to second spin. It is worth to mention that in-phase magnetization (eg. I_{1x}) is also characterized by doublet signal (in-phase) splitted due to 2 states of the coupled spin. Finally, there are 5 more product operators which represent different states of two-spin system - multiple-quantum coherences (4) and non-equilibrium population distribution term (1). However, these terms are not observable and do not have to be further discussed in a context of spectral editing.

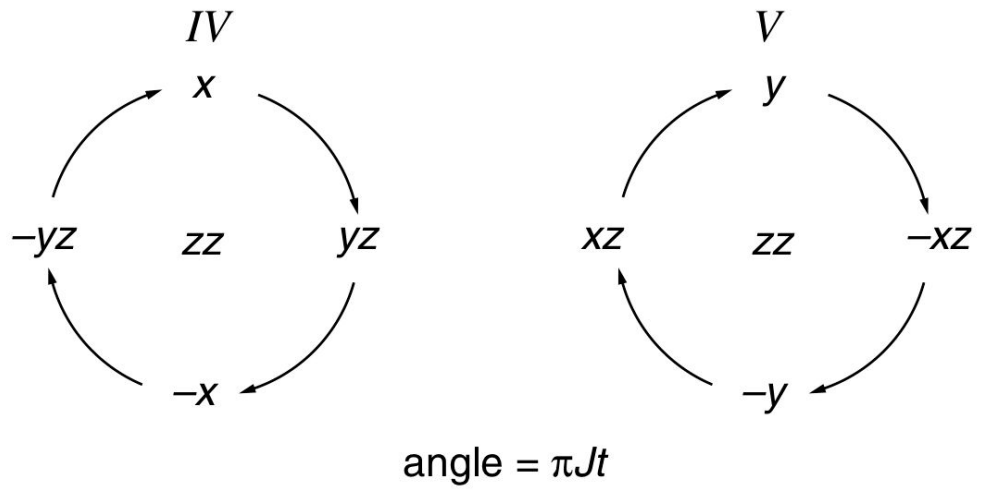

Figure 14. Coupling transitions (Keeler, 2011)

As an example spin-echo sequence for 2-spin coupled system will be given. In previous calculation for single-spin system, it has been shown that spin-echo refocuses the offset induced by a free precession during delay τ. Thus to simplify the equations, the free precession will be ignored in the present calculations. Only the coupling Hamiltonian and the related effect of refocusing pulse will be reconsidered:

1. Evolution under coupling

   $$-I_y \frac{2\pi J_{12} I_{1z} I_{2z}}{} - cos2\pi J_{12}\tau I_{1y} + sin2\pi J_{12} 2I_{1x} I_{2z}$$

2. Refocusing pulse

   $$-cos2\pi J_{12}\tau I_{1y} + sin2\pi J_{12} 2I_{1x} I_{2z} \frac{\omega_1 t_p I_{1x}}{} \frac{\omega_1 t_p I_{2x}}{} \sigma_{ref}$$

   let $\omega_1 t_p = \omega_2 t_p = \pi$

   Refocusing pulse about x-axis for spin 1 has no effect on the operator I_{1x}, as well as the second spin I_{2z}. It simply reverses the sign of I_{1y} (first term). Refocusing pulse about x-axis for spin 2 has no effect on the 1st spin operators and it reverses the sign of I_{2z}.

   $$\sigma_{ref} = cos2\pi J_{12}\tau I_{1y} - sin2\pi J_{12} 2I_{1x} I_{2z}$$

3. Evolution after refocusing

   $$cos2\pi J_{12}\tau I_{1y} - sin2\pi J_{12}\tau 2I_{1x} I_{2z} \frac{2\pi J_{12} I_{1z} I_{2z}}{} \sigma_{echo}$$

   terms dealt separately:

   $$cos2\pi J_{12}\tau I_{1y} \frac{2\pi J_{12} I_{1z} I_{2z}}{} cos2\pi J_{12}\tau cos2\pi J_{12}\tau I_{1y} - cos2\pi J_{12}\tau sin2\pi J_{12}\tau 2I_{1x} I_{2z}$$

$$-sin2\pi J_{12}\tau 2I_{1x}I_{2z}\frac{2\pi J_{12}I_{1z}I_{2z}}{} - cos2\pi J_{12}\tau sin2\pi J_{12}\tau 2I_{1x}I_{2z} - sin2\pi J_{12}\tau sin2\pi J_{12}\tau I_{1y}$$

with a help of trigonometric identities: $2sin\alpha cos\alpha = sin2\alpha$, $cos^2\alpha - sin^2\alpha = cos2\alpha$

$$\sigma_{echo} = cos4\pi J_{12}\tau I_{1y} - sin4\pi J_{12}\tau 2I_{1x}I_{2z}$$

In words, the refocusing pulse has no effect on J-coupling evolution, meaning that the result would be the same during 2τ evolution without 180° pulse. The outcome is irrelevant to the starting point.

If spin 1 and spin 2 are different, such they belong to specific carbohydrate groups or are different nuclei such as 13C and 1H, it is possible to choose to apply refocusing pulse to either or both spins. The sequence, presented above, where 180° was applied to both spins results in refocusing the offset related to a free precession but allows the evolution of coupling to go on for 2τ (until acquisition). However, if the refocusing pulse is applied only to one spin, the following takes place:

1. Evolution under coupling

   $$-I_y\frac{2\pi J_{12}I_{1z}I_{2z}}{} - cos2\pi J_{12}\tau I_{1y} + sin2\pi J_{12}2I_{1x}I_{2z}$$

2. Refocusing pulse applied to spin 1

   $$-cos2\pi J_{12}\tau I_{1y} + sin2\pi J_{12}2I_{1x}I_{2z}\frac{\omega_1 t_p I_{2x}}{}\sigma_{ref}\,,\ \omega_1 t_p = \pi$$

   Refocusing pulse about x-axis for spin 2 has no effect on the 1st spin operators and it reverses the sign of I_{2z} (second term).

   $$\sigma_{ref} = -cos2\pi J_{12}\tau I_{1y} - sin2\pi J_{12}2I_{1x}I_{2z}$$

3. Evolution after refocusing

   $$-cos2\pi J_{12}\tau I_{1y} - sin2\pi J_{12}\tau 2I_{1x}I_{2z}\frac{2\pi J_{12}I_{1z}I_{2z}}{}\sigma_{echo}$$

   $$-cos2\pi J_{12}\tau I_{1y}\frac{2\pi J_{12}I_{1z}I_{2z}}{} - cos2\pi J_{12}\tau cos2\pi J_{12}\tau I_{1y} + cos2\pi J_{12}\tau sin2\pi J_{12}\tau 2I_{1x}I_{2z}$$

   $$-sin2\pi J_{12}\tau 2I_{1x}I_{2z}\frac{2\pi J_{12}I_{1z}I_{2z}}{} - cos2\pi J_{12}\tau sin2\pi J_{12}\tau 2I_{1x}I_{2z} - sin2\pi J_{12}\tau sin2\pi J_{12}\tau I_{1y}$$

   with a help of trigonometric identities: $cos^2\alpha + sin^2\alpha = 1$

   $$\sigma_{echo} = -I_y$$

   The result is the same regardless of the initial transverse orientation.

Practical meaning of above calculations is that one can easily modify J-evolution during a spin-echo experiment. For example if there are 2 coupled carbohydrate groups in one molecule, it is possible to selectively apply pulses to refocus j-evolution or non-selectively let

it evolve to modify shape of the spectrum. It is the basis of many important 2D techniques such as COSY and TOCSY with a special 1D case of spectral editing. The last one is frequently used in in-vivo studies and was implemented into PRESS by means of additional selective inversion pulses - MEGA. When standard spin echo, with τ=1/2J$_{12}$, is acquired without selective inversion (both spins affected), spectrum will be inverted thanks to half-cycle of j-evolution. Alternatively, when the refocusing pulse is selective (or additional selective - MEGA pulse is applied), peaks will have the same phase as at the beginning (not inverted):

$-I_y \xrightarrow{2\pi J_{12} I_{1z} I_{2z}} \xrightarrow{180°_{1,2}} \xrightarrow{2\pi J_{12} I_{1z} I_{2z}} cos4\pi J_{12}\tau I_{1y} - sin4\pi J_{12}\tau 2I_{1x}I_{2z}$, for τ=1/2J$_{12}$

$-I_y \xrightarrow{2\pi J_{12} I_{1z} I_{2z}} \xrightarrow{(180°_{1,2})} \xrightarrow{2\pi J_{12} I_{1z} I_{2z}} I_y$, pulse applied to both spins (edit off)

$-I_y \xrightarrow{2\pi J_{12} I_{1z} I_{2z}} \xrightarrow{180°_{2}} \xrightarrow{2\pi J_{12} I_{1z} I_{2z}} -I_y$, selective refocusing (edit on)

1.4.3 MEGA-PRESS

MEGA-PRESS (MEshcher–GArwood Point RESolved Spectroscopy), named after the authors who first proposed the MEGA suppression scheme (applied to water suppression), is quickly becoming the standard technique used in MRS measurements of GABA. It allows GABA signals to be separated from the stronger overlying signals of other metabolites by taking advantage of known couplings within the GABA molecule (P. G. Mullins et al., 2014).

MEGA suppression consist of 2 frequency selective refocusing pulses with non-balanced crasher gradients to spoil related magnetization. The signal affected by MEGA pulses dephases, thus we lose information encoded at that range of frequencies. However, refocusing pulses reverse j-evolution of coupled spins (edit on), which can be utilised to modify the spectrum at other frequencies. MEGA-PRESS sequence is based on a standard PRESS double spin-echo paradigm with additionally placed 2 MEGA pulses about 2nd refocusing pulse (Figure 15). Considering the timing of that sequence - spin echo and j-evolution, those 2 processes must have the same duration, so j-evolution could be fully reversed at the echo time (acquisition).

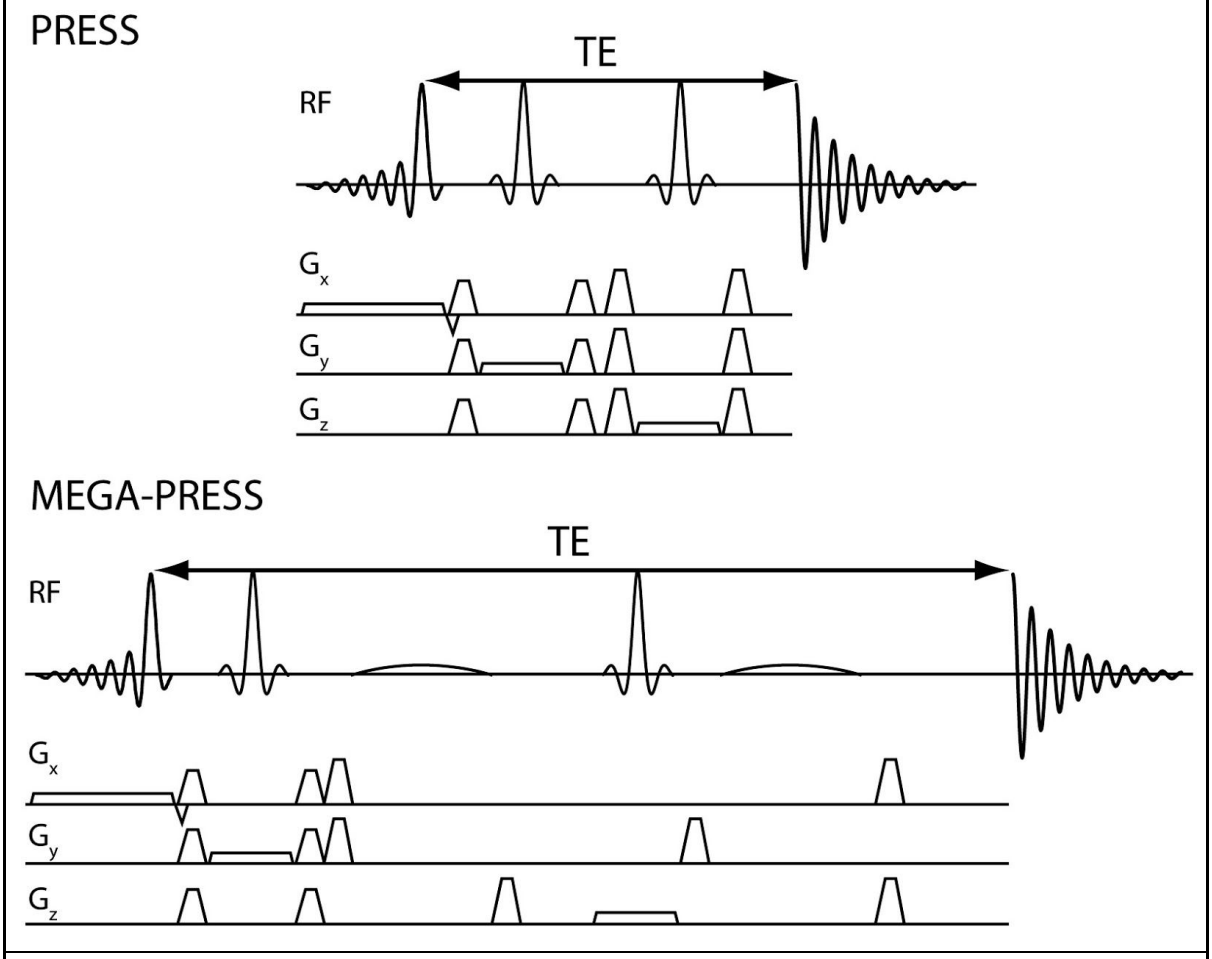

Figure 15. Representative PRESS (a) and MEGA-PRESS (b) pulse sequences, showing the addition of the editing pulses symmetrically around the second 180° pulse. (P. G. Mullins et al., 2014)

MEGA-PRESS acquisition scheme consist of two alternate acquisitions (Figure 16). One of them is set to refocus j-evolution of the selected spins (edit on), the other has to maintain j-evolution but should not differ too much from the first one (edit off). Practically, two approaches are common - (1) apply editing pulse on symmetrically frequency about f_0 (water) or (2) apply sham delays instead of MEGA pulses. In more advanced implementation such as HERMES (Chan et al., 2019) or HERCULES (Oeltzschner et al., 2019) more complicated editing schemes are employed to obtain greater number of edited metabolites during one scan.

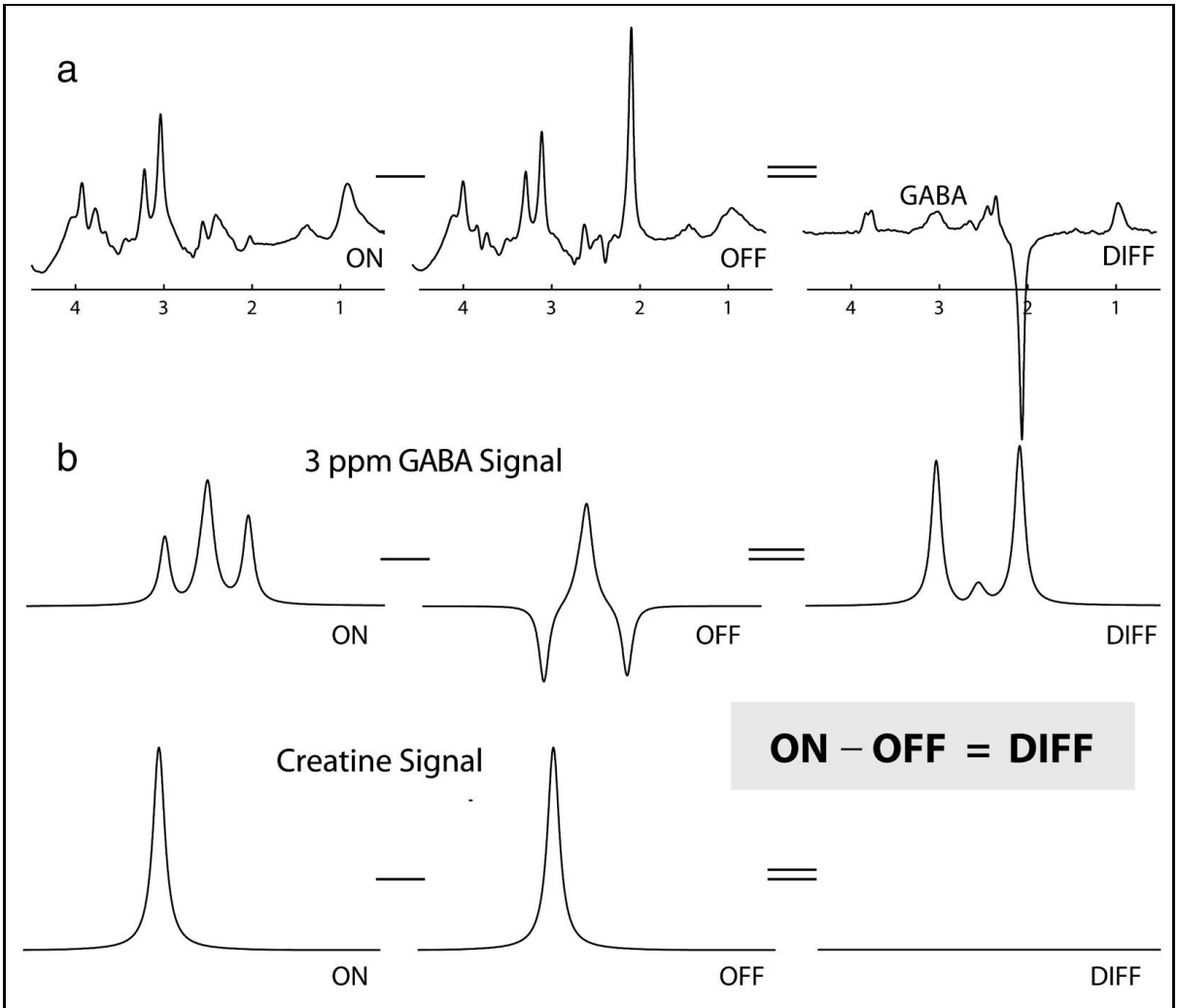

Figure 16. Schematic diagram of MEGA-PRESS editing for GABA. (a) Editing pulses applied at 1.9 ppm modulate the shape of the GABA signals at 3 ppm (b). Subtracting scans acquired without these pulses (labeled OFF) from scans acquired with the editing pulses (ON) removes overlying creatine signals from the edited spectrum, revealing the GABA signal in the difference spectrum (labeled DIFF). (b) shows the effect of editing pulses on signals at 3 ppm only. (P. G. Mullins et al., 2014)

1.4.4 Preprocessing specific to edited MRS

GABA estimation from edited spectroscopy needs to take into account pairs of measurements - edited and non-edited, which are stored in raw data format. Static field usually undergoes long-term drift due to thermal processes i.e. after excessive protocols such as diffusion weighted imaging. Thus, individual spectra should be aligned before accumulation (subtraction) to avoid bias related to frequency drift. All necessary steps regarding GABA preprocessing can be performed in Gannet toolbox (Edden et al., 2014),

which is specifically designed to estimate GABA from the raw data (Siemens, Philips, GE) with the following steps of preprocessing: (1) coil channel combine and phase correction, (2) frequency drift correction, (3) calculation of differential spectrum, (4) fitting GABA with the double peak shape. (5) Then, the result can be corrected for partial volume effects with respect to CSF, GM/WM ratio as well as tissue specific relaxation times (Harris et al., 2015).

1.5 Etiology of developmental dyslexia related to brain biochemistry

Dyslexia is a brain-based difficulty in acquiring fluent reading skills that affects around 10-15% of the population (Shaywitz et al., 1998). It is defined as a specific deficit in reading acquisition that cannot be accounted for by low IQ, poor educational opportunities, or an obvious sensory or neurological damage ("International Statistical Classification of Diseases and Related Health Problems," 2011). Many different etiological theories have been proposed to explain its specific symptoms (Ramus & Ahissar, 2012) such as auditory specific - phonological difficulties, visually specific - magnocellular dysfunction and reduced visual attention. However, none of the proposed theories has been successful enough to take into account all nuances related to reading problems. Thus, dyslexia is considered to be complex, heterogeneous disorder with several candidate etiological theories. Even though still little is known about specific link between neurochemistry and reading, there are at least two theories specifically linked to neurotransmission deficits.

The first theory is based on an insight from evoked potentials measured during auditory speech processing. Based on several studies from 2000s (Georgiou et al., 2010; Goswami et al., 2002, 2011; Hämäläinen et al., 2005; Muneaux et al., 2004; Surányi et al., 2009) one of the authors suggested that low-frequency synchronization deficits may be characteristic to dyslexia (Goswami, 2011). Reading is a complex process, which takes a low-level sensory information and further integrates multisensory inputs into the language processing stream. Impairments in neural synchronization may disturb correct sampling and encoding of auditory input as well as the multisensory integration. A temporal sampling framework was presented to be further tested in speech induced auditory cortex oscillations. Phase locking value, which is a measure of task-induced changes at previously defined frequency range, was used to reveal which frequency band is specifically impaired in dyslexia. Researchers have not come to a conclusion yet, whether the deficits in a range of 2-10 Hz (delta and theta)

(Goswami, 2011) or in 25-35 Hz (low gamma) (Lehongre et al., 2011) are specifically related to dyslexia. The first and would correspond to syllable stress pattern, while the second to a phonemic rate accordingly.

The second theory called Neural noise hypothesis, which is more general, combines previously reported oscillatory deficits with other observations from genetic studies (more detailed information can be found in the next chapter). Authors link neuronal hyperexcitability with heightened noise and instability in information processing related to reading (Hancock et al., 2017). The basis of the theory lies in an excitation-inhibition balance within cortical pyramidal-interneuron networks. Abnormal inhibitory neuron migration at the prenatal stage would result in excessive excitability, disturb the balance and consequently the precise timing in a response to sensory input. Neural noise hypothesis predicts also desynchronization at a network level, which may reflect problems in processing and integration of auditory stimuli.

Both theories would predict abnormal concentrations of neurometobilites i.e. neurotransmitters. In case of cortical excitability it is glutamate (Glu or Glx) to GABA ratio, increased glutamatergic activity (Stagg et al., 2011) or disrupted GABAergic inhibition strictly related to heightened neural noise. However, when broad range oscillatory deficits are observed as in the mentioned temporal sampling framework other abnormalities should be considered too including myelination deficits, neuronal density and viability.

Aforementioned studies regarding differences in cortical oscillations pointed out differences in gamma, theta and delta ranges in electrophysiological signal of dyslexic subjects. Since there has been no conclusive result in EEG yet, magnetic resonance spectroscopy would address previously defined hypotheses from a perspective of brain neurochemistry. Frequency - specific synchronization of neuronal excitability within the gamma band is attributable to a balance between excitation and inhibition (Buzsáki & Wang, 2012). Gamma band neurophysiological correlates of GABA concentrations have been observed in the visual (Edden et al., 2009; Muthukumaraswamy et al., 2009); temporal (Balz et al., 2016) and motor (Gaetz et al., 2014) cortex of healthy adults. In slow frequency theta oscillations glutamate and choline (Cho) presumably act as dominant neurotransmitters. Frontal theta activity was driven by hippocampal glutamatergic activity measure by respective neurotransmitter concentration during an auditory target detection task (Gallinat et

al., 2006). Also acetylcholine release in rodent hippocampus preceded the appearance of theta oscillations (H. Zhang et al., 2010) (for review see Pignatelli et al. (Pignatelli et al., 2012; H. Zhang et al., 2010)).

Presented observations and theories should potentially have a reflection in brain metabolite concentrations i.e. neurotransmitters. Indeed, there have been a few studies concerning neurometabolites in dyslexia. Initial work was carried out by Rae (C. Rae et al., 1998), who found lower choline to NAA ratio in the left temporo-parietal lobe and right cerebellum in 14 dyslexic mens compared to 15 controls. Regrettably, only the confusing choline to NAA ratio, not choline itself, reached significance threshold, which must be always pointed out in the interpretations. Interestingly, substantial lateralization difference in respect to this result was observed in the dyslexic group, whereas not in controls. Ten years later Laycock with collaborators (Laycock et al., 2008) published contradictory results of increased Cho/Cr and Cho/NAA ratios in 6 dyslexic vs 6 control subjects. Subsequently, on a bigger sample of 31 adults Bruno et al. (2013) showed that in the left angular gyrus Cho/Cr ratio is negatively correlated with phonological awareness (PA), a skill closely related to reading (Pennington et al. 1990). Also, in the richest dataset of 75 children (6-10 years old), Pugh and colleagues (Pugh et al., 2014) identified higher Cho/Cr ratios related to poor reading performance (negative correlation) in the visual cortex. Surprisingly, the effect was not significant when PA was considered but only 10 children from the whole examined sample met the criteria for reading disorder. They additionally showed negative correlations between Glu/Cr ratio and reading skill, as well as PA in the same occipital region. It is worth to mention, that this study was the first to measure GABA concentration with reliable editing sequence. However, no significant effects in GABA have been identified in the main analysis from 2014. The group has recently published a follow up study (Del Tufo et al., 2018), where more behavioural tasks were being considered i.e. a cross-modal, audio-visual word matching task. Additionally to previous work they reported that faster reaction times in this task were predicted by lower GABA/Cr and higher NAA/Cr ratios in a subsample of 70 children from the previous study. What is more, the authors showed that the task response time mediates the link between metabolite concentration (Glu, Cho) and reading ability. Consistent with neural noise hypothesis in dyslexia (Hancock et al., 2017), the authors presented supportive arguments regarding mediation role of Glu and Cho levels in the process too. Finally, Lebel

et al. (Lebel et al. 2016) measured neurometabolites' concentration in two regions: the anterior cingulate gyrus (n=56) and left angular gyrus (n=45) in a group of preschool children. In contrast to Bruno et al. (2013) and Pugh et al. (2014), they reported positive correlations between PA and neurotransmitters - Glu, creatine and inositol in anterior cingulate gyrus. Lebel analyzed absolute (water referenced) metabolite concentrations, which minimizes the risk of misinterpretation due to ratio referencing. The above mentioned findings were summarized in Figure 17, which visualizes discrepancies between previous studies i.e. related to brain region, metabolite of reference and behavioural measures.

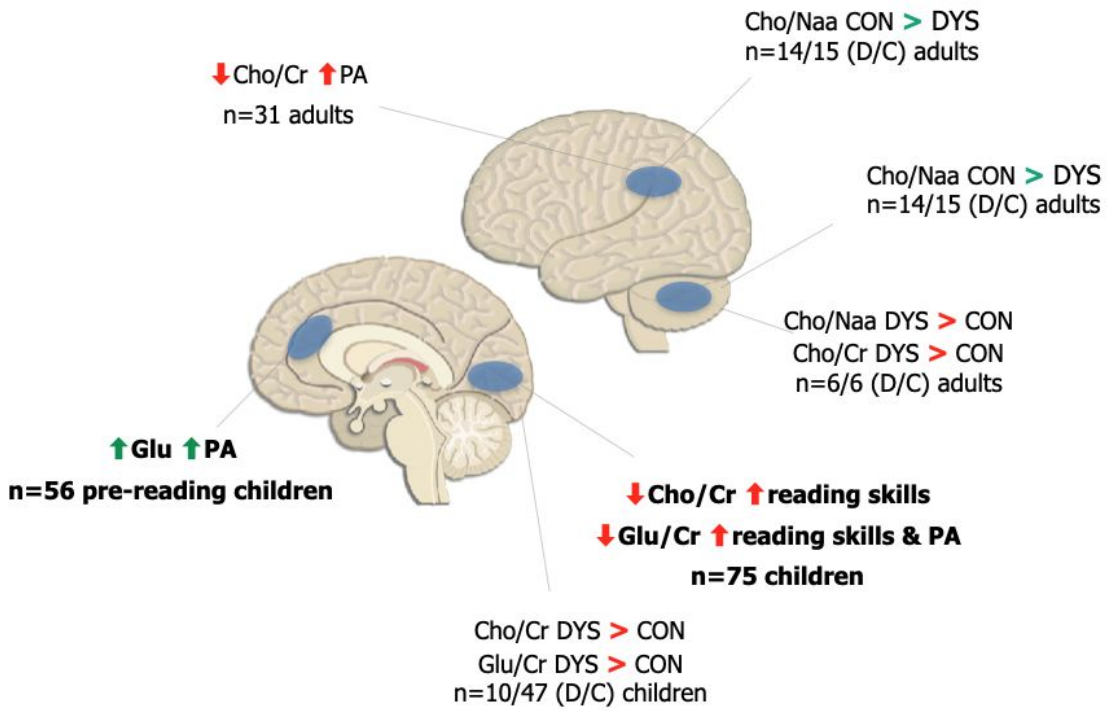

Figure 17. Neurometabolites in dyslexia - state of the art up to date of writing the thesis. Green colour indicates that higher metabolite level is associated with better performance or is characteristic to a control group compared to dyslexic subjects. Red colour represents negative correlation with performance or higher concentration in an experimental group.

Apart from the presented theories, still little is known about typical neurometabolite levels with respect to age and performance in reading related tasks. For example, neurochemistry may inform about underlying cytoarchitectonic differences between typical and dyslexic readers. White matter microstructure can be characterized by a fractional anisotropy (FA) of diffusion imaging. Significant differences between dyslexic and control

groups (both adults and children) were found in FA (Vandermosten et al., 2012), which could be accounted for decreased myelin content especially in the arcuate fasciculus and corpus callosum. At the level of neurometabolites, choline is considered to reflect active myelination (Blüml et al., 1999), membrane turnover (Hattingen et al., 2011) and glial cell density (Gupta et al., 2000). Increased choline is generally interpreted as reflecting either abnormal myelination or excessive cortical connectivity leading to longer communication route and transmission time (Laycock et al., 2008). Another metabolite, which also supports myelination is NAA (Singhal et al., 2017). Additionally, its concentration reflects neuronal density, function or viability (C. D. Rae, 2014). In summary, balanced levels of metabolites are crucial for the brain homeostasis. In regard to previous diffusion weighted, structural and functional imaging studies, spectroscopy can provide valuable insight. Finally, we aim to not only to test the neural noise hypothesis but also to investigate markers of tissue microstructure i.e. NAA and choline levels.

1.6 Neural noise hypothesis

Neural noise is an intrinsic characteristic of neuronal network related to random electrical fluctuations not associated with response to stimuli. Its main source arises from ions crossing cell membrane in a stochastic manner due to non-deliberate opening or closing of ion channels (channel noise) or migration through open or leaking channels (shot noise). Both of them may be generally linked to thermal fluctuation (Brownian motion) causing random movement and collisions of molecules. Another type of noise is related to the continuous and noisy synaptic activity. Stochastic exocytosis of vesicles with neurotransmitters may greatly influence that activity by modulation of ion-flow (excitatory or inhibitory). (Destexhe & Rudolph-Lilith, 2012). Also neighbouring neurons can generate false signals, which propagate within the network. In particular this type of noise is characteristic to cerebral cortex with very high cortical interconnectivity. Operationally, neural noise can be considered as stochastic variability in the neural response to repeated presentations of the same stimulus.

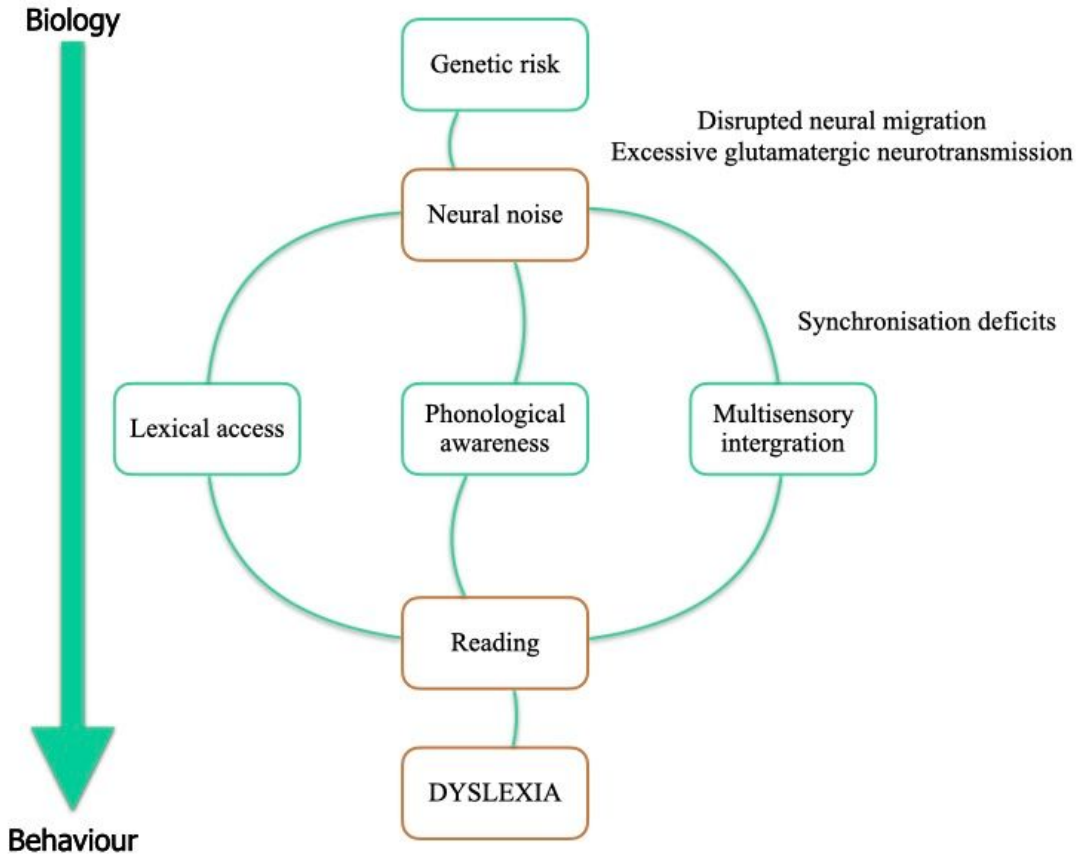

Figure 18. Overview of the neural noise hypothesis of developmental dyslexia (Hancock et al., 2017) based on the link between biological and behavioural observations. Genetic risk related to an overexpression of DCDC2 and KIAA0319 (Grigorenko, 2004) increases chances of an abnormal neural migration and postsynaptic excitability (Meng et al., 2005; Raschle et al., 2011; Wilcke et al., 2009). In consequence heightened neural noise, which can be confirmed by a synchronization deficits (Goswami et al. 2002; Lehongre et al. 2011), correlates with observed deficits in reading components (Fecenec 2008; Pennington et al. 1990) and the reading overall performance.

Enhanced neural noise has been recently proposed as a phenomenon which may play a main role in reading impairment (Hancock et al., 2017). The theory integrates behavioral symptoms specific to dyslexia such as deficits in phonological awareness and multisensory processing with neurobiological alterations such as disrupted oscillation in auditory processing task, functional and structural connectivity and related to it genetic risk (Figure 18). Finally, the authors suggest that neural noise may build a bridge between biology and behaviour in dyslexia.

Dyslexia has strong genetic dependance (Grigorenko, 2004) which can be observed in

overexpression of at least two genes - DCDC2 and KIAA0319. Both of them were correlated with abnormalities in cortical structure, function and reading related behavioural impairments (Meng et al., 2005; Raschle et al., 2011; Wilcke et al., 2009). Rodents homologs of these genes are associated with abnormal neural migration and glutamatergic signalling which greatly supports neural noise hypothesis in that matter. Mice with disrupted function of the homologous DCDC2 gene are characterized with increased glutamate as well as glutamate receptor genes (NMDA) (Che et al., 2014, 2016). DCDC2 is also linked to abnormal pyramidal neurons migration and KIA0319 to both pyramidal and GABAergic interneurons abnormalities. Although translation of these findings is difficult from microstructure abnormalities to reading, the presented neural noise hypothesis gives an opportunity to tackle dyslexia from a different point of view. If neural noise is manifested in excessive glutamatergic excitability or by balance between Glu and GABA, then we could apply research tools adequate to test the hypothesis based on the level of neurotransmitter concentrations.

2 ORIGINAL STUDIES

2.1 APPROACH

It has taken a few years of studies in order to prepare, run and complete a project regarding magnetic resonance spectroscopy in dyslexia. The following part will show how experimental methods have been evaluated to better understand, perform and interpret the measurements. Thanks to amazingly fortunate circumstances and fruitful collaborations with the researchers from Warsaw University of Technology, Mossakowski Centre, Nencki Institute and CNS Lab, it was possible to develop an effective approach for studying neurotransmitter concentration in pediatric population (APPLICATION).

New equipment, which has recently became available for research applications, enabled deep and innovative studies. Two whole-body 3T scanners for humans - GE Discovery and Siemens Trio and a 7T small animal scanner from Bruker were used to collect data for this thesis. Several methods were developed as an own input and implementation but other were introduced thanks to new, fruitful collaborations with producers. Especially the work-in-progress packages were transferred to these scanners and tested in an experimental environment. Application of a new methods presented here should be also considered as an

original input into the field. Lastly, there are several other projects, briefly referenced in the thesis, which could be realised thanks to the new contacts and gathered expertise.

2.1.1 Sequence programming and its phantom evaluation

2.1.1.1 Phantom design

Phantom is an object, whose MR signal resembles an original subject. In spectroscopy phantoms are containers which chemical composition is prepared to be similar to the brain, however, only the metabolites detected by proton spectroscopy are relevant. Some of the designs have also the possibility to measure localized signal dependent on the voxel position. Currently there are very few options on the market including the most popular GE Braino phantom and a few custom-made appliances (M. van der Graaf et al., 2008; Hunjan et al., 2003; Woo et al., 2009) (Figure 19).

Figure 19. Magnetic resonance spectroscopy quality phantoms - from the left: GE Spectro Braino, Woo et al., Graaf et.al (M. van der Graaf et al., 2008; Woo et al., 2009)

These phantoms have one common limitation, that there is only one specific volume of interest, which can be measured or as in case of the more sophisticated design - single smaller container within a bigger volume. Having that in mind, in a collaboration with Warsaw University of Technology, Mossakowski Centre and HIMTECH, we developed a new phantom which would have multiple containers with different mixtures but the same size. Such phantom could serve both for quality assessment as well as training with the possibility

to measure spectra of selected metabolites without their interference in a spectrum. The custom made phantom called PW-MRS consists of 16 cylinders inside a cylindrical container with individual valves to administer liquid to each volume (Figure 20). Phantom can be purchased as a ready to use product from the collaborating manufacturer.

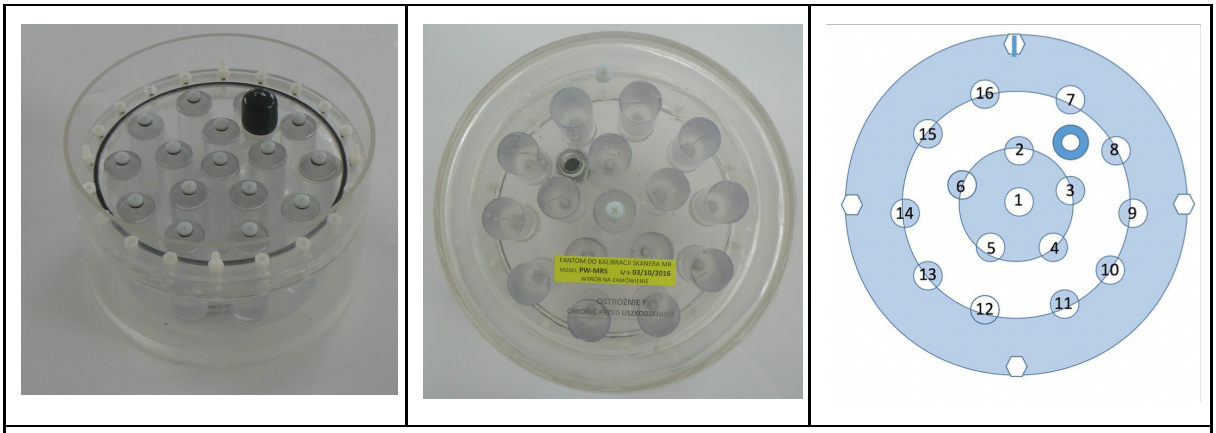

Figure 20. Phantom PW-MRS - overview and a schema with cylinders' numbering

List of mixtures inside respective cylinders:

1. 12.5 mM NAA; 12.5 mM Glu; 10 mM Cr; 7.5 mM mIns; 5.0 mM Lac; 3.0 mM Cho
2. 50 mM NAA
3. 5 mM NAA; 10 mM Cr
4. 25 mM NAA; 10mM Cr
5. 100 mM Glu
6. 100 mM Gln
7. 100 mM Lac
8. 200 mM Tau
9. 200 mM Glc (glucose)
10. 50 mM PCh
11. 50 mM PCr
12. 200 mM mIns
13. 100 mM Act (acetate)

14. 100 mM Ala (alanine)

15. 100 mM Cho

16. 50 mM Cr

Each of the containers (and the main cylinder) was filled with basis fluid consisting of K2HPO4 (72 mM), KH2PO4 (28 mM), TSP (1mM), sodium formate (20mM) solution in double deionized water and buffer (pH 7.0-7.2) (Hunjan et al., 2003).

Apart from the primary application in quality control, the phantom is very useful in training and testing of new sequences. The experiments presented further were done on a single cylinder containing desired mixture or with a use of the full-sized PW-MRS phantom.

2.1.1.2 MEGA-PRESS implementation

7T Bruker small animal scanner, located in the Small Animal Laboratory, Mossakowski Medical Research Centre, PAS, Warsaw was used to set up an experimental bench for MEGA-PRESS implementation. The sequence was programmed with a C language libraries available for ParaVision software.

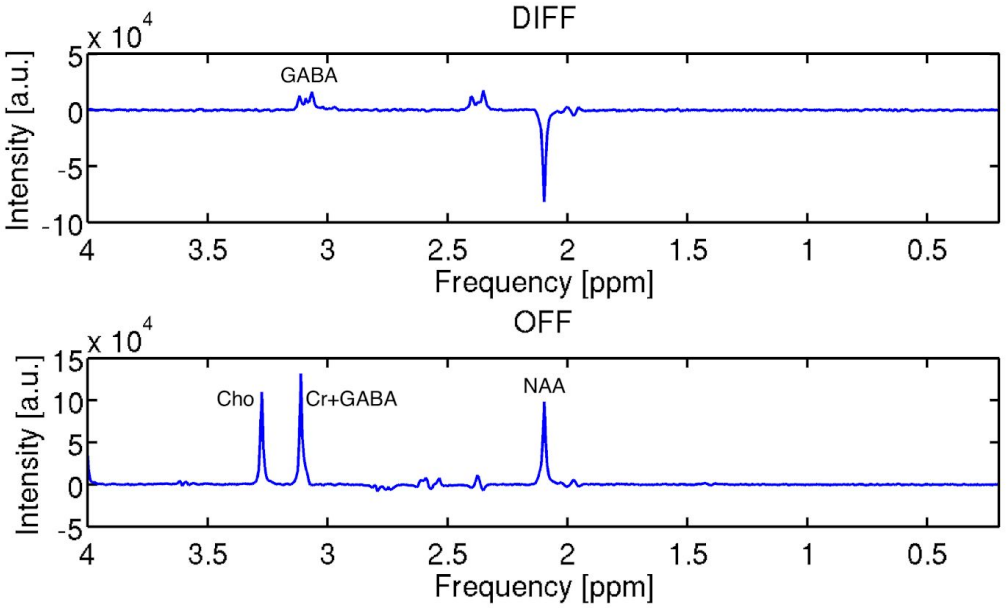

Figure 21. Data acquired on Bruker Biospec 7T (Mossakowski Medical Research Centre, Warsaw) with the use of brain metabolite phantom (NAA 12mM, Cr 10mM, Cho 3mM, GABA 8mM, Lac 5mM, sodium and buffer).

Original vendor PRESS code has been modified to include 2 spectral selective MEGA pulses and allow to modify basics parameters from the GUI of Paravision 5.1. Implementation tests were done on GABA phantoms. Exemplary acquisition was done with 5 brain metabolites' phantom (Figure 21). In-vivo experiment has been performed on rats as a trial in "New therapy in psychotic disorders and Huntington's disease with special focus on cognitive deficits" (NCBiR NoteSzHD) - accepted by local ethical committee. Following experimental modifications were performed:

The effect of non-symmetrical j-evolution

In this experiment, a spacing between MEGA pulses was varied with a fixed echo time to visualize the effect of a mismatch between them in the sequence. When the duration of evolution time before refocusing pulse (forward) is equal to evolution after refocusing pulse (backward) the spin operators presented in introduction simplify resulting in positive or negative phase accumulation. But when the timing is wrong, such in a case $\tau_1 \neq \tau_2$, resultant phase will not decrease to zero. Mathematical equations become more complicated due to multiplication of trigonometric terms. Hence, spectra simulation or phantom tests rather than theoretical equations can effectively visualize the results. Spacing between 2 MEGA pulses was varied from τ_2 = 15.11 ms (maximal mismatch) to 34 ms (correct, symmetrical evolution) with a fixed TE of 68 ms. J-evolution during τ_1 was adjusted to maintain echo position ($\tau_1+\tau_2$=68ms). If the delays are not equal editing efficiency decreases by 41% at 15.11 ms (Figure 22). However, just 16% drop is observed in a range up to 10 ms difference (τ_2 = 29 to 34 ms), which could give an opportunity of sequence optimization even if the condition is not satisfied.

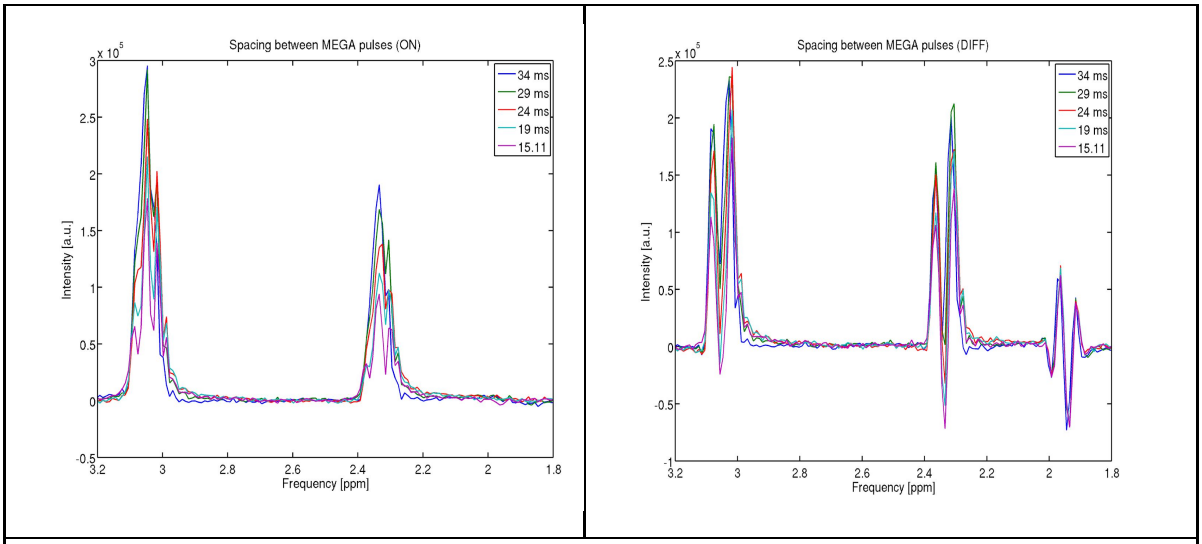

Figure 22. The effect of non-balanced J-evolution. Left - edited spectra with variable efficiency due to non-symmetrical spin evolution (edit ON). Right - edit on and off spectra difference (DIFF). Coupled methylene pair is visible at 1.9 and 3 ppm.

MEGA pulse bandwidth

Pulse bandwidth is an important feature of frequency selective RF pulses. In edited spectroscopy it defines range of a directly affected frequency band. Bandwidth of the pulse is inversely related to the pulse length which has been varied from 25 ms (narrow bandwidth, maximum available width) to 10 ms (broad bandwidth). All pulses have similar effect on edition at 3 ppm methylene group (Figure 23). But, curiously, the shortest pulse introduced undesired attenuation at 2.3 ppm due to its broad frequency spectrum. Nevertheless, pulse bandwidth has little effect on GABA peak at 3 ppms, which opens the possibility to apply broader pulses to affect multiple peaks in more complex editing schemes such as HERMES for GABA, GSH and ethanol simultaneously (Saleh et al., 2016).

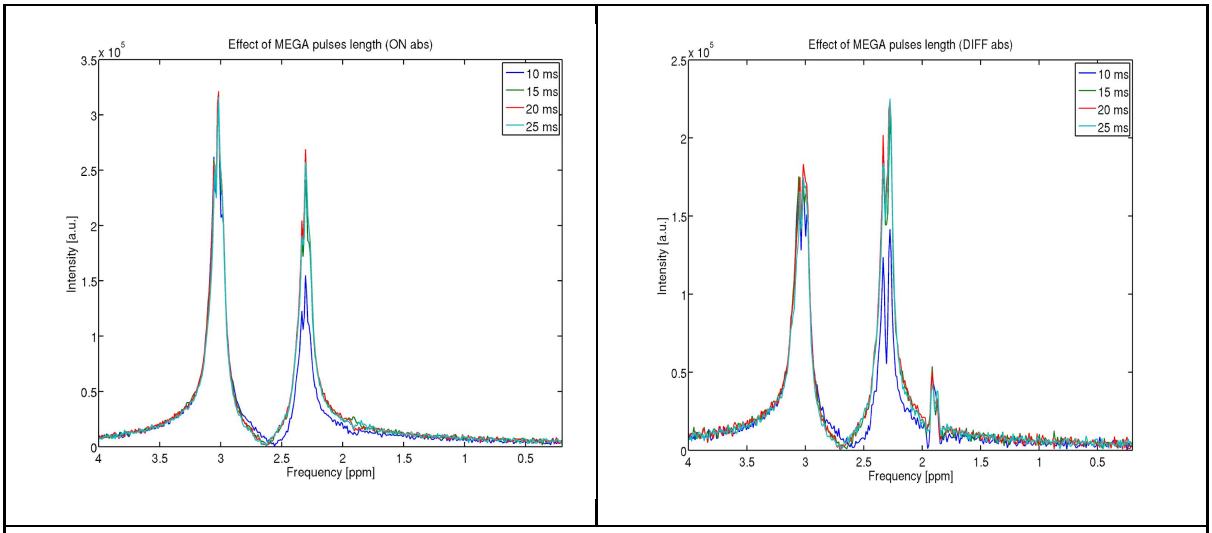

Figure 23. Pulse length adjustment in a range from 10 to 25 ms. On the left side an edited spectrum is presented with a frequency selective pulse operating at frequency of 1.9 ppm. On the right side differential spectrum shows the MEGA-PRESS efficiency (3.1 ppm) as well as an interference with a neighbouring peak at 2.3 ppm.

In-vivo validation

To fully prove correct implementation of the new method the in-vivo test was performed on 3 anesthetized rats. Optimal MEGA pulse length of 15 ms has been chosen as the minimal with no co-editing effects at 2.3 ppm. On one hand, the pulse of the minimal length (10 ms) gives the greatest flexibility in sequence design i.e. length and magnitude of gradient crushers. On the other hand, such a pulse is more prone to frequency mismatch between the pulse and GABA peak, which may occur due to frequency drift during prolonged acquisition. Optimal pulse spacing of 34 ms is based on the J-coupling constants' rates and does not have to be readjusted in the current implementation.

Scans have been performed with the following parameters:

- TR=3000 ms, TE=68 ms
- NA=256x2
- MEGA pulse length = 15 ms
- MEGA pulse spacing = 34 ms
- voxel size 4x4x4 mm

All the scans were successfully acquired and analyzed in Gannet Toolbox (Edden et al.,

2014) (Figure 24). Data import function was rewritten in order to run the analyses on Bruker FID files (*Interface to load Bruker MRS into Gannet toolbox*. Kossowski B.). In-vivo concentration in 3 rats relative to water was estimated respectively - 3.68, 3.02, 2.72 mM, which is reasonable compared to GABA concentration measured in human studies - 2.1 mM (Kossowski et al., 2019).

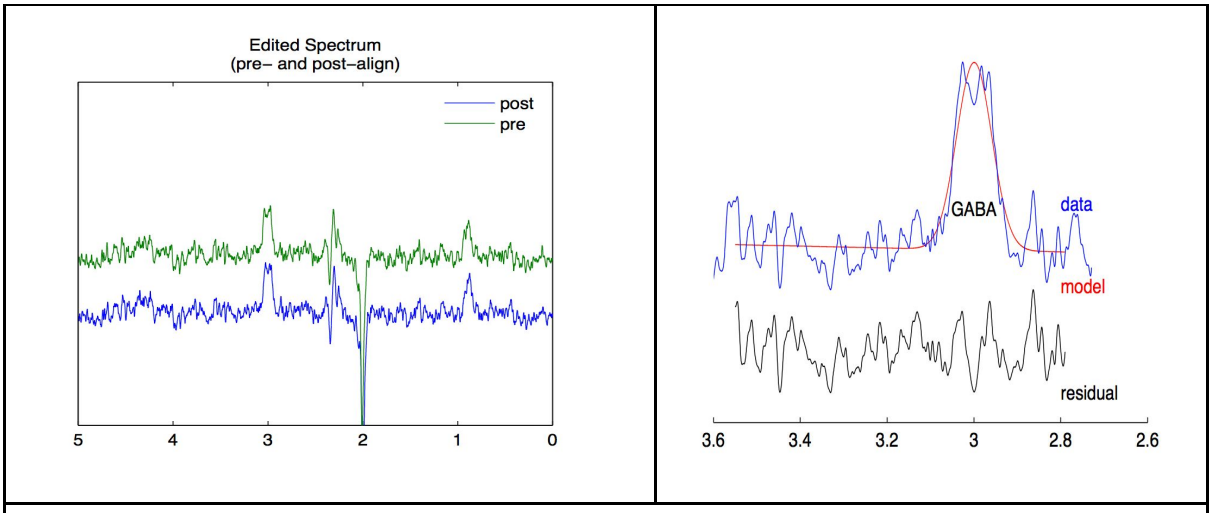

Figure 24. MEGA-PRESS analysis of in-house sequence in-vivo scan performed in Gannet Toolbox. Frequency drift correction on the left visualizes pre- and post- processed average differential spectrum. On the right GABA peak fitting with the defined gaussian model is presented.

Not only the sequence has been implemented and prepared to be used in a research project at Mossakowski Centre but, what is also the most important for the thesis, MEGA-PRESS parameters has been thoroughly studied with all the respective consequences.

2.1.2 Spectroscopy on clinical scanner

Single voxel spectroscopy as well as spectroscopic imaging (multiple voxels spectroscopy) are available on the most clinical scanners but were implemented to address specifically some clinical applications. In case of the single voxel spectroscopy there are PRESS (double-refocused echo) and STEAM (stimulated echo) available in standard (Philips, GE and Siemens). The predefined protocols enable quick, automated acquisition with some basic visualization of the results, however, a lot of optimization is needed in order to improve the results.

GE and Siemens also offer MEGA-PRESS sequence as a work-in-progress package for their products to target editable metabolites such as GABA and lactate. The code is based on a standard, FDA-approved PRESS single-voxel spectroscopy, however, the use of MEGA

pulses has not been yet introduced into a clinical practice. Siemens package named WIP-529 is available on various platforms including VB17 (3T Magnetom Trio, Nencki Institute) and enables use of MEGA-PRESS with limited flexibility. Advanced MR Spectroscopy Package for GE scanners (3T Discovery 750w, CNS Lab) gives the opportunity not only to use MEGA-PRESS but also to modify other features of standard PRESS sequence including pulse shape, 2D spectroscopy (JPRESS), spectral suppression and asymmetric echo.

Calibration with MRS phantom

Calibration procedure based on the MRS phantom acquisition enables absolute metabolite quantification. Phantom design has been optimized to the use in human horizontal-bore scanners and tested on two 3T scanners - Siemens Magnetom Trio and GE MR Discovery 750w. Quality assessment is based on an acquisition of a selected spectrum from the phantom, analysis and comparison between the previous spectrum or respective spectra presented in the manual. Number of quality measures can be derived based on measured MR signal such as signal to noise ratio, peak width and separation, peak position, metabolite concentration etc. Also the image quality control can be performed based on geometrical properties of the cylinders and their relative positions.

Table 2. Recommended acquisition parameters for phantom based calibration and quality control

TR	3000 ms
TE	30 ms
Number of averages - water suppressed (WS)	96
Number of averages - water unsuppressed (WS OFF)	4
Dummy scans	4
Water suppression bandwidth	50 Hz
Bandwidth & number of samples	1200 Hz / 2048 samples
Center frequency	-2,3 ppm relative to water
Acquisition time	~ 5 min WS + 20 s WS OFF

Calibrated PRESS single-voxel spectroscopy consist of a phantom acquisition with the optimized parameter set (Table 2) followed by an in-vivo scan. Phantom metabolite quantification was performed in TARQUIN with an adapted settings (temperature shift, water content). Exemplary calibrated measurement for the central cylinder results in <10% agreement for NAA, Glu, Cr concentrations (Figure 25) comparing to referenced values.

Further protocol optimisation can be done in a reference to the calibration measurement. Consequently GE and Siemens MEGA-PRESS protocols have been evaluated and the parameters of a reference were chosen accordingly: TR=2000 ms, TE=68 ms, Number of averages; 192 (water suppressed) + 4 (non-suppressed), 4 dummy scans, 50 Hz water suppression bandwidth, bandwidth 1200 Hz, editing frequency = 1.7 ppm (in-vitro).

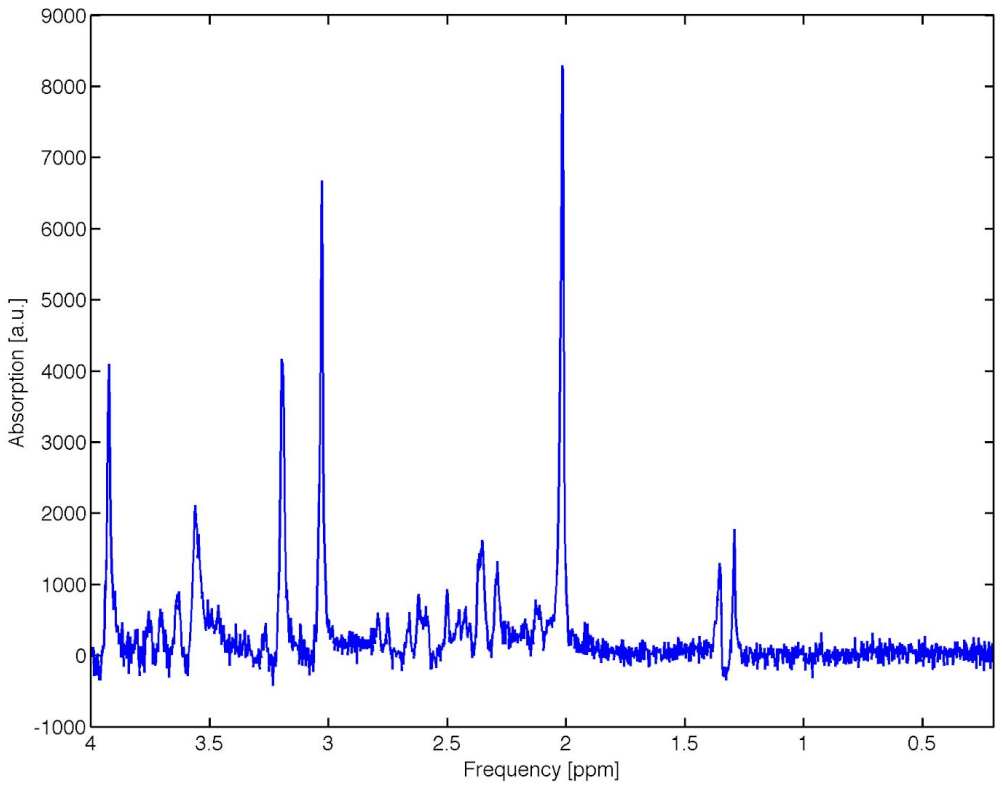

NAA 12,5 mM + Glu 12,5 mM + Cr 10 mM+ mIns 7,5 mM + Lac 5mM + Cho 3mM			
No 1	CONC 11,5; 13,4; 10,2; 8,79; 3,95; 2,45	WNR 31956	FWHM 1,6 Hz

Figure 25. Calibration spectrum obtained with PW-MRS phantom from 1st cylinder. Referenced values and results of analysis performed according to phantom's manual are shown in a table - concentration in mM (CONC), water peak to noise ratio (WNR), water peak width at half of maximum (FWHM).

B0 field calibration

Shimming is a term related to adjustment of homogeneity in local static magnetic field B0. According to Larmor equation, the signal frequency is strictly dependant on magnetic induction so as its spatial distribution. Thus, local variability in magnetic field causes broadening of spectroscopy peaks, which can be clearly visualized in the following example. PW-MRS phantom was used to test shimming procedure on Siemens Magnetom Trio, which

can be automatic and/or manual. Automatic procedure is based on an acquisition of B0 field map and optimization procedure, which can either calculate corrections needed for global or local field harmonization. In case of spectroscopy coarse global shimming followed by local shimming is used as a standard. However, we noticed that optimization algorithm often calculates corrections factors (shimming coils current) out of physically available range resulting in a truncated, incorrect setting. Repetition of the global shimming procedure may help but it takes a lot of time as the previous settings need to be manually reset to default ones. Surprisingly, manual shimming in case of local linear shimming (X, Y, Z) within a voxel, which is done by changing coil currents during continuous observation of changes in the shape of water peak, outperforms the automatic procedure and quickly improves the lineshape (Figure 26). However, to initiate an adequate starting point it is beneficial to run the automatic shimming first. Such a procedure consisting of automatic followed by manual shimming was introduced for use in Laboratory of Brain Imaging and applied in presented studies.

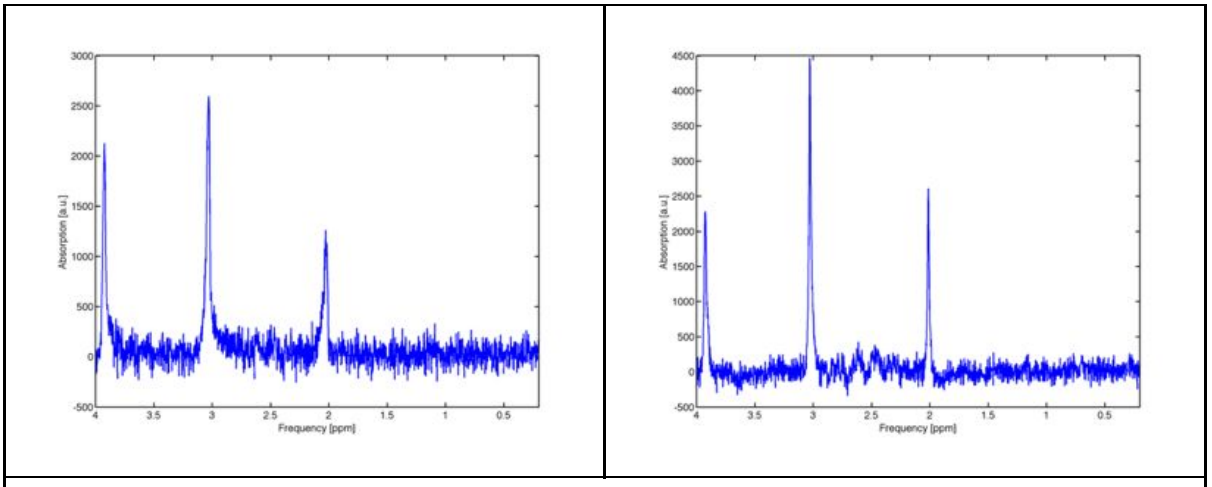

Figure 26. Shimming in a voxel placed within container no 3. Left - automatic procedure, right - automatic procedure followed by manual adjustment. Linewidth and SNR improvement is dramatical and visible despite automatic scaling of y-axis.

J-evolution artifacts

If only one specific frequency is being consider, the voxel position is precisely determined. Signals of different frequencies, however, would have different positions spreaded in space according to their chemical shift. Consequently, distant peaks would be observable from different, spatially shifted voxels. That effect would break assumptions for

single, homogenous voxel i.e. when different paths of j-evolution take place within a voxel (section 1.4.2). The effect has been observed since high-field scanners become available, because the chemical shifts and voxel displacement consequently scale up with B0. With an employment of relevant simulation, it is possible to predict the shape of the selected spectra and hypothetically apply post-processing correction to the results, however it is the most often neglected (Figure 28) (Lange et al., 2006).

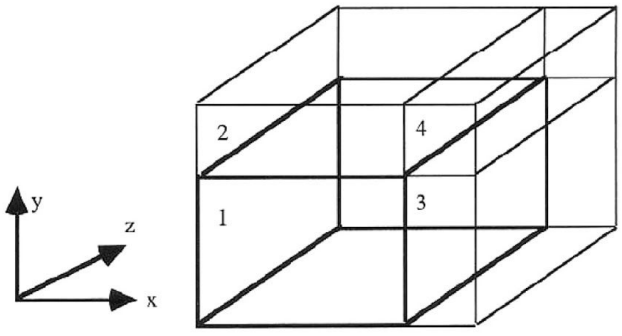

$$V_1 = \left(1 - \frac{\Delta\omega_{CS}}{\Delta\omega_{RF}}\right)^2 \cdot V$$

$$V_2 = V_3 = \frac{\Delta\omega_{CS}}{\Delta\omega_{RF}} \cdot \left(1 - \frac{\Delta\omega_{CS}}{\Delta\omega_{RF}}\right) \cdot V$$

$$V_4 = \left(\frac{\Delta\omega_{CS}}{\Delta\omega_{RF}}\right)^2 \cdot V$$

Region	1st 180°	2nd 180°	Observable Magnetization
1	non-selective	non-selective	$S_1 \sim V_1 \cdot \cos(\pi \cdot J \cdot TE)$
2	non-selective	selective	$S_2 \sim V_2 \cdot \cos(\pi \cdot J \cdot 2t_1)$
3	selective	non-selective	$S_3 \sim V_3 \cdot \cos(\pi \cdot J \cdot (TE - 2t_1))$
4	selective	selective	$S_4 \sim V_4$

Figure 27. Illustration of 4 different pools within a voxel. Selective/non-selective feature refers to spectral characteristic of 2 refocusing pulses. Ideally both refocusing pulses are non-selective with a regard to 2 spin-system such as lactate, which enables j-evolution. Other non-ideal cases describes j-evolution due to selective refocusing of one or both spin groups. Source: (Lange et al., 2006)

Practical visualization can be made for J-evolution of lactate, which is an example of two-spin coupling with J=6.9Hz (2/J=288ms) resonating at 1.3 and 3.6 ppms (3rd group at 4.25 ppm). From the introduction we know that such a system is subjected to j-evolution with an inversion at 144 ms only when the same conditions are fulfilled for the both spins. However, it has been shown (Figure 28), that the assumption is broken due to inevitable voxel displacement. Thus some parts of voxel would give an expected inverted signal, but the mismatched volume will contribute to other evolution paths i.e. with the opposite sign of the signal. The effect is so complicated that only spectro-spatial simulation or empirical

measurements may help. Such measurement can be done with the use of PW-MRS phantom, where only lactate is observable in cylinder no 7. With an increase of echo time, we would expect a decrease of signal due to T2 relaxation. However, the signal at 144 ms, which should be inverted within the whole voxel is much weaker than at 288 ms. It is now clear that some parts of the voxel give rise to inverted (negative), but mismatched volume to non-inverted positive and they cancel each other out (Figure 29). If one wants to minimize this artifact and estimate more reasonable lactate concentration longer inversion time is recommended as well as the use of high-bandwidth refocusing pulses.

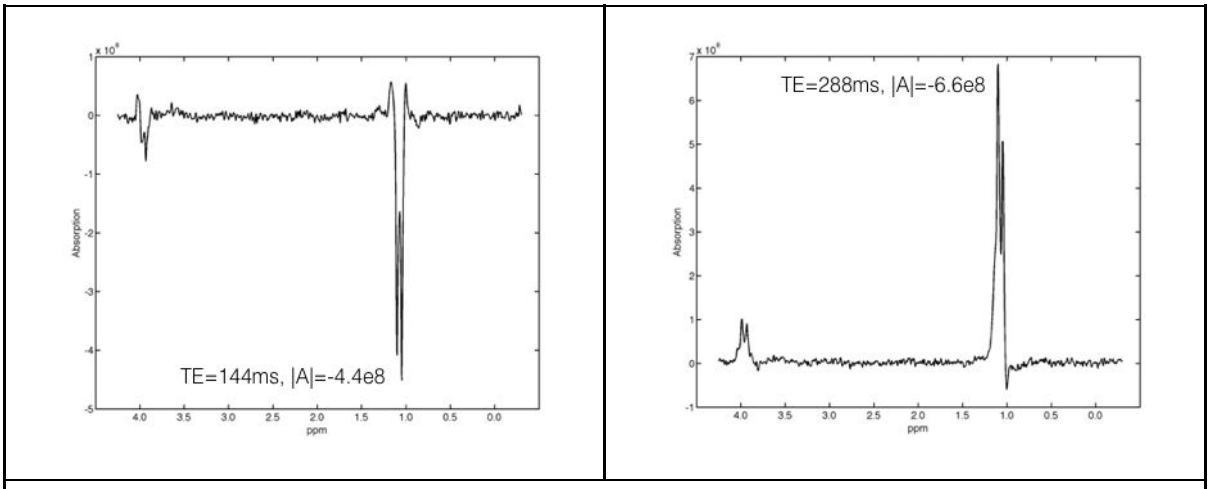

Figure 29. Lactate signal measured with conventional PRESS at 3T. Left - inversion at 144 ms and right - evolution refocusing at 288 ms. Signal magnitude ratio is 4:6 respectively, which is unintuitive result of chemical shift voxel displacement.

Importantly, one should keep in mind that j-evolution artifact will be presented in case of GABA edited spectroscopy. Refocusing pulse bandwidth can be increased to the highest available value depending on the gradient performance or ideally adiabatic pulses should be used (much better performance and minimal hardware demand).

Integration of imaging modalities into MR spectroscopy

Single voxel spectroscopy refers to data acquired in some specific region of interest. That region should always be deliberately defined using any kind of imaging data we can acquire along the experiment eg. FLAIR or T2w for lesions and T1w for gyrus/sulcus localization. After the experiment, the radiologist would expect to receive spectroscopy data (preferably preprocessed by physicists) and at least 3 orthogonal images reconstructed in

parallel planes for voxel orientation. Both clinical scanners used here enable acquisition of parallel planes or reconstruction based on other 3D acquisition. However, only graphical visualization of a voxel is available, which is not numerically accessible and cannot be used for further analysis.

Research applications (and clinical application in the future) would require 3-dimensional representation of a voxel in image space, which could be easily accessible and used for visualization and data processing. The later is critically important, when water signal referencing is performed, because water concentration differs significantly between CSF, WM and GM. Even though, there is a kind of recipe, which can be used to extract voxel position and orientation from RAW data (Quadrelli et al., 2016) (at least for Siemens), there had been no such a tool, which could automatically convert spectroscopy data to a voxel mask (an image) to be overlaid onto an anatomical scan before.

RDA2NIFTI is our in-house MATLAB script, which enables voxel visualization on a reference image (Figure 30). To my knowledge it is the first tool available online which works reliably well with RDA Siemens spectroscopy files converting them to reusable NIFTI mask. Some efforts have been done by GANNET developers in that matter, but its functionality is prone to some unexpected errors and it needs to be run along with the whole GABA preprocessing. Hence, the code has been developed for the purpose of the current and future investigations as an alternative to erroneous GANNET functionality and shared with GANNET developers to improve that feature. RDA2NIFTI is publicly available in the NITRC repository (rda2nifti - Siemens spectroscopy to voxel mask converter, Kossowski B.).

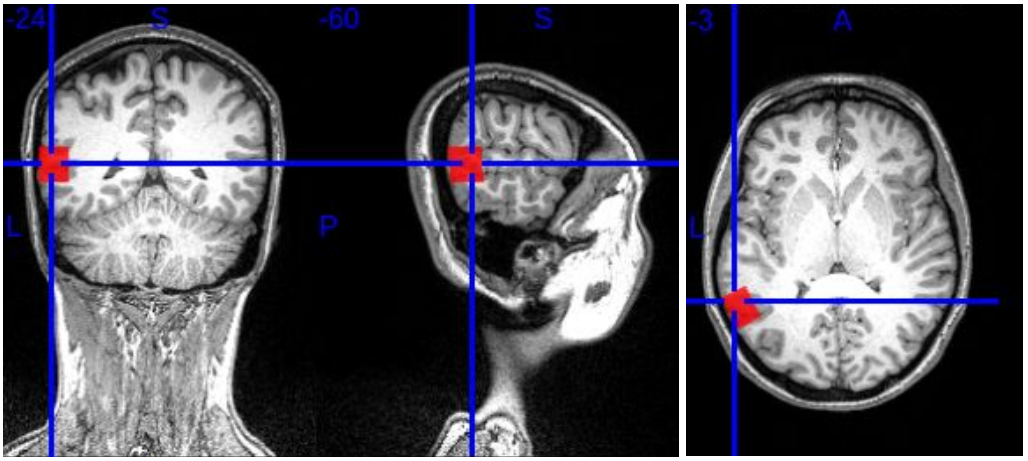

Figure 30. Voxel mask created from Siemens spectroscopy file (RDA) and overlaid on an anatomical image with a use of the in-house script (rda2nifti - Siemens spectroscopy to voxel mask converter, Kossowski B.)

For GE scanners, there is a research package called Advanced Spectroscopy (AMRSP) and semiLaser released with a piece of MATLAB code, which can similarly reproduce a voxel mask based on RAW spectroscopy and image data (Figure 31). However, in contrast to our Siemens implementation it has to rely on overcomplicated voxel position defined in a reference to an anatomical image. Algorithm needs to solve the inverse problem whether the given voxel in an anatomical, high resolution image belongs to a spectroscopic voxel definition. It can take several minutes depending on the image resolution in contrast seconds in case of rda2nifti, which does not require excessive computations.

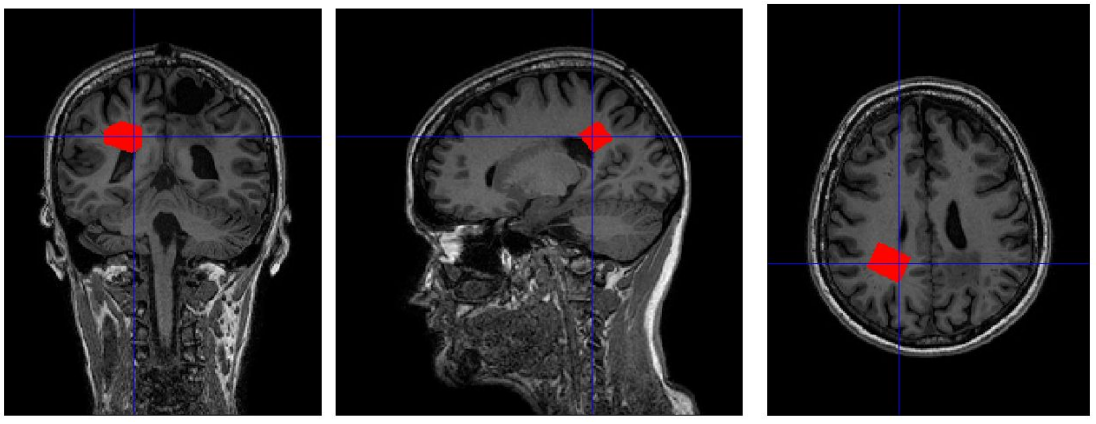

Figure 31. Voxel mask created from GE spectroscopy file (PFile) and overlaid on an anatomical image with a use of a MATLAB script by R. Noeske (GE)

Preprocessing pipeline

DICOM standard provides recommendations to store both original and already analyzed MRS data in a common way. However, producers give a limited access to raw data due to the low pressure from regular customers on that matter. Producers developed the specific data formats in order to exchange information between their own software, which can be reused in more advanced applications. On GE scanners all the respective measurements are saved within one so called Pfile. However, the content of the file depends on the sequence implementation and scanner's software version. On Siemens spectroscopic data is stored in 2 raw data formats. Siemens RDA files consist of the data already accumulated across different coil receivers and averages (single time domain vector). TWIX files, which are more general to all types of acquisition (similarly to GE pfiles) consist of all the data registered during the acquisition (averages, channels etc.). Due to complicated acquisition schemes used for GABA it is necessary to access low level unprocessed data for an extended preprocessing of MEGA-PRESS. Standard GABA preprocessing pipeline consist of: (1) coil channel combine and phase correction, (2) frequency drift correction, (3) calculation of differential spectrum, (4) peak fitting. Finally, all the results can be corrected in respect to CSF, GM and WM ratios (5) (Harris et al., 2015).

Due to the growing interest of advanced spectroscopic methods there is more and more software available including LCModel, TARQUIN and jMRUI, which are the most popular. Especially designed software for MEGA-PRESS preprocessing is Gannet MATLAB toolbox. There are also a few packages, which provides routines needed to read and preprocess edited spectroscopy such as FID-A, OpenMrsLab. Here we decided to use Gannet, which provides a complete, easy to adapt pipeline for GABA measurement and LCModel as a gold standard in non-edited spectral fitting.

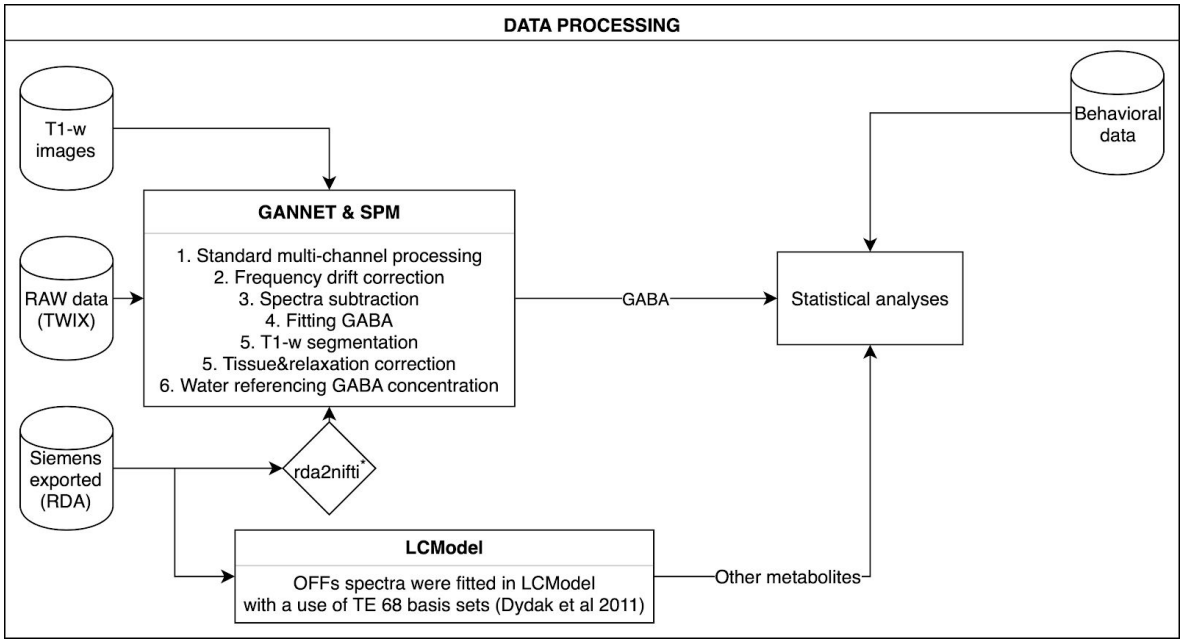

Figure 32. Data preprocessing diagram for Siemens RDA and TWIX spectroscopy data formats accompanied by reference images

Thus, as it is depicted in Figure 32, data preprocessing involved 3 types of data - structural (T1w), accumulated spectroscopy (RDA), raw spectroscopy (TWIX). Preprocessing pipeline has been developed and evaluated on the phantom data. Applied modification involved: custom voxel mask conversion (rda2nifti) and LCModel reference water concentration tissue adjustment. GABA estimates with all applied correction are presented in a visual report from Gannet analysis (Figure 33).

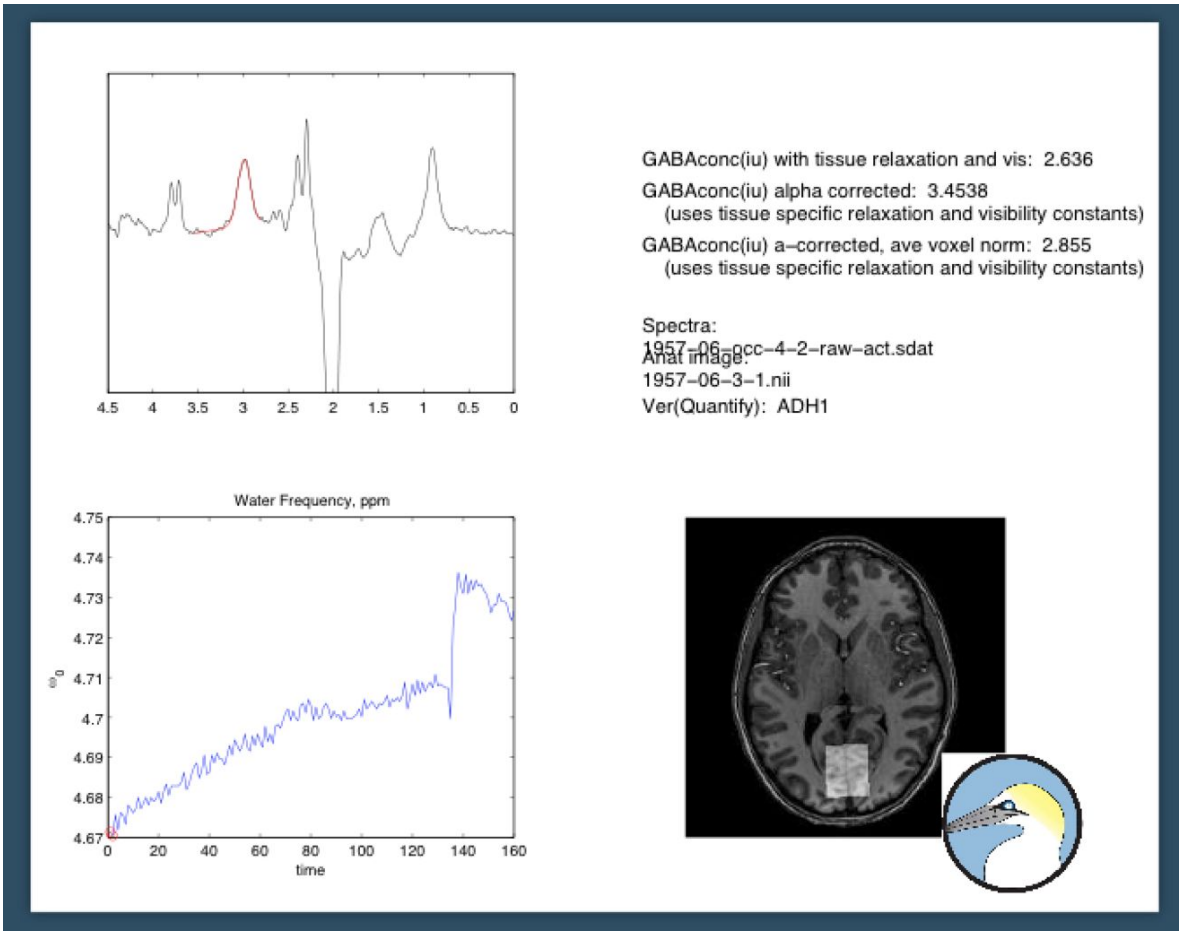

Figure 33. GABA estimation report generated by Gannet shows differential spectrum (top-left corner), estimates (top-right), frequency drift (bottom-left) and voxel position (bottom-right) (Edden et al., 2014)

2.1.3 Reproducibility and power analysis

Reproducibility tells us about the reliability of measurement based on data from a representative sample. Variance and mean estimates are needed to perform power analysis to reveal sample size of experimental groups needed to detect a change of a hypothesized size. Repeatability, however, which is based on test-retest data of the same participant would tell more about the precision of the instruments. It is very useful in new methods' assessment such as in case of semiLaser but does not inform us how to prepare to an application project. Both standard and edited spectroscopy are highly repeatable when a well-defined measurement protocol is used (<5%). Consequently, between subjects variance or

physiological variance need to be considered as major confounds. In order to estimate variability related to those factors the data from a cohort of 68 healthy, 21-45 y/o (35 females, 33 males, M age in years = 27.5) participants was analysed.

All participants underwent structural imaging and localized spectroscopy on a 3T GE Discovery 750w with 70cm wide bore, using a body transmit coil for excitation and an eight-channel receive coil. The structural scan was performed for voxel placement using Spoiled Gradient Recalled Acquisition in Steady State (SPGR) with the following parameters: TR/TI/TE = 6.576/400/2.1 ms, 1×1×1 mm3, duration 7 min 3 sec. Spectroscopic data were acquired with MEGA-PRESS single voxel sequence (TR/TE = 1800/68ms bandwidth = 2367 Hz, 128 acquisitions, duration 7 min 40 sec), with chemical shift selective (CHESS) water suppression. Volume of interest (20×20×20 mm3) was placed in precentral gyrus gray matter. Unsuppressed water signals were acquired for each location for eddy current compensation and phase correction. 4096 complex points were acquired on each spectrum.

Spectra were analyzed in Gannet MATLAB Toolbox (Edden et al., 2014) with a standard preprocessing pipeline, which includes water filtering, phasing, frequency drift correction and fitting. The software estimates NAA, Cr and GABA peaks as well as non-suppressed water reference signal. Four subjects were not correctly loaded due to corrupted data. Average spectra from the remaining participants (Figure 34) confirm good spectra quality as well as excellent performance of automatic preprocessing and a frequency alignment.

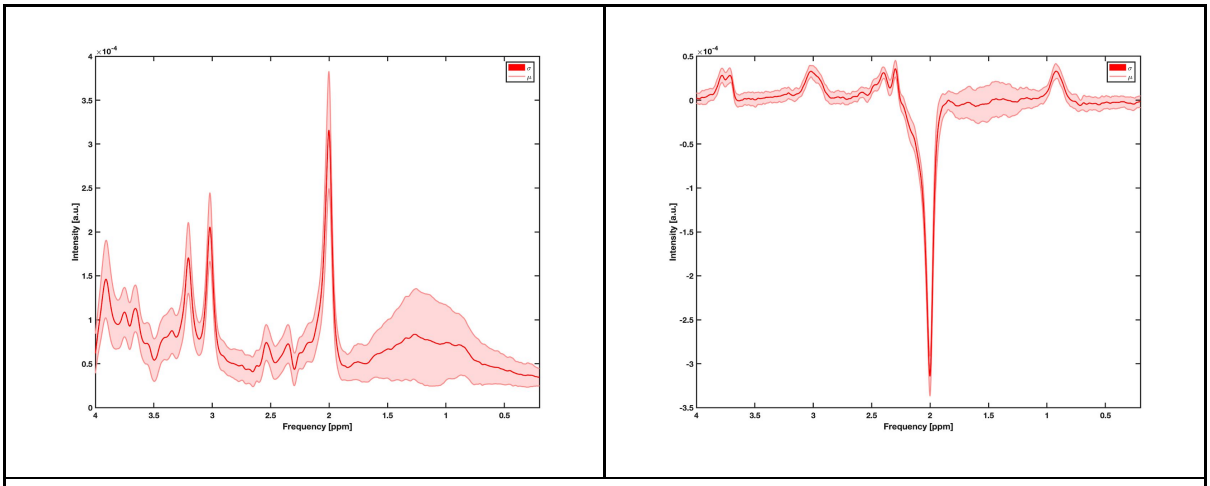

Figure 34. Averaged spectrum from a cohort of 64 healthy, adult subjects. Shaded margins show a standard deviation range. A picture on the left shows average non-edited spectrum, whereas right picture difference between non-edited and GABA edited spectra.

Additionally, summary quality measures are listed in the Table 3. Both FWHM, which estimates field homogeneity within a voxel as well as SNR measures prove reliable, above average quality of the dataset. Mean SNR of the GABA peak is above 6, which is sufficient for fitting algorithm to converge, however the value is rather low comparing to currently available datasets (Mikkelsen et al., 2017). Creatine peak has 9 Hz width at the half of maximum, however there are unexpected outliers on both sides resulting in <5 and >20 Hz shimming, which should be additionally inspected.

Table 3. Quality measures estimated with the results of Gannet preprocessing.

	Cr FWHM [Hz]	**GABA SNR [ratio]**
Valid	64	64
Mean	9.263	6.333
Std. Deviation	2.942	2.463
Minimum	1.916	1.673
Maximum	28.355	16.729

Finally, the collected data gives an opportunity to estimate a mean GABA concentration and a respective group variance. Further, different methods of GABA referencing - Cr and water peak ratios can be tested to find the most reproducible results. Descriptive statistics shown in Table 4 will be used to calculate minimum sample size in order to detect 10% difference of GABA estimate between experimental groups.

Table 4. Descriptive statistics of GABA and NAA estimates based on Gannet results

	GABA/water [a.u.]	GABA/Cr [ratio]
Valid	64	64
Mean	3.423	0.110
Std. Deviation	0.990	0.031
Minimum	1.230	0.044
Maximum	5.774	0.196

Above descriptive statistics based on a representative sample of 64 individual spectra give an opportunity to perform power analysis. Power of a statistical tests reveals the probability of detecting a significant difference between the groups (rejecting the null hypothesis). With a reasonable p threshold of 0.05 and power of 0.8 (80% chances) following calculations have been performed for 10% concentration difference from the average:

Table 5. Power analysis for a 10% difference from an average GABA concentration based on 64 healthy subjects

	GABA/water [a.u.]	GABA/Cr [ratio]
sig. level	0.05	0.05
power	0.8	0.8
group difference	0.34	0.01
min size of each group	**133**	**125**

In summary, power analysis is a very useful in a process of project preparation, which informs us about reproducibility of our results in a wider context. On one hand, GABA variability in a given sample is much too high to expect conclusive results with classical hypothesis testing. On the other hand, the acquisition protocol and preprocessing pipeline used here have not been fully optimised yet. There are a few points that should be improved in the target project, which may greatly reduce the between subject variance:

1. Tissue type correction for absolute GABA concentration based on segmented anatomical images.
2. SNR increase with longer TR, more averages.
3. Improved coil sensitivity in cortical regions with a use of multiple chanel coil.
4. Reduced motion which would help in data preprocessing.

We have taken those observations into account during protocol setup for a study concerning developmental dyslexia. The 8-channel birdcage coil used for the power analyses was replaced by 32-channel coil with much higher signal to noise ratio in the regions of interest (factor>2). TR and number of averages were increased to summarical amplify SNR by a factor of 1.3 (marginal effect of TR change with an assumed T1=1200ms). Eventually, the voxel volume from 8 cm^3 was increased to 13.5 cm^3 with an expected linear gain in SNR respectively (factor ~1.7). In a studied sample we expected to reduce the standard deviation minimally by a factor of 3 (from 0.99 to 0.33 i.u.). The sample size needed to detect 10% effect with the reduced standard deviation is 16 in each of the groups. It is worth to mention that GABA due to specific acquisition has the highest variance among other metabolites of interest such as NAA, Cho, Glu.

2.1.4 Conclusion

I have performed hundreds of measurements and simulations to better understand, test and apply MR spectroscopy. Three different devices have been used including two 3T human scanners and 7T small animal scanner. All of the appliances were placed in research sites of Polish Academy of Sciences in Warsaw, which enabled establishing a collaboration between institutes. Thanks to GE and Siemens collaboration the work-in-progress packages of semiLASER and MEGA-PRESS could be installed and evaluated. Additionally, I independently programmed these advanced features at 7T Bruker scanner. All of that helped me to better understand, what obstacles we can face during application of our methods.

Finally, we have decided to use 3T Siemens scanner available at the Nencki Institute, which was justified by the performance of the device. With regard to Master Research Agreement signed by Siemens and the director of Nencki Institute, we could apply MEGA-PRESS (WIP-529) as a method to measure single voxel spectroscopy of commonly observable metabolites and GABA. The method was not only innovative but also enabled us

to compare the results with the state-of-the-art research in dyslexia. We also identified the problems, which previously prevented making a correct estimation of metabolite concentration (voxel mask, preprocessing pipeline) without internal referencing to Cr or NAA. Finally, additional software - LCModel, GANNET and in-house scripts (rda2nifti) have been evaluated and applied.

2.2 APPLICATION

2.2.1 Research question

The main objective of the project is to determine whether the concentration of metabolites can serve as a biomarker of a developmental dyslexia. According to the previous studies choline, glutamate and GABA are the candidates compounds of brain metabolism, which are hypothetically responsible for abnormal neural synchronization in reading disorder. Those metabolites may serve as neurotransmitters in human brain, however the impaired tissue cytoarchitecture is also being considered by a levels of choline and NAA.

Until now, only few studies have examined neurometabolites concentration in the context of dyslexia (Bruno et al., 2013; Laycock et al., 2008; Lebel et al., 2016; Pugh et al., 2014; C. Rae et al., 1998), while their findings show hardly any consistency. There are several factors which might have influenced this inconsistency. First, subjects at a very different age were previously studied such as adults, pre-reading children and school-age children. Second, various brain regions were targeted (left temporo-parietal, occipital, anterior cingulate cortices and cerebellum) Third, despite the fact that the acquisition of a single-voxel MRS has a limited number of parameters (TE, TR etc.), the analyses could have been performed in a many ways. Specifically, if internal signal reference is not available e.g. additional water signal measurement, some researchers calculated metabolite ratios (Glu/Cr, Cho/Cr, Cho/NAA, NAA/Cr etc.) with an assumption that the denominator remains stable across the participants. This is particularly problematic in case of exploratory research such as dyslexia especially when age of the participants is one of the confounding factors.

To address and solve discrepancies between the previous studies we decided to acquire representative samples in both adult and children samples. Due to presumably different creatine levels between the two age groups and to minimize variance in respect to tissue type

we took an effort to calculate and compare absolute metabolite concentrations. A specifically designed and pre-tested pipeline incorporates information from both spectroscopy and images. As a reference we used locally measured water signal with an additional short MRS sequence and corrected for water tissue variations. Finally, we compared different reference scaling methods and suggest directions for future research.

In our study we implemented the state of the art statistical modelling in order to minimize the influence of nuisance factors such as age and voxel composition. We present results in a clear way with limited interpretation when multiple comparisons corrected threshold has not been met. Until now, there have been only one other study (Lebel et al., 2016) regarding dyslexia, where a similar pipeline has been used. Despite previous literature on age-related changes (Blüml et al., 2013), some researchers reported metabolite ratios, which could lead to potential confusion in the field. Particularly, when differences in metabolite concentrations have opposite directions between the studies, such as choline/creatine and choline/NAA ratios, we could ask whether there is one or two factors playing roles together. To overcome some of the discrepancies between our study and previous literature we decided to also provide full overview of the results processed in regard to other papers - metabolite ratios and gray matter partial regression.

In order for the reader to compare current findings with the previous literature we report all effects surviving the nominal significance of $p < 0.05$ (Laycock et al., 2008; Pugh et al., 2014; C. Rae et al., 1998), but focus more on results surviving more stringent statistical threshold corrected for multiple comparisons.

Hypotheses

1. Dyslexic individuals have heightened level of glutamate compared to controls (as predicted by the neural noise hypothesis).
2. Glutamate and choline levels predict individual differences in reading ability as they were identified by previous studies of Pugh et al. (2013) and Lebel et al. (2016).
3. Cytoarchitecture abnormalities characteristic to dyslexia are reflected by concentration of choline, NAA and creatine.
4. The concentration of NAA, choline, glutamate, creatine changes with age of participants.

Explorative research questions

5. Does GABA concentration, in addition to glutamate, differentiate control from dyslexic group (as predicted by the neural noise hypothesis)?
6. Does the age of participants influence the metabolite differences related to dyslexia diagnosis as suggested by the discrepancies in the previous results i.e. choline level in Rae et al. (1998) vs Pugh et al. (2014)?
7. Is internal referencing to Cr, Cho or NAA legitimate in non-uniform samples such in case of children with dyslexia? Which reference method is recommended to compare distant age groups?

2.2.2 Methods

The study was funded by a Preludium grant "Neural Correlates of Dyslexia" (2015/17/N/HS6/03013) conducted at the Nencki Institute from 2015 to 2018. Original publication was published in 2019 in Nature Scientific Reports under the title "Dyslexia and age related effects in the neurometabolites concentration in the visual and temporo-parietal cortex" (Kossowski et al., 2019). The study was approved by the Warsaw University Ethical Committee and carried out in accordance to the provisions of the World Medical Association Declaration of Helsinki.

2.2.2.1 Participants

Since we aimed to control for the age-related effects, we recruited both children and adults for the current study. All participants had to meet the inclusion criteria, such as right-handedness, normal vision and hearing, no diagnosis of the neurological illness, psychiatric diagnosis, or brain damage. All participants were native Polish speakers. Adult participants gave written consent, while children agreed orally, and their parents signed the consent as well.

Adults

Thirty-six adult volunteers (12 females, 24 males, M age in years = 27.3, std = 3.8) were recruited to the study. Inclusion to the group with dyslexia was based on the three different criteria, and the participants had to meet at least two of them. The first criterion was

dyslexia diagnosis, which, however, was not commonly diagnosed in Poland in the 1980s. Nonetheless, 14 subjects indeed obtained dyslexia diagnosis in their childhood. The second criterion was based on the Adult Reading History Questionnaire (ARHQ) score, a measure commonly used to screen for the reading problems in families in the dyslexia research. As suggested by Black et al. (2012) (Black et al., 2012), the criterion was met in the ARHQ score was higher than 40. The third criterion was based on the number of pseudowords read per minute. This criterion was met if the subject obtained a score lower than the group median (Med = 69, Mean = 76.36). Four subjects without the former dyslexia diagnosis met the criteria of high ARHQ score and a low number of pseudowords read per minute; they were thus included in the group with dyslexia. All 14 subjects with former dyslexia diagnosis also met one of the two additional criteria. As a result, 18 subjects with dyslexia were included. Subjects from the control group (18 participants) were never diagnosed with dyslexia, had ARHQ scores lower than 40, and their reading score was above the group median. The control group was matched for age and sex to the dyslexic group, and all subjects completed higher education (see Table 6).

Children

Fifty-two children (22 girls, 30 boys, M age in years = 11.06, std = 0.97) were recruited to the study. They were selected from the larger pediatric sample examined in a different study conducted at the Nencki Institute. Within that study, they were examined with the battery of tests for diagnosis of dyslexia (*Diagnoza dysleksji u uczniów klasy III szkoły podstawowej: przewodnik diagnostyczny*, 2008), and Wechsler's IQ test (Matczak et al., 1997). Children selected for the current study were readers diagnosed with dyslexia (26 children), and typical readers (26 children) matched for age and sex. All the children had average or above-average IQ and were born at term.

Table 6. Demographic data of participants

Characteristic	Adults				Children			
	Dyslexic N=18	**Control N=18**	**t | χ2**	**p**	**Dyslexic N=26**	**Control N=26**	**t | χ2**	**p**
Age	30.28 ± 4.09	28.02 ± 3.40	1.804 (34)	0.080	10.90 ± 0.98	11.21 ± 0.95	1.136 (50)	0.261
Male	13 (72.2%)	11 (61.1%)	0.500 (1)	0.480	15 (57.7%)	15 (57.7%)	0.000 (1)	1.000
ARHQ	55.78 ± 7.18	25.39 ± 11.11	9.772	<0.001	-	-	-	-

2.2.2.2 Data acquisition and analysis

Magnetic resonance data

Study was performed on 3T scanner Siemens Magnetom TRIO equipped with 32CH receiving coil. Work-in-progress package for MEGA-PRESS spectroscopy (WIP-529) was installed to acquire single-voxel spectroscopy spectrum including GABA signal. Two different brain regions – occipital (visual) cortex and left temporo-parietal cortex were targeted by single voxel spectroscopy. Voxels were placed based on 3 plane T1-weighted images (TR = 3000 ms, TI = 900 ms, 1 × 1 × 1 mm resolution) (Gunter et al., 2017) with a use of synthetic image as a template provided for reference (Figure 35).

DATA ACQUISITION

MR scanner

Siemens Magnetom TRIO 3T, Rx - 32CH Head Coil, Tx - Whole-body coil

Anatomical scan

T1 MP-RAGE 1x1x1 mm, TR=2530 ms, TI=1100 ms

Voxel 1 - Visual cortex

Calibration (3D-FieldMap, Manual shimming)
Water-suppressed scan - 192 AVGs
Water reference scan - 16 AVGs

MEGA-PRESS WIP 529, 15x30x30 mm voxel,
TR=2000ms, TE=68ms, NA = 192 OFFs + 192 ONs
TA = 12 min 48 s

Voxel 2 - Temporo-parietal lobe

As above

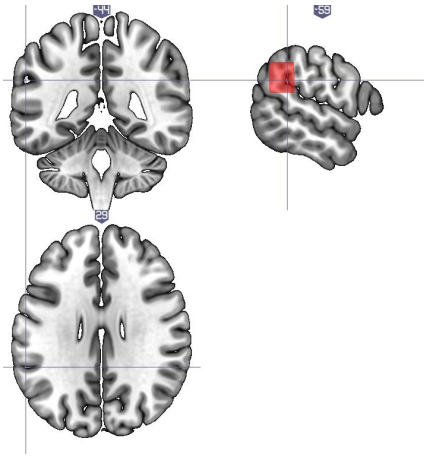

Figure 35. Data acquisition scheme and voxels' position.

Acquisition parameters were set to TR = 2000 ms and TE = 68 ms, which corresponds to GABA inversion without editing pulses. Acquisition protocol consisting of 2 phases - anatomy scan and spectroscopy (Figure 35) was validated in the group of adults. We decided to implement more advanced shimming strategy with manual fine tuning based on results from PW-MRS phantom. Spectra were averaged 192 times resulting in 12 min 50 s of a single acquisition in adults. However, we identified several irreversibly corrupted data sets due to bad calibration or subjects' motion. Therefore, we decided to shorten the acquisition time in the group of children to 96 averages (6 min 25 s) and repeat measurements in case of strong artifacts (with the subject's consent) to minimize the data loss. The voxel size was 30 × 30 × 15 mm in both the visual cortex and left temporo-parietal cortex in adults. Whereas, in children the temporo-parietal voxel was slightly reduced (from 30 × 30 × 15 to 25 × 25 × 15 mm) to better correspond with angular gyrus anatomical features. Visual cortex voxel was of the same size in both age groups. We think that such modifications were legitimate, since resultant SNR enabled estimation of all metabolites of interest (apart from GABA) with a variance of estimate below 15% (CRLB < 15% (Kreis, 2016). The acquisition parameters were similar to other recent studies where standard PRESS sequence was used (Bruno et al., 2013; Lebel et al., 2016).

For both voxel positions we acquired water unsuppressed scan (NA = 16) to reference the metabolites concentrations. Internal reference based on water signal was additionally

corrected with a use of tissue composition derived from individual T1-weighted anatomical images to better estimate true water concentration with respect to tissue specific relaxation times.

Metabolite quantification

First, non-edited metabolite spectrum was analyzed in LCModel with optimised for non-standard echo time (68 ms) basis set consisting of 14 metabolite priors (Dydak et al., 2011). Spectra were assessed visually and quantitatively with a regard to SNR, shape of baseline, residual noise, symmetry and width of singlets (NAA, Cr) and voxel position. Both water-referenced (mM) as well as creatine ratios were extracted. Secondly, raw data was analyzed in Gannet (Edden et al., 2014) in order to estimate GABA concentration from the difference between edited and non-edited spectra. Spectra misaligned during frequency drift correction during GANNET preprocessing were disqualified from the analysis. Tissue specific correction factor was calculated based on priors resulting from segmentation in SPM8 into GM/WM/CSF fractions of a voxel and respective relaxation times (Gasparovic et al., 2006) within Gannet and reapplied to LCModel to improve estimates. Selected metabolites from tissue corrected LCModel analysis as well as GABA estimates from Gannet were treated as the most appropriate, final data. However, different scaling and preprocessing methods were also presented in supplementary results for reference to previous studies. Other methods include creatine and NAA ratios (Bruno et al., 2013; Laycock et al., 2008; C. Rae et al., 1998), as well as use grey matter content as a covariate (Pugh et al., 2014). They are explained in more detail in Discussion and should be used with a great caution related to potential bias and limitations.

Despite, the voxel position was set up according to visual checklist consisting of reference images, it is very rare in MR spectroscopy papers to share individual or group reports. It is mainly due to additional effort needed to extract voxel position from non-standard vendor specific data type. It is worth to mention that in our study voxel position was registered and overlaid on T1w anatomical scans thanks to in-house Matlab script rda2nifti written specially for that purpose. Then images were normalized to MNI space for comparison and visualization.

Behavioral measures

On site, the day scan was performed, subjects were tested on words and pseudowords reading speed (Szczerbiński & Pelc-Pękala, 2013) and rapid automatized naming (RAN) (Fecenec, 2008). RAN test consisted of a multiple categories of objects accumulated into two categories: objects & colors and letters & digits. Subjects with dyslexia and controls were compared for the number of words and pseudowords read in one minute. The summarical times for the two RAN test subsets were compared between the groups as a measure of lexical access. Children, but not adults were additionally tested with a battery of phonological awareness tasks based on pseudowords in which both syllable and phoneme manipulation was included (*Diagnoza dysleksji u uczniów klasy III szkoły podstawowej: przewodnik diagnostyczny*, 2008). Results of behavioral measures are presented in the Table 7.

Statistical model

Metabolite of interest (Glu, GABA, Cho, tNAA and Cr) were analyzed in 2x2 ANOVA model with group (adults/children) and diagnosis (dyslexic/typical readers) as factors. We investigated main effect of group, diagnosis as well as interaction between them. Then, if it was statistically justified, we performed post-hoc tests to analyze differences between specific subgroups. Also brain-behaviour correlations between metabolite concentration and additional behavioral measures (reading, lexical access and phonological awareness) were studied. Only results, which survived conservative Bonferroni correction for 5 metabolites were further visualized with asterisks and highlighted in interpretation. Nonetheless, p values reported in the text are not corrected for multiple comparisons to better correspond with previous studies from the field. Additionally, we employed bayesian ANOVA to estimate ratio of the likelihood probability (Bayes factor) of two competing hypotheses (Kass & Raftery, 1995). Here we assume that for Bayes factor above 3 there is a substantial evidence for alternative hypothesis as compared to null and symmetrically below 1/3 for null as compared to alternative. Bayes factor does not require multiple comparison correction (Gelman et al., 2012).

2.2.3 Results

2.2.3.1 Behavioural results

In adults, ARHQ score showed strong negative correlation with word reading ($r = -0.57$, $p < 0.001$) and pseudoword reading ($r = -0.73$, $p < 0.001$). In both reading tasks, adults with dyslexia performed significantly lower than adult control group ($t=5,456$ & $t=6,456$, $p < 0.001$). Dyslexic adults were also significantly slower than controls at naming letters and numbers in RAN task, but had similar performance in the objects and colors subtests. This pattern of results remained unchanged when 3 subjects were excluded from the analysis due to spectral artifacts. It is important to mention that both ARHQ and pseudowords reading test were used to classify subjects to the groups in adult sample.

Children with dyslexia had significantly lower performance than children from the control group in all behavioral tests - word and pseudoword reading, both subscales of RAN, and phonological awareness tasks. This pattern of results was not affected by the exclusion of up to 18 subjects with spectral artifacts in the worst case of GABA analysis. Descriptive statistics and results of the statistical comparisons between the dyslexic and control groups are presented in the Table 7.

Table 7. Behavioural results in adult and children.

Characteristic	Adults				Children			
	Dyslexic N=18	**Control N=18**	**t**	**p**	**Dyslexic N=26**	**Control N=26**	**t**	**p**
Words/min	115.67 ± 12.45	142.50 ± 16.74	-5.456	<0.001	47.62 ± 16.61	95.5 ± 20.11	-9.361	<0.001
Pseudowords/min	62.28 ± 10.39	90.44 ± 15.33	-6.456	<0.001	33.27 ± 6.55	57.92 ± 14.74	-7.794	<0.001
RAN (objects and colors) in sec	62.61 ± 7.35	59.11 ± 8.98	1.280	0.209	95.88 ± 15.71	80.65 ± 11.86	3.947	<0.001
RAN (letters and numbers) in sec	37.44 ± 4.13	32.72 ± 5.88	2.788	0.009	57.04 ± 10.49	47.92 ± 9.41	3.298	0.002
Phonological awareness (sten)					3.50 ± 1.70	5.46 ± 2.02	3.781	<0.001

2.2.3.2 MR spectroscopy

Quality

Spectra were assessed based on the criteria presented in section 2.2.2.2. In adults strong artifacts declassified 4 spectra from visual cortex and 3 from temporo-parietal lobe. Additionally, Gannet data preprocessing routine failed during frequency drift correction in 2 spectra from visual cortex, which disabled further GABA estimation. Finally, analysed dataset consisted of 33 spectra from temporo-parietal lobe (17 dyslexic subjects), 32 spectra (16 dyslexic subjects) from visual cortex in LCModel analysis. Respective GABA estimates were calculated for all spectra but aforementioned 2, which reduced number of spectra from visual cortex to 30 (15 dyslexic) due to computational problems. In a group of 52 children, one participant was unable to maintain still during both scans. More detailed visual inspection revealed artifacts in 8 more spectra from temporo-parietal lobe and 1 from visual cortex. Moreover, Gannet preprocessing was not satisfactory in 3 temporo-parietal spectra and 1 visual cortex. As a result, 43 spectra from temporo-parietal lobe (20 dyslexic children) and 50 from visual cortex (25 dyslexic children) feed into main dataset, with reduced number of

GABA estimates to 40 (17 dyslexic) and 49 (25 dyslexic) in both regions respectively. Overall data quality, depicted in averaged spectra from both groups in Figure 36, characterize narrow peak width (good separation between Cho and Cr), smooth baseline and slightly increased variability in temporo-parietal lobe comparing to visual cortex in both groups. GABA edited spectra quality improved significantly in consequence to the observations made in the reproducibility test (section 2.1.3) in adults but not children sample. Finally, GABA estimates in adults, in visual cortex (2.68 ± 0.23) resulted in the estimated power of 0.88 (alpha 0.05, n=15 in each of the groups, effect size of 10%). Whereas, power of the statistical test in children in visual cortex was 0.36 despite the bigger sample (alpha 0.05, n=25 in each of the groups, effect size of 10%).[1]

[1] Power estimates are calculated for two-sample T-tests separately for each of the groups for comparison. Methodologically correct would be to calculate power for ANOVA test instead.

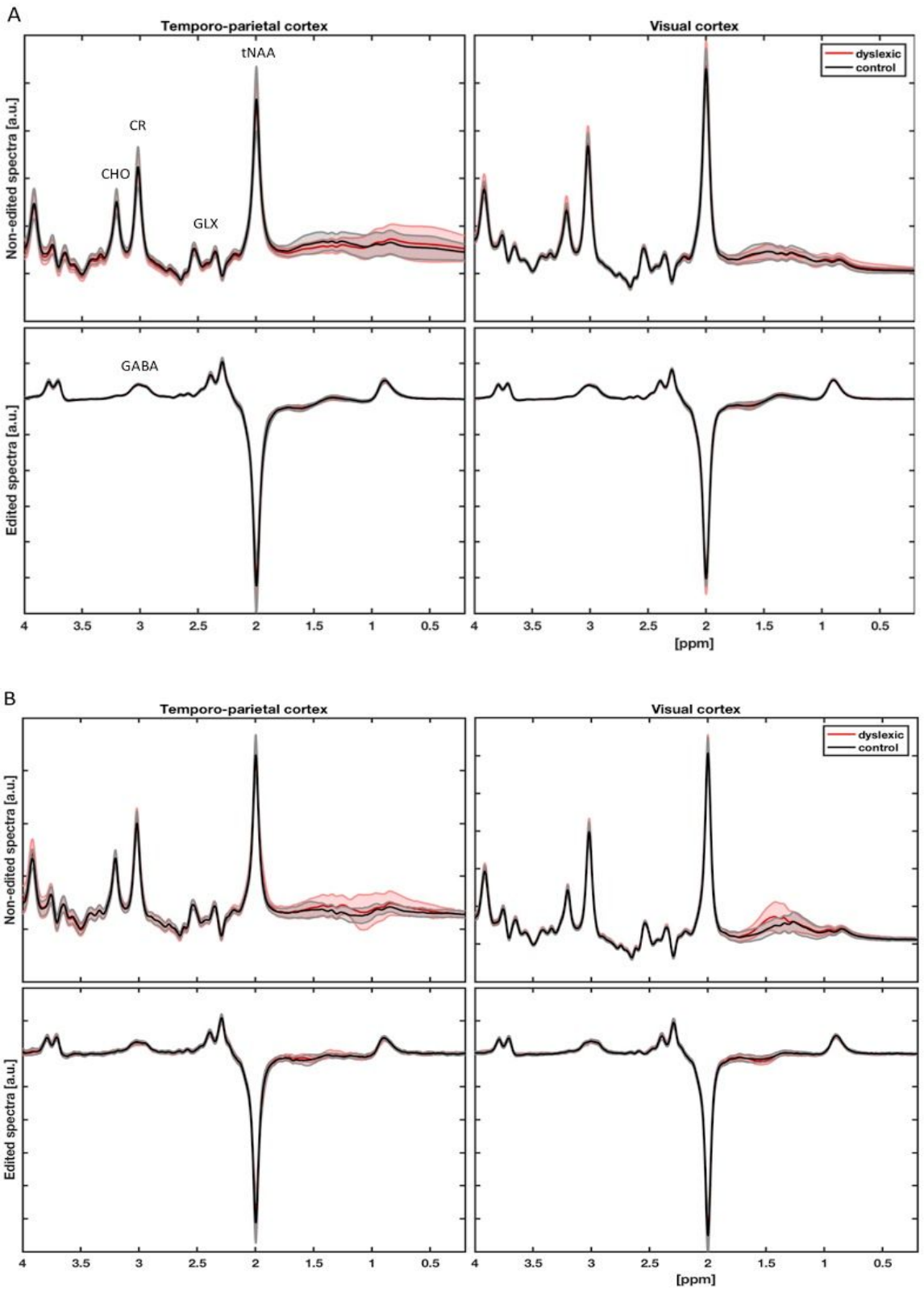

Figure 36. Average spectra - adults (A) and children (B)

Thanks to the fact that voxel position could be overlaid on structural scans (see method for description) we were able to report normalized and averaged voxels in Figure 37. The images show consistent voxel positioning in both regions and groups.

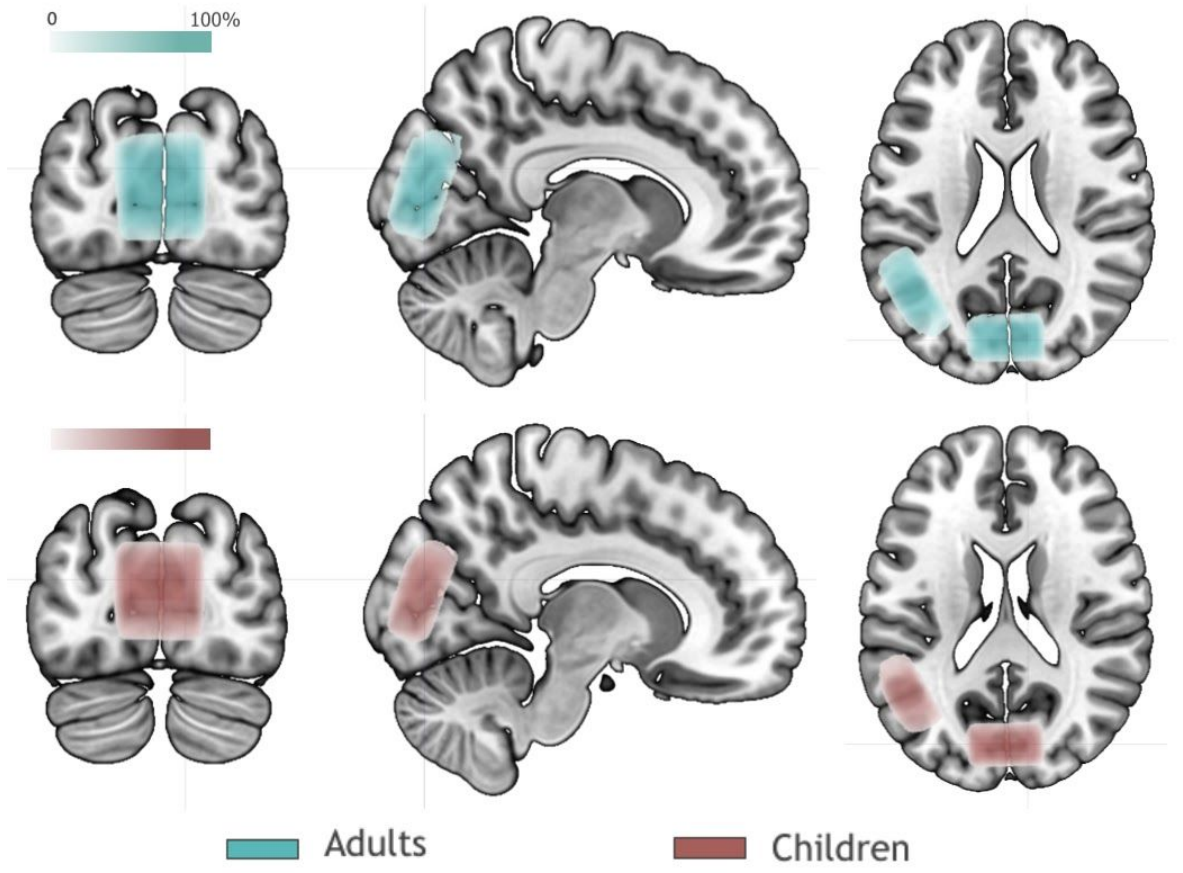

Figure 37. Averaged voxel positions in colour scale corresponding to percentage overlap.

Group differences

Choline

Statistical model revealed a significant main effect of age group in both left temporo-parietal cortex and visual cortex ($F(1,72)=30.68$, $p<0.001$, $BF10>1000$ and$F(1,78)=30.19$, $p<0.001$, $BF10>1000$ respectively). Adults were characterized by higher choline concentration than children (14.1% in temporo-parietal and 10.1% in visual cortex voxels). Interactions between age group and diagnosis reached nominal significance without correction for a number of tested metabolites ($F(1,72)=5.15$, $p=0.026$, $BF10=2.459$ in left temporo-parietal cortex;$F(1,78)=6.52$, $p=0.013$, $BF10=4.007$ in visual cortex). Dyslexic children compared to control children had lower by 7.6% absolute choline concentration in the left temporo-parietal ($p=0.05$, $BF10=1.438$) and by 5.5% in visual cortex ($p=0.031$, $BF10=1.466$) (see Figure 1). In adults the difference between the experimental groups did not reach significance in neither regions, although dyslexic adults tended to have higher choline concentration than controls. Therefore there was no main effect of dyslexia.

Glutamate and glutamine (Glu & Glx)

A main effect of age group was found for both Glu and Glx ($F(1,78)=52.03$, $p<0.001$, $BF10>1000$ and $F(1,78)=33.53$, $p<0.001$, $BF10>1000$ respectively) in visual cortex with children having higher concentration of neurotransmitters than adults (17.9% - Glu and 13.6% - Glx). In the left tempo-parietal cortex the effect of age group was not significant. There was also no significant effect of diagnosis nor interaction between age group and diagnosis in neither Glu nor Glx.

Gamma-aminobutyric acid (GABA)

In both brain areas, neither main effects of age group and diagnosis nor interaction between these factors reached significance for GABA.

Creatine (Cr)

Children had lower concentration of Cr than adults by 17.8% in temporo-parietal

(F(1,72)=42.79, p<0.001, BF10>1000) and by 5.7% in the visual cortex (F(1,78)=12.22, p=0.001, BF10=37.307). There was no significant effect of diagnosis nor interaction.

Total N-acetyl-aspartate (tNAA)

In the visual cortex, but not in the left temporo-parietal cortex, subjects with dyslexia had on average lower concentration of tNAA by 4.5% than typically reading controls (F(1,78)=7.52, p=0.008, BF10=9.811). The effect remained significant (F(1,76)=7.23, p=0.009, BF10=4.598) after removal of two control children with outlying tNAA concentration (>3SD above mean). There was also a significant effect of age group in the left temporo-parietal cortex (F(1,72)=23.73, p<0.001, BF10>1000), where children had lower concentration of tNAA than adults by 10.8%.

See tables for summary statistics - Table 8, Table 9 and Figure 38 for results visualization.

Table 8. Concentration of metabolites of interest in the left temporo parietal cortex.

	control children	dyslexic children	control adults	dyslexic adults
glu	8.619 ± 1.133	8.176 ± 1.496	8.218 ± 1.151	7.754 ± 0.986
glx	10.564 ± 1.303	10.049 ± 1.558	10.168 ± 1.372	9.562 ± 1.118
tNAA	12.888 ± 1.278	12.193 ± 1.311	14.196 ± 1.539	13.985 ± 1.405
Cho	1.829 ± 0.227	1.691 ± 0.227	2.002 ± 0.245	2.103 ± 0.212
GABA	2.577 ± 0.767	2.515 ± 0.919	2.383 ± 0.172	2.423 ± 0.190

Table 9. Concentration of metabolites of interest in the visual cortex.

	control children	dyslexic children	control adults	dyslexic adults
glu	8.977 ± 1.501	8.866 ± 0.774	7.553 ± 0.465	7.105 ± 0.408
glx	11.395 ± 1.748	11.144 ± 0.952	10.081 ± 0.707	9.389 ± 0.531
tNAA	15.152 ± 1.451	14.283 ± 0.782	15.381 ± 0.760	14.976 ± 0.744
Cho	1.460 ± 0.165	1.380 ± 0.108	1.546 ± 0.121	1.615 ± 0.095
GABA	2.712 ± 0.684	2.488 ± 0.382	2.699 ± 0.258	2.663 ± 0.197

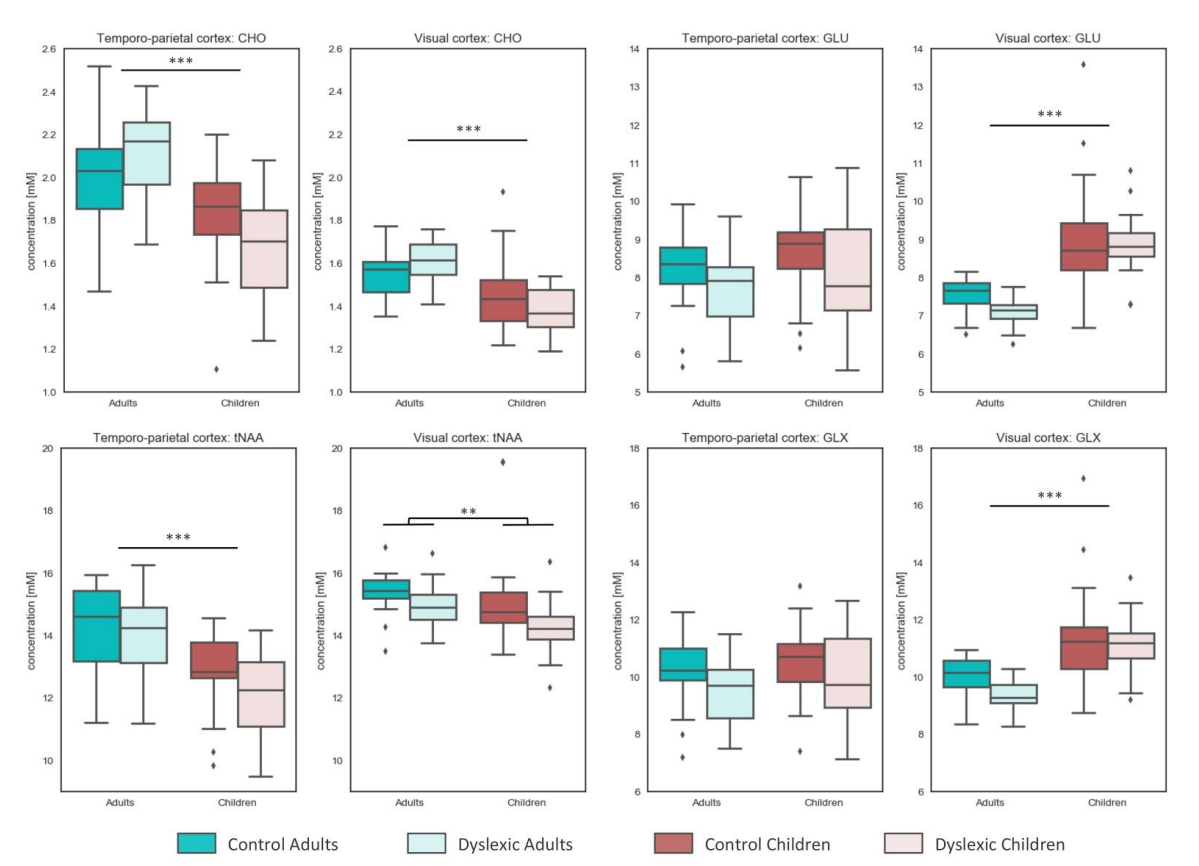

Figure 38. Group comparison in 2x2 model. Significant effect of age group is annotated in Cho (both regions), Glu & Glx (visual cortex) and tNAA (temporo-parietal cortex). Effect of diagnosis was identified in tNAA concentration in visual cortex. Anecdotal evidence for interaction between age group and diagnosis is in choline estimates (both regions, $p_{unc}<0.05$).

Brain-behaviour correlations

Correlations between behavioural measures and metabolite concentrations need to be performed separately for children and adults, because the respective tests results differ significantly between the groups. Next, the correlation coefficients were compared between the groups to identify potential differences between younger and less experienced readers to older experienced group.

Choline concentration correlated with RAN objects and colors in both age groups, however, in with different direction (Figure 39). In adults higher concentration of metabolite predicted slower naming speed ($r = 0.449$, $p = 0.01$ in the visual cortex; $r = 0.516$, $p = 0.002$** in the left temporo-parietal cortex), whereas in children negative correlation did

not approach significance threshold corrected for multiple comparisons ($r = -0.109$, $p = 0.45$ in the visual cortex; $r = -0.299$, $p = 0.052$ in the left temporo-parietal cortex). Nevertheless, there was a significant difference in correlation coefficients between the groups ($z = 2.51$, $p = 0.012$ for visual cortex; $z = 3.64$, $p < 0.001$ for the temporo-parietal).

Despite the following results did not survive conservative Bonferroni corrected alpha threshold, we present them to correspond with the previous literature. Word reading speed was positively correlated with choline in the visual cortex in children ($r = 0.284$, $p = 0.045$). tNAA concentration in the temporo-parietal cortex was negatively related to the time needed to name objects and colors ($r = -0.372$, $p = 0.014$). Interestingly, glutamate in the left temporo-parietal cortex was positively correlated with RAN objects and colors ($r = 0.367$, $p = 0.036$ - Glu; $r = 0.385$, $p = 0.027$ - Glx) only in adults.

It is worth to mention that no significant correlations were found between metabolite concentrations and phonological awareness in children (PA was not measured in adults).

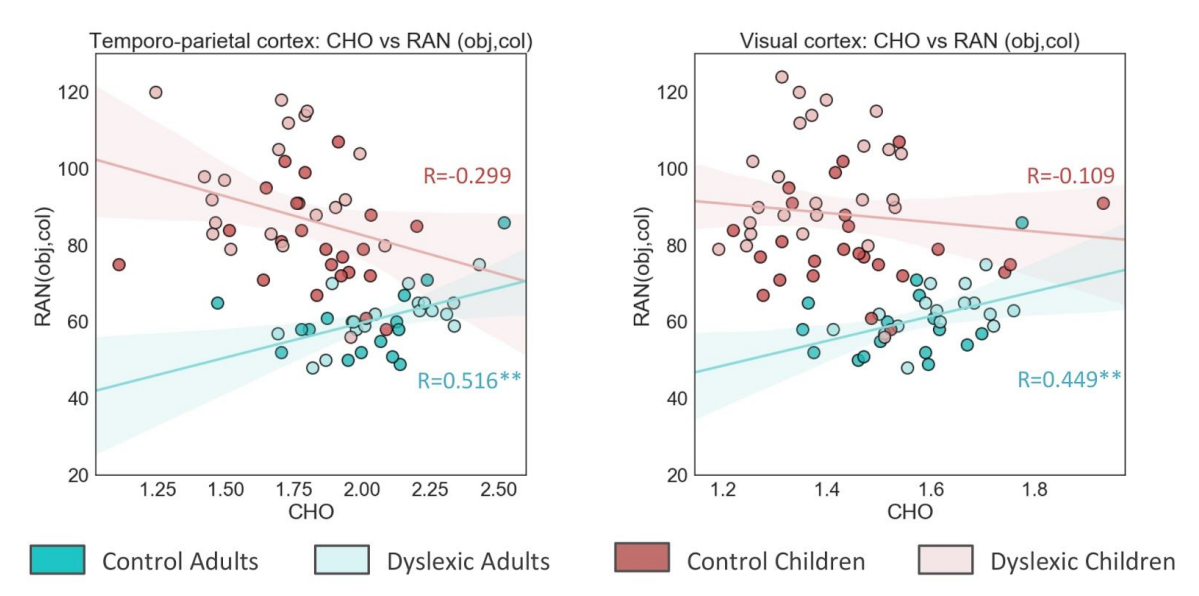

Figure 39. Brain-behaviour correlations between RAN (objects & colors) and choline concentration in the temporo-parietal lobe (left) and the visual cortex (right). Significant results are marked with asterisk (**p<0.01).

Influence of reference factor on the results

Since previous studies differ in strategies of referencing metabolite signal we performed supplementary group analyses. First, water referenced concentration of metabolites was

analysed without correction for tissue volume fractions. Second creatine ratios were calculated and additionally to both results an inhomogeneous voxel composition was controlled by gray matter volume (GMV) within a voxel by the means of multiple regression. This approach is different than the one presented above in such a way that the absolute quantification utilized percentage of different tissue classes and respective relaxation times to better estimate referenced water concentration, in contrast to including gray matter as a linear covariate. Tissue composition would affect both water and metabolite estimates. We decided to present water referenced concentrations, where water content within tissue classes is taken into consideration. However, variability of estimates may also reflect inhomogeneous distribution of metabolite within a voxel (i.e. neurotransmitters in a cortex). Then, a model with a gray matter volume as a covariate would better predict the results.

Additional tests were not corrected for multiple comparisons. The results are presented in Table 10 and Table 11.

Choline

In both temporo-parietal and visual cortex, the interaction between age group and diagnosis reached nominal significance irrespective of scaling or correction methods (see Tables 7 and 8). In the temporo-parietal cortex, congruently with the main analysis (corrected for tissue composition), control children had higher choline concentration than dyslexic children, while the difference in adults, although going in a different direction, did not reach significance. In the visual cortex, the difference in adults was significant with higher choline concentration in dyslexic than control adults, while the difference in children with higher concentration in control than dyslexic (as in the main analysis) did not reach significance. Adults on average had higher concentration of choline than children and the age effect was more stable in the temporo-parietal cortex than in the visual cortex.

Glutamate and glutamine (Glu & Glx)

In the visual cortex there was a stable effect of age group, with children having higher Glu and Glx concentrations than adults. In the temporo-parietal cortex this effect, although present, was less stable. Scaling to creatine, instead of water, irrespective of GMV correction

resulted in a diagnosis effect in the temporo-parietal cortex, with lower Glu/creatine and Glx/creatine in dyslexic than control individuals.

Gamma-aminobutyric acid (GABA)

No significant effects for GABA were observed in the visual cortex. Scaling to creatine, instead of water, irrespective of GMV correction resulted in the main effect of age group in the temporo-parietal cortex, with higher GABA/creatine concentration in children than adults.

Total N-acetyl-aspartate (tNAA)

The effects of age group and diagnosis changed a lot depending on scaling and correction. Scaling to creatine, reversed age effect in the temporo-parietal cortex with children having higher concentration of tNAA/creatine than adults (adults had higher concentration of tNAA than children). Additionally, a trend for diagnosis effect appeared with higher tNAA/creatine in controls than dyslexics. In the visual cortex depending on scaling and correction either only age effect or trends for diagnosis or interaction of two factors were found.

Table 10. Concentration of metabolites in control (CON) and dyslexic (DYS) adults (AD) and children (CH) in the left temporo-parietal cortex. Each metabolite is scaled either to water (for e.g. CHO) or creatine (for e.g. CHO/CR) and additionally adjusted for GMV by the means of linear regression.

Table 11. Concentration of metabolites in control (CON) and dyslexic (DYS) adults (AD) and children (CH) in the visual cortex. Each metabolite is scaled either to water (for e.g. CHO) or creatine (for e.g. CHO/CR) and additionally adjusted for GMV by the means of linear regression.

TABELE ZAJMUJĄ 1 STRONĘ HORYZONTALNIE

PLIK - *tabele scaling factors.pdf*

Table 10. Concentration of metabolites in control (CON) and dyslexic (DYS) adults (AD) and children (CH) in the left temporo-parietal cortex. Each metabolite is scaled either to water (for e.g. CHO) or creatine (for e.g. CHO/CR) and additionally adjusted for GMV by the means of linear regression.

	No adjustment for tissue composition						Adjustment for GMV					
Metabolite	**CON AD**	**DYS AD**	**CON CH**	**DYS CH**	**Main effects**	**Post-hoc**	**CON AD**	**DYS AD**	**CON CH**	**DYS CH**	**Main effects**	**Post-hoc**
CHO	1.65 ±0.22	1.74 ±0.19	1.52 ±0.21	1.36 ±0.22	AGE*** GR x AGE*	AD>CH CON>DYS (CH)	0.09 ±0.96	0.52 ±0.89	-0.00 ±0.91	-0.62 ±1.11	AGE** GR x AGE*	AD>CH CON>DYS (CH)
CHO/CR	0.21±0.02	0.22 ±0.02	0.24 ±0.03	0.22 ±0.03	GR x AGE**	CON>DYS (CH)	-0.59 ±0.65	-0.18 ±0.84	0.63 ±0.95	-0.08 ±0.92	AGE** GR x AGE**	AD>CH CON>DYS (CH)
GLU	6.70 ±0.98	6.42 ±0.88	6.95 ±1.33	6.83 ±1.58	AGE***	CH>AD	0.12 ±0.84	-0.14 ±0.71	0.12 ±1.12	0.01 ±1.32	-	
GLU/CR	0.87 ±0.07	0.82 ±0.09	1.14 ±0.19	1.05 ±0.13	AGE*** GR*	CH>AD CON>DYS	-0.32 ±0.39	-0.59 ±0.46	0.69 ±1.06	0.22 ±0.72	AGE*** GR*	CH>AD CON>DYS
GLX	8.36 ±1.19	7.98 ±1.00	8.62 ±1.47	8.32 ±1.67	AGE***	CH>AD	0.17 ±0.92	-0.13 ±0.74	0.17 ±1.13	-0.07 ±1.26	-	
GLX/CR	1.08 ±0.07	1.02 ±0.09	1.40 ±0.23	1.29 ±0.14	AGE*** GR*	CH>AD CON>DYS	-0.33 ±0.37	-0.64 ±0.46	0.73 ±1.13	0.24 ±0.71	AGE*** GR*	CH>AD CON>DYS
GABA	2.02 ±0.13	2.06 ±0.17	2.19 ±0.65	2.13 ±0.75	-		-0.11 ±0.27	-0.08 ±0.33	0.24 ±1.26	0.11 ±1.45	-	
GABA /CR	0.09 ±0.00	-0.09 ±0.01	0.12 ±0.03	0.11 ±0.04	AGE**	CH>AD	-0.31 ±0.18	-0.16 ±0.36	0.39 ±1.23	0.16 ±1.41	AGE*	CH>AD
tNAA	11.64 ±1.43	11.50 ±1.23	10.62 ±1.41	10.15 ±1.27	AGE***	AD>CH	0.31 ±1.03	0.24 ±0.97	-0.04 ±1.07	-0.36 ±0.98	AGE*	AD>CH
tNAA/CR	1.51 ±0.09	1.49 ±0.13	1.69 ±0.22	1.58 ±0.16	AGE** GRt	CH>AD CON>DYS	-0.30 ±0.48	-0.39 ±0.67	0.59 ±1.12	-0.003 ±0.82	AGE** GRt	CH>AD CON>DYS

AD - adults; CH - children; ***p<0.001; **p<0.01; *p<0.05; tp<0.1

Table 11. Concentration of metabolites in control (CON) and dyslexic (DYS) adults (AD) and children (CH) in the visual cortex. Each metabolite is scaled either to water (for e.g. CHO) or creatine (for e.g. CHO/CR) and additionally adjusted for GMV by the means of linear regression.

	No adjustment for tissue composition						Adjustment for GMV					
Metabolite	**CON AD**	**DYS AD**	**CON CH**	**DYS CH**	**Main effects**	**Post-hoc**	**CON AD**	**DYS AD**	**CON CH**	**DYS CH**	**Main effects**	**Post-hoc**
CHO	1.18 ±0.09	1.28 ±0.08	1.16 ±0.12	1.11 ±0.10	AGE*** GR x AGE**	AD>CH DYS>CON (AD)	-0.15 ±0.85	0.53 ±0.75	0.04 ±1.12	-0.29 ±0.92	GR x AGE*	DYS>CON (AD)
CHO/CR	0.15 ±0.01	0.16 ±0.01	0.15 ±0.01	0.15 ±0.01	AGE** GR x AGE**	AD>CH DYS>CON (AD)	-0.29 ±1.02	0.38 ±1.27	0.12 ±0.69	-0.17 ±0.97	GR x AGE*	DYS>CON (AD)
GLU	5.87 ±0.31	5.71 ±0.31	7.09 ±1.13	7.14 ±0.48	AGE***	CH>AD	-0.44 ±0.37	-0.26 ±0.39	0.37 ±1.36	0.26 ±0.78	AGE**	CH>AD
GLU/CR	0.75 ±0.03	0.72 ±0.06	0.94 ±0.09	0.95 ±0.07	AGE**	CH>AD	-0.59 ±0.63	-0.28 ±0.53	0.40 ±0.84	0.38 ±0.87	AGE***	CH>AD
GLX	7.79 ±0.34	7.52 ±0.35	9.01 ±1.33	8.95 ±0.56	AGE***	CH>AD	-0.34 ±0.38	-0.28 ±0.43	0.38 ±1.39	0.16 ±0.78	AGE**	CH>AD
GLX/CR	0.99±0.04	0.95 ±0.08	1.19 ±0.11	1.19 ±0.09	AGE**	CH>AD	-0.44 ±0.74	-0.27 ±0.68	0.40 ±0.74	0.28 ±0.89	AGE***	CH>AD
GABA	2.14 ±0.18	2.17 ±0.17	2.21 ±0.56	2.04 ±0.31	-		0.01 ±0.48	0.11 ±0.45	0.18 ±1.49	-0.28 ±0.83	-	
GABA /CR	0.11 ±0.01	0.11 ±0.01	0.12 ±0.02	0.11 ±0.02	-		-0.06 ±0.45	-0.01 ±0.31	0.27 ±1.39	-0.21 ±1.05	-	
tNAA	11.78 ±0.44	11.79 ±0.57	12.02 ±1.18	11.43 ±0.44	GR x AGEt	CON>DYS (CH)	-0.001 ±0.56	-0.01 ±0.72	0.33 ±1.49	-0.40 ±0.55	GRt	CON>DYS
tNAA/CR	1.52±0.05	1.52 ±0.11	1.59 ±0.07	1.54 ±0.07	AGE*	CH>AD	-0.16 ±0.76	-0.04 ±1.35	0.45 ±0.82	-0.28 ±0.93	GR x AGEt	CON>DYS (CH)

AD - adults; CH - children; ***p<0.001; **p<0.01; *p<0.05; tp<0.1

2.2.4 Discussion

In collaboration with Laboratory of Brain Imaging, Laboratory of Language Neurobiology at the Nencki Institute and Warsaw University of Technology we were able to conduct research with a new MR spectroscopy method in a group of 88 participants. This thesis gives a broader view of a whole preparation process starting from theoretical and preclinical considerations towards sophisticated etiological model of dyslexia. For the first time, we were able to test both age and dyslexia related effects in order to identify differences specific to language development period. From previously analyzed regions we chose two - occipital cortex and left temporo-parietal lobe including angular gyrus to see whether abnormal metabolite levels are common for both of them. What is more, we applied MEGA-PRESS spectroscopy to reliably measure GABA concentration. Thus, collected dataset is unique in a context of dyslexia and also aging and has a great value in the field of the human brain biochemistry.

2.2.4.1 Age related effects

We observed several maturational changes in all metabolites of interest apart from GABA. In the visual cortex but not temporo-parietal lobe adults were characterized with lower glutamate concentration. The result is in line with other MR spectroscopy datasets (Marsman et al., 2013; Shimizu et al., 2017) and can be explained by age-related reduction of glutamatergic NMDA receptors (Peterson & Cotman, 1989) and reduced glutamate-glutamine cycle flux (Boumezbeur et al., 2010). Such differences are linked rather to elevated metabolic activity in children (Segovia et al., 2001) but should not influence cognitive functions in our sample (21-40 y/o) as this concern is present only at a later age in other research. Opposite to glutamate, choline level was higher in adults than children in both regions of interest. As it was described in Applications of 1H-MRS in neurology (section 1.3), choline is considered to be a marker of membrane turnover. It has been also shown that choline measured with phosphorus spectroscopy (31P-MRS) increases with age (Blüml et al., 1999) (the method enabled detailed identification of compounds to glycerophosphorylcholine and glycerophosphorylethanolamine). Higher signal of free choline measured with 1H-MRS may also reflect impaired uptake of acetylcholine related to aging (Katz-Brull et al., 2002). Generally speaking, our result is in line with life-span dynamic of tissue growth measured by

other MR-related parameters - relaxometry and diffusion (Yeatman et al., 2014). Interestingly, previously reported discrepancies in choline in dyslexia presumably depend also on age of participants (anecdotal interaction was detected in our study).

Cr and tNAA, markers of energy deposit and cortical microstructure, are usually considered to be stable across healthy participants. However, when we investigated age as a factor it has became clear that there is a significant age effect there such as children have lower levels of both metabolites. In a independent sample consisting of 309 spectra from 0 to 18 y/o, a positive correlation with age was detected in both metabolites up to 12 years (Blüml et al., 2013). In current study we were also able to identify the effect of both age and dyslexia on tNAA level. Thus, referencing to tNAA could not be performed to prevent from confusion between the effects of numerator and denominator. Also referencing to Cr should be generally discouraged i.e. in groups with a large age span. Thus, in the future it should be carefully considered, which is the optimal option to prevent from further confusion as with the study of C. Rae where NAA was used as a reference metabolite (C. Rae et al., 1998) to emphasize Cho and Cr differences. Ideally, full datasets should be made available to reanalyze the data with a common approach for better comparison between the studies.

2.2.4.2 Dyslexia

This study aimed to disentangle inconsistencies between previous studies regarding potential neurometabolite abnormalities in dyslexia, specifically for choline and glutamate level. Surprisingly, we did not find supporting evidence for group differences in case of these neurometabolites, calling into question the use of traditional, non-task related magnetic resonance spectroscopy in dyslexia. On the one hand in our study, glutamate concentration was related to slower naming speed in adult sample. On the other hand this result did not survive corrections for multiple comparisons and glutamate did not correlate in children with any behavioral measure. Previously researchers reported mixed results for glutamate - positive correlation with PA in pre-reading children (Lebel et al., 2016) in anterior cingulate cortex as well as negative correlation with PA and reading performance in beginner readers (Pugh et al., 2014) in the visual cortex. Regarding choline concentration is has been examined several times - in left angular gyrus (2 times), visual cortex and cerebellum (2 times). However, there are two contradictory results in cerebellum with lower Cho/NAA in dyslexic males (C. Rae et al., 1998) and increased Cho/NAA (Cho/Cr as well) in dyslexic

adults (Laycock et al., 2008) compared to controls. What is more, lower Cho/NAA ratio in dyslexia obtained by Rae et al., (1998) in temporo-parietal cortex, was also further questioned by Bruno et al. (2013), who found negative correlation between choline and phonological awareness in 31 adults (Bruno et al., 2013) (such as lower results in PA are associated with higher choline). Eventually, Pugh and colleagues (2014) also reported negative correlation in Cho/Cr with reading performance in visual cortex (Pugh et al., 2014) (higher choline associated with poorer performance). It is also worth to mention recently published negative result for choline in anterior cingulate cortex in children with an anecdotal evidence for negative correlation between choline and silent reading score limited to dyslexic female subsample (Horowitz-Kraus et al., 2018). Apart from Rae et al., (1998), who might have found mixed effect of Cho & NAA, the other authors showed the most consistent data with unfortunately no obvious interpretation available yet. It is due to choline proton resonance signal, which may arise from multiple of compounds reflecting membrane turnover, neurotransmission or active myelination as well. Impaired auditory sampling theory predicted correspondence between theta band oscillation deficits and glutamate or choline concentrations. Indeed, higher choline in both occipital and temporo-parietal cortex was related with slower naming speed in the RAN test in adults but not in children here. This result, however not confirmed in children, would be in line with Pugh et al. (2014), Bruno et al. (2013) and SK. Laycock et al. (2008) findings of negative relation between choline and phonological awareness, which is considered to be linked with RAN speed (Wagner et al., 1993). Additionally we have found anecdotal evidence for interaction between dyslexia and age driven by lower choline concentration in dyslexic compared to control children. That stands in contrast to previous studies as well as correlation in adults presented here. We suppose that choline level might change with age reflecting various cognitive and maturational processes. According to our results it is not clear how to interpret contradictory group and correlation results in two age groups. Further studies involving phosphorus spectroscopy or combined multimodal proton resonance imaging should be performed to enable more detailed evaluation.

Eventually, dyslexic individuals, irrespective of age, had significant lower tNAA than controls in the occipital cortex. Similar result was recently confirmed by Del Tufo et al., (2018), who found positive correlation between NAA/Cr ratio and response time in

multimodal word matching tasks (Del Tufo et al., 2018) in the same region of interest. NAA is considered to be a marker of neural health and viability but also plays a role in myelin synthesis (C. D. Rae, 2014). Reduced tNAA in all examined dyslexic subjects suggest microstructure abnormalities. Concentration of tNAA is positively correlated with water diffusion directionality in white matter tracts (FA) (Tang et al., 2007). Other diffusion weighted imaging studies identified lower FA in both temporo-parietal lobe (Vandermosten et al., 2012) and occipital lobe (Steinbrink et al., 2008). Interestingly, occipital cortex was for a long time a focus of fMRI studies on dyslexia, showing abnormalities in processing of visual motion (Eden et al., 1996) and symbols (Price & Ansari, 2011). Lower tNAA was not predicted by presented etiological theories, however, it is the most prominent result presented here, which clearly indicates abnormalities in tissue microstructure, which persist regardless of age.

2.2.4.3 Neural noise hypothesis

Neural noise presented by Hancock et al., 2017 is a holistic model for developmental dyslexia taking into consideration genetic risk, neuroimaging and behavioural observations. Its important part comprises implications from genes responsible for abnormal neural migration and glutamatergic activity. Obviously, a direct tissue microscopy in a representative sample is unavailable in dyslexia, however, MR spectroscopy enables a non-invasive insight into brain cytoarchitecture and biochemistry. Several spectroscopic dataset have been acquired up to the date of writing this thesis. Despite discrepancies between them in age of participants, regions of interest, quantification methods (see Etiology of developmental dyslexia, section 1.5), is should be noted that glutamate and choline concentrations seem to repeatedly appear in a context of dyslexia studies. According to that, we expected that glutamate and perhaps GABA estimates could differentiate the groups at least in children sample. Indeed, glutamate in the left temporo-parietal cortex was positively correlated with RAN objects and colors in adults ($r = 0.367$, $p = 0.036$ - Glu; $r = 0.385$, $p = 0.027$ - Glx), but no evidence for group difference has been found. On the one hand, we did not find support for neural noise hypothesis. On the other hand, we suppose that it might me not optimal to measure neurotransmitters concentration during non-specific task. Actually, to maintain participants comfort during long acquisition periods, we presented them videos on the screen. Thus, metabolite concentration averaged from almost 9 min acquisition

would reflect metabolic activity perhaps elevated due to visual stimulation (in both regions), but not the level related to the release of neurotransmitters evoked by specific stimuli (Stanley & Raz, 2018). Authors also noted that glutamate concentration varies more when participants were not constraint to perform one simple task such as looking at a fixation cross. It is possible that videos presented by us might increase variability leading to inconclusive results.

Due to several technological improvements (see section 1.1.1) MR spectroscopy has recently become capable to acquire meaningful data also in new domain - time of an experiment. Task-related metabolite fluctuations known as functional MRS (fMRS) have been already measured in neurotransmitters - Glu, GABA and surprisingly also in lactate (Cleve et al., 2015; Mangia et al., 2007; P. Mullins et al., 2005). It is terrifically attractive to tackle dyslexia from point of view of task related glutamate and GABA concentration. According to two well known in a field meta analyses both task-related (block design) metabolic states (Stanley & Raz, 2018) as well as event-related glutamate release curve (P. G. Mullins, 2018), may give a completely new insight into behavioural research. We also presume that neural noise hypothesis needs to be tested in such a task-specific paradigm to eventually resolve the inconsistencies in findings.

In future we plan to study task-modulated neurochemistry (concentration of main excitatory and inhibitory neurotransmitters in the human brain - glutamate (Glu and Glx) and gamma-aminobutyric acid (GABA)) of the left ventral occipito-temporal (vOT) cortex during word reading in dyslexic and typical readers. Hypoactivation in the left vOT during reading found in functional magnetic resonance imaging (fMRI) studies is specific to dyslexia and results from atypical neurodevelopmental trajectory during reading acquisition (Chyl et al., 2019). At the same time, functional magnetic resonance spectroscopy (fMRS) in contrast to blood oxygenation level dependent (BOLD) signal in fMRI allows for direct measurement of the neuronal response to stimuli and can distinguish between excitatory and inhibitory neural activity. It yields a more direct measure of behaviorally relevant neural activity and is considerably less sensitive to vascular changes. So far research has shown using low level visual stimulation that visual flashing checkerboard increase glutamate level compared to passive visual fixation in primary visual cortex (Ip et al., 2017; Kurcyus et al., 2018). To date, fMRS has not been tested during reading paradigm. It is also unknown if task-related brain

neurochemistry is associated with individual differences in reading skill and whether task-modulated neurochemical measures could distinguish between typical and dyslexic readers.

2.2.4.4 Limitations

Although the study was carefully designed to disentangle age and region specific differences, we could not avoid pitfalls leading to some limitations of our results. Firstly, we did focus on minimizing motion artifacts in our data especially in the group of children. In order to catch the attention during long acquisition protocol (~40min) we decided to show videos appropriate to the age. Knowing how much variability it could introduce to our data i.e. glutamate (Stanley & Raz, 2018), we could have missed the difference in glutamate concentration not related to the explicit visual stimulation. What is more, recently other authors who also displayed movies during measurements were not able to confirm dyslexia effects for glutamate in anterior cingulate cortex (Horowitz-Kraus et al., 2018). However, watching movies seems to be more ecological scenario and enables generalization of our result to conditions not constrained to observation of a fixation cross. Secondly, SNR was significantly lower in children group than in adults (26.12 vs 50.25) due to shortened acquisition (both voxels) and smaller voxel in temporo-parietal lobe. Nevertheless, more specific quality measure (Cramer-Rao lower bound) was controlled for the level of spectra modelling and all metabolites of interest withstood conservative threshold of CRLB<15%. In case of voxel position and composition all the results presented here were referenced to locally measured water signal and corrected for tissue types. We then assume that despite acquisition inconsistency, we took all necessary steps to minimize the difference in variance within the groups to the acceptable level (2.11 in adults vs 1.76 in children for tNAA).

2.2.5 Conclusions

This thesis describes the magnetic resonance spectroscopy experiment starting from review of literature, through methodological studies in a theory and practice, ending with a application study in a research of dyslexia. The highlight of presented research are hypotheses accompanied by more explorative research questions. To sum up the previous considerations here a short synthesis will be presented in the relevant order.

1. In contrast to the predictions based on the neural noise hypothesis, dyslexic

individuals were not characterized with a heightened levels of glutamate neither in adult, nor children sample. However, an effect of dyslexia for glutamate scaled to creatine was detected in both regions and age groups but became non-significant after multiple comparison correction . This coincidental finding should be rather accounted for confounding difference in creatine concentration between the age groups, than to dyslexia itself. It also confirms the limited interpretation when metabolite ratios are being reported. As an anecdote also the positive correlation between glutamate and rapid naming task hardly reached Bonferroni corrected alpha threshold.

2. Despite the fact that previous researchers (i.e. Pugh et al. and Lebel et al.) pointed to glutamate and choline levels as predictors of individual differences in reading ability, in the current study none of them were confirmed. Interestingly, RAN as a measure of lexical access correlated positively with choline concentration in a way that higher choline level corresponds to slower responses.
3. Dyslexic individuals, irrespective of age, had significantly lower tNAA than controls in the occipital cortex. NAA considered to be a marker of neural health and viability but also plays a role in myelin synthesis. Reduced tNAA in all dyslexic subjects suggests microstructure abnormalities. Lower tNAA was not predicted by presented etiological theories, however, it is the most prominent result presented here, which clearly indicates abnormalities in tissue microstructure, which persist regardless of age.
4. It should be pointed out as a main finding of the presented research that all hypothesized metabolites change with age such as NAA, choline and creatine are higher in adults, whereas glutamate is lower. On one hand, the increased concentration of metabolites reflects changes in cell density, myelination, membrane content and energy deposit. On the other hand, glutamate level decreases due to lower number of NMDA receptors and lower glutamate-glutamine cycle flux.
5. Although we did not find any significant results in GABA concentration we succeed to establish a sophisticated measurement. The power of statistical tests in adults and children subsamples was 0.88 and 0.36 respectively. Variability was greatly reduced in adults due to technical improvements. However, the variability of estimates in younger participants was much higher than expected and could led to the false negative results. More research on bigger samples with at least 60 participants in each

group or with an even improved data quality is needed to resolve the problem.

6. Within the presented 2x2 model we have been able for the first time to test an interaction between participants' age and diagnosis. In a result the nominally significant interaction (without correction for multiple comparisons) was identified in choline such as dyslexic children were characterized with lower metabolite concentration than controls. The effect of diagnosis in adults was not significant itself however, due to observed interaction we know that the choline level difference related to diagnosis changes with age of participants.
7. Since the creatine concentration significantly differed between the group of children and adults we are not able to perform legitimate analyses to compare our results with the previous studies. The same conclusion is valid for NAA and choline, which were also used as references before. However, to simulate an effect of different referencing strategies we performed supplementary group analyses where the main results were confirmed. Nevertheless, it should be noted that water referencing used here with a proper tissue corrections is the most advisable method and the one with least assumptions to be made. In other words, absolute metabolite concentration has a simple, universal interpretation.

3 References

Anderson, C. M., & Swanson, R. A. (2000). Astrocyte glutamate transport: review of properties, regulation, and physiological functions. *Glia*, *32* (1), 1–14.

Bak, L. K., Schousboe, A., Sonnewald, U., & Waagepetersen, H. S. (2006). Glucose is necessary to maintain neurotransmitter homeostasis during synaptic activity in cultured glutamatergic neurons. *Journal of Cerebral Blood Flow and Metabolism: Official Journal of the International Society of Cerebral Blood Flow and Metabolism*, *26* (10), 1285–1297.

Balz, J., Keil, J., Roa Romero, Y., Mekle, R., Schubert, F., Aydin, S., Ittermann, B., Gallinat, J., & Senkowski, D. (2016). GABA concentration in superior temporal sulcus predicts gamma power and perception in the sound-induced flash illusion. *NeuroImage*, *125*, 724–730.

Barker, P. B. (2001). N - Acetyl Aspartate—A Neuronal Marker? In *Annals of Neurology* (Vol. 49, Issue 4, pp. 423–424). https://doi.org/10.1002/ana.90.abs

Bihan, D. L., Le Bihan, D., & Schild, T. (2017). Human brain MRI at 500 MHz, scientific perspectives and technological challenges. In *Superconductor Science and Technology* (Vol. 30, Issue 3, p. 033003). https://doi.org/10.1088/1361-6668/30/3/033003

Black, J. M., Tanaka, H., Stanley, L., Nagamine, M., Zakerani, N., Thurston, A., Kesler, S., Hulme, C., Lyytinen, H., Glover, G. H., Serrone, C., Raman, M. M., Reiss, A. L., & Hoeft, F. (2012). Maternal history of reading difficulty is associated with reduced language-related gray matter in beginning readers. *NeuroImage*, *59* (3), 3021–3032.

Bloch, F. (1946). Nuclear Induction. In *Physical Review* (Vol. 70, Issues 7-8, pp. 460–474).

https://doi.org/10.1103/physrev.70.460

Blüml, S., Seymour, K. J., & Ross, B. D. (1999). Developmental changes in choline- and ethanolamine-containing compounds measured with proton-decoupled 31P MRS in in vivo human brain. In *Magnetic Resonance in Medicine* (Vol. 42, Issue 4, pp. 643–654). https://doi.org/3.0.co;2-n">10.1002/ (sici)1522-2594 (199910)42:4<643::aid-mrm5>3.0.co;2-n

Blüml, S., Wisnowski, J. L., Nelson, M. D., Jr, Paquette, L., Gilles, F. H., Kinney, H. C., & Panigrahy, A. (2013). Metabolic maturation of the human brain from birth through adolescence: insights from in vivo magnetic resonance spectroscopy. *Cerebral Cortex* , *23* (12), 2944–2955.

Bottomley, P. (1985). 4480228 Selective volume method for performing localized NMR spectroscopy. In *Magnetic Resonance Imaging* (Vol. 3, Issue 1, pp. iv – v). https://doi.org/10.1016/0730-725x (85)90032-3

Boumezbeur, F., Mason, G. F., de Graaf, R. A., Behar, K. L., Cline, G. W., Shulman, G. I., Rothman, D. L., & Petersen, K. F. (2010). Altered brain mitochondrial metabolism in healthy aging as assessed by in vivo magnetic resonance spectroscopy. *Journal of Cerebral Blood Flow and Metabolism: Official Journal of the International Society of Cerebral Blood Flow and Metabolism*, *30* (1), 211–221.

Bruno, J. L., Lu, Z.-L., & Manis, F. R. (2013). Phonological processing is uniquely associated with neuro-metabolic concentration. *NeuroImage*, *67*, 175–181.

Buzsáki, G., & Wang, X.-J. (2012). Mechanisms of gamma oscillations. *Annual Review of Neuroscience*, *35*, 203–225.

Chan, K. L., Oeltzschner, G., Saleh, M. G., Edden, R. A. E., & Barker, P. B. (2019). Simultaneous editing of GABA and GSH with Hadamard-encoded MR spectroscopic

imaging. *Magnetic Resonance in Medicine: Official Journal of the Society of Magnetic Resonance in Medicine / Society of Magnetic Resonance in Medicine*, *82* (1), 21–32.

Che, A., Girgenti, M. J., & LoTurco, J. (2014). The Dyslexia-Associated Gene Dcdc2 Is Required for Spike-Timing Precision in Mouse Neocortex. In *Biological Psychiatry* (Vol. 76, Issue 5, pp. 387–396). https://doi.org/10.1016/j.biopsych.2013.08.018

Che, A., Truong, D. T., Fitch, R. H., & LoTurco, J. J. (2016). Mutation of the Dyslexia-Associated Gene Dcdc2 Enhances Glutamatergic Synaptic Transmission Between Layer 4 Neurons in Mouse Neocortex. *Cerebral Cortex* , *26* (9), 3705–3718.

Chemical shift artifact. (n.d.). Questions and Answers in MRI. Retrieved February 24, 2020, from http://mriquestions.com/chemical-shift-artifact.html

Christiansen, P., Toft, P. B., Gideon, P., Danielsen, E. R., Ring, P., & Henriksen, O. (1994). MR-visible water content in human brain: A proton MRS study. In *Magnetic Resonance Imaging* (Vol. 12, Issue 8, pp. 1237–1244). https://doi.org/10.1016/0730-725x(94)90088-9

Chyl, K., Kossowski, B., Dębska, A., Łuniewska, M., Marchewka, A., Pugh, K. R., & Jednoróg, K. (2019). Reading Acquisition in Children: Developmental Processes and Dyslexia-Specific Effects. *Journal of the American Academy of Child and Adolescent Psychiatry*, *58* (10), 948–960.

Cleve, M., Gussew, A., & Reichenbach, J. R. (2015). In vivo detection of acute pain-induced changes of GABA+ and Glx in the human brain by using functional 1H MEGA-PRESS MR spectroscopy. *NeuroImage*, *105*, 67–75.

Del Tufo, S. N., Frost, S. J., Hoeft, F., Cutting, L. E., Molfese, P. J., Mason, G. F., Rothman, D. L., Fulbright, R. K., & Pugh, K. R. (2018). Neurochemistry Predicts Convergence of Written and Spoken Language: A Proton Magnetic Resonance Spectroscopy Study of

Cross-Modal Language Integration. *Frontiers in Psychology*, *9*, 1507.

Destexhe, A. & Rudolph-Lilith, M. (2012). Neuronal Noise. Springer Science & Business Media.

Diagnoza dysleksji u uczniów klasy III szkoły podstawowej: przewodnik diagnostyczny. (2008).

Donne, D. G., & Gorenstein, D. G. (1997). A pictorial representation of product operator formalism: Nonclassical vector diagrams for multidimensional NMR. In *Concepts in Magnetic Resonance* (Vol. 9, Issue 2, pp. 95–111). https://doi.org/3.0.co;2-h">10.1002/(sici)1099-0534 (1997)9:2<95::aid-cmr4>3.0.co;2-h

Dydak, U., Jiang, Y.-M., Long, L.-L., Zhu, H., Chen, J., Li, W.-M., Edden, R. A. E., Hu, S., Fu, X., Long, Z., Mo, X.-A., Meier, D., Harezlak, J., Aschner, M., Murdoch, J. B., & Zheng, W. (2011). In vivo measurement of brain GABA concentrations by magnetic resonance spectroscopy in smelters occupationally exposed to manganese. *Environmental Health Perspectives*, *119* (2), 219–224.

Edden, R. A. E., Muthukumaraswamy, S. D., Freeman, T. C. A., & Singh, K. D. (2009). Orientation discrimination performance is predicted by GABA concentration and gamma oscillation frequency in human primary visual cortex. *The Journal of Neuroscience: The Official Journal of the Society for Neuroscience*, *29* (50), 15721–15726.

Edden, R. A. E., Puts, N. A. J., Harris, A. D., Barker, P. B., & Evans, C. J. (2014). Gannet: A batch-processing tool for the quantitative analysis of gamma-aminobutyric acid–edited MR spectroscopy spectra. *Journal of Magnetic Resonance Imaging: JMRI*, *40* (6), 1445–1452.

Eden, G. F., VanMeter, J. W., Rumsey, J. M., Maisog, J. M., Woods, R. P., & Zeffiro, T. A.

(1996). Abnormal processing of visual motion in dyslexia revealed by functional brain imaging. *Nature*, *382* (6586), 66–69.

Ertürk, M. A., Wu, X., Eryaman, Y., Van de Moortele, P.-F., Auerbach, E. J., Lagore, R. L., DelaBarre, L., Vaughan, J. T., Uğurbil, K., Adriany, G., & Metzger, G. J. (2017). Toward imaging the body at 10.5 tesla. *Magnetic Resonance in Medicine: Official Journal of the Society of Magnetic Resonance in Medicine / Society of Magnetic Resonance in Medicine*, *77* (1), 434–443.

Fecenec, D. (2008). *Test szybkiego nazywania: zeszyt testowy - wersja S*.

Frahm, J., Michaelis, T., Merboldt, K. D., Bruhn, H., Gyngell, M. L., & Hänicke, W. (1990). Improvements in localized proton NMR spectroscopy of human brain. Water suppression, short echo times, and 1 ml resolution. In *Journal of Magnetic Resonance (1969)* (Vol. 90, Issue 3, pp. 464–473). https://doi.org/10.1016/0022-2364 (90)90051-a

Gaetz, W., Bloy, L., Wang, D. J., Port, R. G., Blaskey, L., Levy, S. E., & Roberts, T. P. L. (2014). GABA estimation in the brains of children on the autism spectrum: measurement precision and regional cortical variation. *NeuroImage*, *86*, 1–9.

Gallinat, J., Kunz, D., Senkowski, D., Kienast, T., Seifert, F., Schubert, F., & Heinz, A. (2006). Hippocampal glutamate concentration predicts cerebral theta oscillations during cognitive processing. *Psychopharmacology*, *187* (1), 103–111.

Gasparovic, C., Song, T., Devier, D., Bockholt, H. J., Caprihan, A., Mullins, P. G., Posse, S., Jung, R. E., & Morrison, L. A. (2006). Use of tissue water as a concentration reference for proton spectroscopic imaging. *Magnetic Resonance in Medicine: Official Journal of the Society of Magnetic Resonance in Medicine / Society of Magnetic Resonance in Medicine*, *55* (6), 1219–1226.

Gelman, A., Hill, J., & Yajima, M. (2012). Why We (Usually) Don't Have to Worry About

Multiple Comparisons. In *Journal of Research on Educational Effectiveness* (Vol. 5, Issue 2, pp. 189–211). https://doi.org/10.1080/19345747.2011.618213

Georgiou, G. K., Protopapas, A., Papadopoulos, T. C., Skaloumbakas, C., & Parrila, R. (2010). Auditory temporal processing and dyslexia in an orthographically consistent language. In *Cortex* (Vol. 46, Issue 10, pp. 1330–1344). https://doi.org/10.1016/j.cortex.2010.06.006

Goswami, U. (2011). A temporal sampling framework for developmental dyslexia. *Trends in Cognitive Sciences*, *15* (1), 3–10.

Goswami, U., Thomson, J., Richardson, U., Stainthorp, R., Hughes, D., Rosen, S., & Scott, S. K. (2002). Amplitude envelope onsets and developmental dyslexia: A new hypothesis. *Proceedings of the National Academy of Sciences of the United States of America*, *99* (16), 10911–10916.

Goswami, U., Wang, H.-L. S., Cruz, A., Fosker, T., Mead, N., & Huss, M. (2011). Language-universal sensory deficits in developmental dyslexia: English, Spanish, and Chinese. *Journal of Cognitive Neuroscience*, *23* (2), 325–337.

Graaf, R. A. de, & de Graaf, R. A. (2019). *In Vivo NMR Spectroscopy*. https://doi.org/10.1002/9781119382461

Graaf, M. van der, van der Graaf, M., Julià-Sapé, M., Howe, F. A., Ziegler, A., Majós, C., Moreno-Torres, A., Rijpkema, M., Acosta, D., Opstad, K. S., van der Meulen, Y. M., Arús, C., & Heerschap, A. (2008). MRS quality assessment in a multicentre study on MRS-based classification of brain tumours. In *NMR in Biomedicine* (Vol. 21, Issue 2, pp. 148–158). https://doi.org/10.1002/nbm.1172

Grigorenko, E. L. (2004). Genetic bases of developmental dyslexia: A capsule review of heritability estimates. In *Enfance* (Vol. 56, Issue 3, p. 273).

https://doi.org/10.3917/enf.563.0273

Gunter, J. L., Borowski, B. J., Thostenson, K., Arani, A., Reid, R. I., Cash, D. M., Thomas, D. L., Zhang, H., DeCarli, C. S., Fox, N. C., Thompson, P. M., Tosun, D., Weiner, M., & Jack, C. R. (2017). [IC-P-137]: ADNI-3 MRI PROTOCOL. In *Alzheimer's & Dementia* (Vol. 13, Issue 7S_Part_2, pp. P104–P105). https://doi.org/10.1016/j.jalz.2017.06.2411

Gupta, R. K., Cloughesy, T. F., Sinha, U., Garakian, J., Lazareff, J., Rubino, G., Rubino, L., Becker, D. P., Vinters, H. V., & Alger, J. R. (2000). Relationships Between Choline Magnetic Resonance Spectroscopy, Apparent Diffusion Coefficient and Quantitative Histopathology in Human Glioma. *Journal of Neuro-Oncology*, *50* (3), 215–226.

Hahn, E. L., & Maxwell, D. E. (1952). Spin Echo Measurements of Nuclear Spin Coupling in Molecules. In *Physical Review* (Vol. 88, Issue 5, pp. 1070–1084). https://doi.org/10.1103/physrev.88.1070

Hajek, M., & Dezortova, M. (2008). Introduction to clinical in vivo MR spectroscopy. *European Journal of Radiology*, *67* (2), 185–193.

Hämäläinen, J., Leppänen, P. H. T., Torppa, M., Müller, K., & Lyytinen, H. (2005). Detection of sound rise time by adults with dyslexia. *Brain and Language*, *94* (1), 32–42.

Hancock, R., Pugh, K. R., & Hoeft, F. (2017). Neural Noise Hypothesis of Developmental Dyslexia. In *Trends in Cognitive Sciences* (Vol. 21, Issue 11, p. 909). https://doi.org/10.1016/j.tics.2017.08.003

Hangel, G., Strasser, B., Považan, M., Gruber, S., Chmelík, M., Gajdošík, M., Trattnig, S., & Bogner, W. (2015). Lipid suppression via double inversion recovery with symmetric frequency sweep for robust 2D-GRAPPA-accelerated MRSI of the brain at 7 T. In *NMR*

in Biomedicine (Vol. 28, Issue 11, pp. 1413–1425). https://doi.org/10.1002/nbm.3386

Harris, A. D., Puts, N. A. J., & Edden, R. A. E. (2015). Tissue correction for GABA-edited MRS: Considerations of voxel composition, tissue segmentation, and tissue relaxations. *Journal of Magnetic Resonance Imaging: JMRI*, *42* (5), 1431–1440.

Harris, A. D., Saleh, M. G., & Edden, R. A. E. (2017). Edited1H magnetic resonance spectroscopy in vivo: Methods and metabolites. In *Magnetic Resonance in Medicine* (Vol. 77, Issue 4, pp. 1377–1389). https://doi.org/10.1002/mrm.26619

Hattingen, E., Magerkurth, J., Pilatus, U., Hübers, A., Wahl, M., & Ziemann, U. (2011). Combined 1H and 31P spectroscopy provides new insights into the pathobiochemistry of brain damage in multiple sclerosis. In *NMR in Biomedicine* (Vol. 24, Issue 5, pp. 536–546). https://doi.org/10.1002/nbm.1621

Hingerl, L., Strasser, B., Moser, P., Hangel, G., Motyka, S., Heckova, E., Gruber, S., Trattnig, S., & Bogner, W. (2019). Clinical High-Resolution 3D-MR Spectroscopic Imaging of the Human Brain at 7 T. In *Investigative Radiology* (p. 1). https://doi.org/10.1097/rli.0000000000000626

Horowitz-Kraus, T., Brunst, K. J., & Cecil, K. M. (2018). Children With Dyslexia and Typical Readers: Sex-Based Choline Differences Revealed Using Proton Magnetic Resonance Spectroscopy Acquired Within Anterior Cingulate Cortex. *Frontiers in Human Neuroscience*, *12*, 466.

Hunjan, S., Adalsteinsson, E., Kim, D.-H., Harsh, G. R., Boyer, A. L., Spielman, D., & Xing, L. (2003). Quality assurance of magnetic resonance spectroscopic imaging–derived metabolic data. In *International Journal of Radiation Oncology*Biology*Physics* (Vol. 57, Issue 4, pp. 1159–1173). https://doi.org/10.1016/s0360-3016 (03)01564-5

International Statistical Classification of Diseases and Related Health Problems. (2011). In

Encyclopedia of Clinical Neuropsychology (pp. 1347–1347). https://doi.org/10.1007/978-0-387-79948-3_3055

Ip, I. B., Berrington, A., Hess, A. T., Parker, A. J., Emir, U. E., & Bridge, H. (2017). Combined fMRI-MRS acquires simultaneous glutamate and BOLD-fMRI signals in the human brain. *NeuroImage*, *155*, 113–119.

Kass, R. E., & Raftery, A. E. (1995). Bayes Factors. In *Journal of the American Statistical Association* (Vol. 90, Issue 430, p. 773). https://doi.org/10.2307/2291091

Katz-Brull, R., Koudinov, A. R., & Degani, H. (2002). Choline in the aging brain. In *Brain Research* (Vol. 951, Issue 2, pp. 158–165). https://doi.org/10.1016/s0006-8993(02)03155-4

Keeler, J. (2011). *Understanding NMR Spectroscopy*. John Wiley & Sons.

Kossowski, B. *Interface to load Bruker MRS into Gannet toolbox*. GitHub. Retrieved April 20, 2020, from https://github.com/bkossows/gannet-bruker

Kossowski, B. *rda2nifti - Siemens spectroscopy to voxel mask converter*. NITRC. Retrieved October 2, 2019, from https://www.nitrc.org/projects/rda2nifti/

Kossowski, B., Chyl, K., Kacprzak, A., Bogorodzki, P., & Jednoróg, K. (2019). Dyslexia and age related effects in the neurometabolites concentration in the visual and temporo-parietal cortex. *Scientific Reports*, *9* (1), 5096.

Kossowski, B., Orzeł, J., Bogorodzki, P., Wilson, M., Setkowicz, Z., & P. Gazdzinski, S. (2017). Follow-up analyses on the effects of long-term use of high fat diet on hippocampal metabolite concentrations in Wistar rats: Comparing Tarquin quantification of 7.0T rat metabolites to LCModel. *Biology, Engineering and Medicine*, *2* (4). https://doi.org/10.15761/BEM.1000129

Kreis, R. (2004). Issues of spectral quality in clinical 1H-magnetic resonance spectroscopy

and a gallery of artifacts. *NMR in Biomedicine*, *17* (6), 361–381.

Kreis, R. (2016). The trouble with quality filtering based on relative Cramér-Rao lower bounds. *Magnetic Resonance in Medicine: Official Journal of the Society of Magnetic Resonance in Medicine / Society of Magnetic Resonance in Medicine*, *75* (1), 15–18.

Kurcyus, K., Annac, E., Hanning, N. M., Harris, A. D., Oeltzschner, G., Edden, R., & Riedl, V. (2018). Opposite Dynamics of GABA and Glutamate Levels in the Occipital Cortex during Visual Processing. *The Journal of Neuroscience: The Official Journal of the Society for Neuroscience*, *38* (46), 9967–9976.

Ladd, M. E., Bachert, P., Meyerspeer, M., Moser, E., Nagel, A. M., Norris, D. G., Schmitter, S., Speck, O., Straub, S., & Zaiss, M. (2018). Pros and cons of ultra-high-field MRI/MRS for human application. *Progress in Nuclear Magnetic Resonance Spectroscopy*, *109*, 1–50.

Lance, D., & Michael, G. (1998). *LASER: Adiabatic Single Shot Localization with J-Refocusing*. https://cds.ismrm.org/ismrm-1998/PDF2/p0358.pdf

Lange, T., Dydak, U., Roberts, T. P. L., Rowley, H. A., Bjeljac, M., & Boesiger, P. (2006). Pitfalls in lactate measurements at 3T. *AJNR. American Journal of Neuroradiology*, *27* (4), 895–901.

Laule, C., Vavasour, I. M., Kolind, S. H., Li, D. K. B., Traboulsee, T. L., Wayne Moore, G. R., & MacKay, A. L. (2007). Magnetic resonance imaging of myelin. In *Neurotherapeutics* (Vol. 4, Issue 3, pp. 460–484). https://doi.org/10.1016/j.nurt.2007.05.004

Laycock, S. K., Wilkinson, I. D., Wallis, L. I., Darwent, G., Wonders, S. H., Fawcett, A. J., Griffiths, P. D., & Nicolson, R. I. (2008). Cerebellar Volume and Cerebellar Metabolic Characteristics in Adults with Dyslexia. In *Annals of the New York Academy of Sciences*

(Vol. 1145, Issue 1, pp. 222–236). https://doi.org/10.1196/annals.1416.002

Lebel, C., MacMaster, F. P., & Dewey, D. (2016). Brain metabolite levels and language abilities in preschool children. *Brain and Behavior*, *6* (10), e00547.

Lehongre, K., Ramus, F., Villiermet, N., Schwartz, D., & Giraud, A.-L. (2011). Altered Low-Gamma Sampling in Auditory Cortex Accounts for the Three Main Facets of Dyslexia. In *Neuron* (Vol. 72, Issue 6, pp. 1080–1090). https://doi.org/10.1016/j.neuron.2011.11.002

Löffelholz, K., Klein, J., & Köppen, A. (1993). Chapter 23: Choline, a precursor of acetylcholine and phospholipids in the brain. In *Cholinergic Function and Dysfunction* (pp. 197–200). https://doi.org/10.1016/s0079-6123 (08)62399-7

Mangia, S., Tkác, I., Gruetter, R., Van de Moortele, P.-F., Maraviglia, B., & Uğurbil, K. (2007). Sustained neuronal activation raises oxidative metabolism to a new steady-state level: evidence from 1H NMR spectroscopy in the human visual cortex. *Journal of Cerebral Blood Flow and Metabolism: Official Journal of the International Society of Cerebral Blood Flow and Metabolism*, *27* (5), 1055–1063.

Marsman, A., Mandl, R. C. W., van den Heuvel, M. P., Boer, V. O., Wijnen, J. P., Klomp, D. W. J., Luijten, P. R., & Hilleke E, H. P. (2013). Glutamate changes in healthy young adulthood. *European Neuropsychopharmacology: The Journal of the European College of Neuropsychopharmacology*, *23* (11), 1484–1490.

Martin, E., Capone, A., Schneider, J., Hennig, J., & Thiel, T. (2001). Absence of N-acetylaspartate in the human brain: impact on neurospectroscopy? *Annals of Neurology*, *49* (4), 518–521.

Matczak, A., (tłumacz), A. P., Ciarkowska, W., & Wechsler, D. (1997). *Skala inteligencji D. Wechslera dla dzieci - wersja zmodyfikowana (WISC - R): podręcznik*.

Meng, H., Smith, S. D., Hager, K., Held, M., Liu, J., Olson, R. K., Pennington, B. F., DeFries, J. C., Gelernter, J., O'Reilly-Pol, T., Somlo, S., Skudlarski, P., Shaywitz, S. E., Shaywitz, B. A., Marchione, K., Wang, Y., Paramasivam, M., LoTurco, J. J., Page, G. P., & Gruen, J. R. (2005). DCDC2 is associated with reading disability and modulates neuronal development in the brain. *Proceedings of the National Academy of Sciences of the United States of America*, *102* (47), 17053–17058.

Michaelis, T., Merboldt, K. D., Hänicke, W., Gyngell, M. L., Bruhn, H., & Frahm, J. (1991). On the identification of cerebral metabolites in localized 1H NMR spectra of human brain in vivo. *NMR in Biomedicine*, *4* (2), 90–98.

Mikkelsen, M., Barker, P. B., Bhattacharyya, P. K., Brix, M. K., Buur, P. F., Cecil, K. M., Chan, K. L., Chen, D. Y.-T., Craven, A. R., Cuypers, K., Dacko, M., Duncan, N. W., Dydak, U., Edmondson, D. A., Ende, G., Ersland, L., Gao, F., Greenhouse, I., Harris, A. D., … Edden, R. A. E. (2017). Big GABA: Edited MR spectroscopy at 24 research sites. *NeuroImage*, *159*, 32–45.

Möhler, H. (2006). GABAA receptor diversity and pharmacology. In *Cell and Tissue Research* (Vol. 326, Issue 2, pp. 505–516). https://doi.org/10.1007/s00441-006-0284-3

Mullins, P. G. (2018). Towards a theory of functional magnetic resonance spectroscopy (fMRS): A meta-analysis and discussion of using MRS to measure changes in neurotransmitters in real time. *Scandinavian Journal of Psychology*, *59* (1), 91–103.

Mullins, P. G., McGonigle, D. J., O'Gorman, R. L., Puts, N. A. J., Vidyasagar, R., Evans, C. J., Cardiff Symposium on MRS of GABA, & Edden, R. A. E. (2014). Current practice in the use of MEGA-PRESS spectroscopy for the detection of GABA. *NeuroImage*, *86*, 43–52.

Mullins, P., Rowland, L., Jung, R., & Sibbittjr, W. (2005). A novel technique to study the

brain's response to pain: Proton magnetic resonance spectroscopy. In *NeuroImage* (Vol. 26, Issue 2, pp. 642–646). https://doi.org/10.1016/j.neuroimage.2005.02.001

Muneaux, M., Ziegler, J. C., Truc, C., Thomson, J., & Goswami, U. (2004). Deficits in beat perception and dyslexia: evidence from French. *Neuroreport*, *15* (8), 1255–1259.

Muthukumaraswamy, S. D., Edden, R. A. E., Jones, D. K., Swettenham, J. B., & Singh, K. D. (2009). Resting GABA concentration predicts peak gamma frequency and fMRI amplitude in response to visual stimulation in humans. *Proceedings of the National Academy of Sciences of the United States of America*, *106* (20), 8356–8361.

Nadler, J. V., & Cooper, J. R. (1972). N-ACETYL-l-ASPARTIC ACID CONTENT OF HUMAN NEURAL TUMOURS AND BOVINE PERIPHERAL NERVOUS TISSUES. In *Journal of Neurochemistry* (Vol. 19, Issue 2, pp. 313–319). https://doi.org/10.1111/j.1471-4159.1972.tb01341.x

Narayana, P. A., Fotedar, L. K., Jackson, E. F., Bohan, T. P., Butler, I. J., & Wolinsky, J. S. (1989). Regional in vivo proton magnetic resonance spectroscopy of brain. In *Journal of Magnetic Resonance (1969)* (Vol. 83, Issue 1, pp. 44–52). https://doi.org/10.1016/0022-2364 (89)90290-4

Nordengen, K., Heuser, C., Rinholm, J. E., Matalon, R., & Gundersen, V. (2015). Localisation of N-acetylaspartate in oligodendrocytes/myelin. *Brain Structure & Function*, *220* (2), 899–917.

Oeltzschner, G., Saleh, M. G., Rimbault, D., Mikkelsen, M., Chan, K. L., Puts, N. A. J., & Edden, R. A. E. (2019). Advanced Hadamard-encoded editing of seven low-concentration brain metabolites: Principles of HERCULES. *NeuroImage*, *185*, 181–190.

Peterson, C., & Cotman, C. W. (1989). Strain-dependent decrease in glutamate binding to the

N-methyl-D-aspartic acid receptor during aging. *Neuroscience Letters*, *104* (3), 309–313.

Pignatelli, M., Beyeler, A., & Leinekugel, X. (2012). Neural circuits underlying the generation of theta oscillations. *Journal of Physiology, Paris*, *106* (3-4), 81–92.

Platt, S. R. (2007). The role of glutamate in central nervous system health and disease--a review. *Veterinary Journal* , *173* (2), 278–286.

Poullet, J.-B., Sima, D. M., Simonetti, A. W., De Neuter, B., Vanhamme, L., Lemmerling, P., & Van Huffel, S. (2007). An automated quantitation of short echo time MRS spectra in an open source software environment: AQSES. In *NMR in Biomedicine* (Vol. 20, Issue 5, pp. 493–504). https://doi.org/10.1002/nbm.1112

Prescot, A. P., Prisciandaro, J. J., Miller, S. R., Ingenito, G., Kondo, D. G., & Renshaw, P. F. (2018). Two-Dimensional Proton Magnetic Resonance Spectroscopy versus J-Editing for GABA Quantification in Human Brain: Insights from a GABA-Aminotransferase Inhibitor Study. *Scientific Reports*, *8* (1), 13200.

Price, G. R., & Ansari, D. (2011). Symbol processing in the left angular gyrus: evidence from passive perception of digits. *NeuroImage*, *57* (3), 1205–1211.

Provencher, S. W. (2001). Automatic quantitation of localized in vivo 1H spectra with LCModel. *NMR in Biomedicine*, *14* (4), 260–264.

Pugh, K. R., Frost, S. J., Rothman, D. L., Hoeft, F., Del Tufo, S. N., Mason, G. F., Molfese, P. J., Mencl, W. E., Grigorenko, E. L., Landi, N., Preston, J. L., Jacobsen, L., Seidenberg, M. S., & Fulbright, R. K. (2014). Glutamate and choline levels predict individual differences in reading ability in emergent readers. *The Journal of Neuroscience: The Official Journal of the Society for Neuroscience*, *34* (11), 4082–4089.

Purcell, E. M., Torrey, H. C., & Pound, R. V. (1946). Resonance Absorption by Nuclear

Magnetic Moments in a Solid. In *Physical Review* (Vol. 69, Issues 1-2, pp. 37–38). https://doi.org/10.1103/physrev.69.37

Quadrelli, S., Mountford, C., & Ramadan, S. (2016). Hitchhiker'S Guide to Voxel Segmentation for Partial Volume Correction of in Vivo Magnetic Resonance Spectroscopy. In *Magnetic Resonance Insights* (Vol. 9, p. MRI.S32903). https://doi.org/10.4137/mri.s32903

Rae, C. D. (2014). A guide to the metabolic pathways and function of metabolites observed in human brain 1H magnetic resonance spectra. *Neurochemical Research*, *39* (1), 1–36.

Rae, C., Lee, M. A., Dixon, R. M., Blamire, A. M., Thompson, C. H., Styles, P., Talcott, J., Richardson, A. J., & Stein, J. F. (1998). Metabolic abnormalities in developmental dyslexia detected by 1H magnetic resonance spectroscopy. *The Lancet*, *351* (9119), 1849–1852.

Ramus, F., & Ahissar, M. (2012). Developmental dyslexia: the difficulties of interpreting poor performance, and the importance of normal performance. *Cognitive Neuropsychology*, *29* (1-2), 104–122.

Rango, M., Castelli, A., & Scarlato, G. (1997). Energetics of 3.5 s neural activation in humans: a 31P MR spectroscopy study. *Magnetic Resonance in Medicine: Official Journal of the Society of Magnetic Resonance in Medicine / Society of Magnetic Resonance in Medicine*, *38* (6), 878–883.

Raschle, N. M., Chang, M., & Gaab, N. (2011). Structural brain alterations associated with dyslexia predate reading onset. *NeuroImage*, *57* (3), 742–749.

Roth, K., Hubesch, B., Meyerhoff, D. J., Naruse, S., Gober, J. R., Lawry, T. J., Boska, M. D., Matson, G. B., & Weiner, M. W. (1989). Noninvasive quantitation of phosphorus metabolites in human tissue by NMR spectroscopy. In *Journal of Magnetic Resonance*

(1969) (Vol. 81, Issue 2, pp. 299–311). https://doi.org/10.1016/0022-2364 (89)90062-0

Rothman, D. L., Petroff, O. A., Behar, K. L., & Mattson, R. H. (1993). Localized 1H NMR measurements of gamma-aminobutyric acid in human brain in vivo. *Proceedings of the National Academy of Sciences of the United States of America*, *90* (12), 5662–5666.

Rothman, D. L., Sibson, N. R., Hyder, F., Shen, J., Behar, K. L., & Shulman, R. G. (1999). In vivo nuclear magnetic resonance spectroscopy studies of the relationship between the glutamate-glutamine neurotransmitter cycle and functional neuroenergetics. *Philosophical Transactions of the Royal Society of London. Series B, Biological Sciences*, *354* (1387), 1165–1177.

Rowley, N. M., Madsen, K. K., Schousboe, A., & Steve White, H. (2012). Glutamate and GABA synthesis, release, transport and metabolism as targets for seizure control. *Neurochemistry International*, *61* (4), 546–558.

Saleh, M. G., Oeltzschner, G., Chan, K. L., Puts, N. A. J., Mikkelsen, M., Schär, M., Harris, A. D., & Edden, R. A. E. (2016). Simultaneous edited MRS of GABA and glutathione. *NeuroImage*, *142*, 576–582.

Segovia, G., Porras, A., Del Arco, A., & Mora, F. (2001). Glutamatergic neurotransmission in aging: a critical perspective. *Mechanisms of Ageing and Development*, *122* (1), 1–29.

Shaywitz, S. E., Shaywitz, B. A., Pugh, K. R., Fulbright, R. K., Constable, R. T., Mencl, W. E., Shankweiler, D. P., Liberman, A. M., Skudlarski, P., Fletcher, J. M., Katz, L., Marchione, K. E., Lacadie, C., Gatenby, C., & Gore, J. C. (1998). Functional disruption in the organization of the brain for reading in dyslexia. *Proceedings of the National Academy of Sciences of the United States of America*, *95* (5), 2636–2641.

Shimizu, M., Suzuki, Y., Yamada, K., Ueki, S., Watanabe, M., Igarashi, H., & Nakada, T. (2017). Maturational decrease of glutamate in the human cerebral cortex from childhood

to young adulthood: a H-MR spectroscopy study. *Pediatric Research*, *82* (5), 749–752.

Singhal, N. K., Huang, H., Li, S., Clements, R., Gadd, J., Daniels, A., Kooijman, E. E., Bannerman, P., Burns, T., Guo, F., Pleasure, D., Freeman, E., Shriver, L., & McDonough, J. (2017). The neuronal metabolite NAA regulates histone H3 methylation in oligodendrocytes and myelin lipid composition. *Experimental Brain Research. Experimentelle Hirnforschung. Experimentation Cerebrale*, *235* (1), 279–292.

Slice-selective excitation. (n.d.). Questions and Answers in MRI. Retrieved July 10, 2019, from http://mriquestions.com/slice-selective-excitation.html

Smith, Q. R. (2000). Transport of Glutamate and Other Amino Acids at the Blood-Brain Barrier. In *The Journal of Nutrition* (Vol. 130, Issue 4, p. 1016S – 1022S). https://doi.org/10.1093/jn/130.4.1016s

Spin echo. (n.d.). Wikipedia. Retrieved May 4, 2020, from https://en.wikipedia.org/wiki/Spin_echo

Stagg, C. J., Bestmann, S., Constantinescu, A. O., Moreno, L. M., Allman, C., Mekle, R., Woolrich, M., Near, J., Johansen-Berg, H., & Rothwell, J. C. (2011). Relationship between physiological measures of excitability and levels of glutamate and GABA in the human motor cortex. *The Journal of Physiology*, *589* (Pt 23), 5845–5855.

Stanley, J. A., & Raz, N. (2018). Functional Magnetic Resonance Spectroscopy: The "New" MRS for Cognitive Neuroscience and Psychiatry Research. In *Frontiers in Psychiatry* (Vol. 9). https://doi.org/10.3389/fpsyt.2018.00076

Steinbrink, C., Vogt, K., Kastrup, A., Müller, H.-P., Juengling, F. D., Kassubek, J., & Riecker, A. (2008). The contribution of white and gray matter differences to developmental dyslexia: Insights from DTI and VBM at 3.0 T. *Neuropsychologia*, *46* (13), 3170–3178.

Strasser, B., Považan, M., Hangel, G., Hingerl, L., Chmelik, M., Gruber, S., Trattnig, S., & Bogner, W. (2017). (2 1)D-CAIPIRINHA accelerated MR spectroscopic imaging of the brain at 7T. In *Magnetic Resonance in Medicine* (Vol. 78, Issue 2, pp. 429–440). https://doi.org/10.1002/mrm.26386

Surányi, Z., Csépe, V., Richardson, U., Thomson, J. M., Honbolygó, F., & Goswami, U. (2009). Sensitivity to rhythmic parameters in dyslexic children: a comparison of Hungarian and English. In *Reading and Writing* (Vol. 22, Issue 1, pp. 41–56). https://doi.org/10.1007/s11145-007-9102-x

Szczerbiński, M., & Pelc-Pękala, O. (2013). *Zestaw metod diagnozy trudności w czytaniu: Test Dekodowania*.

Tang, C. Y., Friedman, J., Shungu, D., Chang, L., Ernst, T., Stewart, D., Hajianpour, A., Carpenter, D., Ng, J., Mao, X., Hof, P. R., Buchsbaum, M. S., Davis, K., & Gorman, J. M. (2007). Correlations between Diffusion Tensor Imaging (DTI) and Magnetic Resonance Spectroscopy (1H MRS) in schizophrenic patients and normal controls. *BMC Psychiatry*, *7*, 25.

Thomas, M. A., Albert Thomas, M., Hattori, N., Umeda, M., Sawada, T., & Naruse, S. (2003). Evaluation of two-dimensional L-COSY and JPRESS using a 3?T MRI scanner: from phantoms to human brainin vivo. In *NMR in Biomedicine* (Vol. 16, Issue 5, pp. 245–251). https://doi.org/10.1002/nbm.825

Thomas, M. A., Albert Thomas, M., Yue, K., Binesh, N., Davanzo, P., Kumar, A., Siegel, B., Frye, M., Curran, J., Lufkin, R., Martin, P., & Guze, B. (2001). Localized two-dimensional shift correlated MR spectroscopy of human brain. In *Magnetic Resonance in Medicine* (Vol. 46, Issue 1, pp. 58–67). https://doi.org/10.1002/mrm.1160

Thulborn, K. R., & Ackerman, J. J. H. (1983). Absolute molar concentrations by NMR in

inhomogeneous B1. A scheme for analysis of in vivo metabolites. In *Journal of Magnetic Resonance (1969)* (Vol. 55, Issue 3, pp. 357–371). https://doi.org/10.1016/0022-2364 (83)90118-x

Tofts, P. S. (1988). The noninvasive measurement of absolute metabolite concentrations in vivo using surface-coil NMR spectroscopy. In *Journal of Magnetic Resonance (1969)* (Vol. 80, Issue 1, pp. 84–95). https://doi.org/10.1016/0022-2364 (88)90059-5

Vandermosten, M., Boets, B., Wouters, J., & Ghesquière, P. (2012). A qualitative and quantitative review of diffusion tensor imaging studies in reading and dyslexia. *Neuroscience and Biobehavioral Reviews*, *36* (6), 1532–1552.

Wagner, R. K., Torgesen, J. K., Laughon, P., & Simmons, K. (1993). Development of young readers' phonological processing abilities. In *Journal of Educational Psychology* (Vol. 85, Issue 1, pp. 83–103). https://doi.org/10.1037/0022-0663.85.1.83

Wang, Y., & Li, S. J. (1998). Differentiation of metabolic concentrations between gray matter and white matter of human brain by in vivo 1H magnetic resonance spectroscopy. *Magnetic Resonance in Medicine: Official Journal of the Society of Magnetic Resonance in Medicine / Society of Magnetic Resonance in Medicine*, *39* (1), 28–33.

Watanabe, A., Kato, N., & Kato, T. (2002). Effects of creatine on mental fatigue and cerebral hemoglobin oxygenation. *Neuroscience Research*, *42* (4), 279–285.

Wilcke, A., Weissfuss, J., Kirsten, H., Wolfram, G., Boltze, J., & Ahnert, P. (2009). The role of gene DCDC2 in German dyslexics. *Annals of Dyslexia*, *59* (1), 1–11.

Wilson, M., Andronesi, O., Barker, P. B., Bartha, R., Bizzi, A., Bolan, P. J., Brindle, K. M., Choi, I.-Y., Cudalbu, C., Dydak, U., Emir, U. E., Gonzalez, R. G., Gruber, S., Gruetter, R., Gupta, R. K., Heerschap, A., Henning, A., Hetherington, H. P., Huppi, P. S., … Howe, F. A. (2019). Methodological consensus on clinical proton MRS of the brain:

Review and recommendations. *Magnetic Resonance in Medicine: Official Journal of the Society of Magnetic Resonance in Medicine / Society of Magnetic Resonance in Medicine*, *82* (2), 527–550.

Wilson, M., Reynolds, G., Kauppinen, R. A., Arvanitis, T. N., & Peet, A. C. (2011). A constrained least-squares approach to the automated quantitation of in vivo1H magnetic resonance spectroscopy data. In *Magnetic Resonance in Medicine* (Vol. 65, Issue 1, pp. 1–12). https://doi.org/10.1002/mrm.22579

Woo, D.-C., Choi, C.-B., Kim, S.-S., Rhim, H.-S., Jahng, G.-H., Baek, H.-M., Nalcioglu, O., & Choe, B.-Y. (2009). Development of a QA phantom and protocol for proton magnetic resonance spectroscopy. In *Concepts in Magnetic Resonance Part B: Magnetic Resonance Engineering* (Vol. 35B, Issue 3, pp. 168–179). https://doi.org/10.1002/cmr.b.20144

Wray, S., & Tofts, P. S. (1986). Direct in vivo measurement of absolute metabolite concentrations using 31P nuclear magnetic resonance spectroscopy. *Biochimica et Biophysica Acta*, *886* (3), 399–405.

Wyss, M., & Schulze, A. (2002). Health implications of creatine: can oral creatine supplementation protect against neurological and atherosclerotic disease? *Neuroscience*, *112* (2), 243–260.

Yeatman, J. D., Wandell, B. A., & Mezer, A. A. (2014). Lifespan maturation and degeneration of human brain white matter. *Nature Communications*, *5*, 4932.

Zhang, H., Lin, S.-C., & Nicolelis, M. A. L. (2010). Spatiotemporal coupling between hippocampal acetylcholine release and theta oscillations in vivo. *The Journal of Neuroscience: The Official Journal of the Society for Neuroscience*, *30* (40), 13431–13440.

Zhang, J. M. (2013). *Human Brain Glutamate, Glutamine, γ-Aminobutyric Acid Proton Magnetic Resonance Spectral Quantification with the Fast Pade Transform* (J. R. Alger (Ed.)). University of California, Los Angeles .